

12
3-3-92 JS①

PNL-7975
UC-702

Model Assessment of Protective Barriers: Part III

Status of FY 1990 Work

**M. J. Fayer
M. L. Rockhold
D. J. Holford**

February 1992

**Prepared for the U.S. Department of Energy
under Contract DE-AC06-76RLO 1830**

**Pacific Northwest Laboratory
Operated for the U.S. Department of Energy
by Battelle Memorial Institute**



PNL-7975

REPRODUCTION OF THIS DOCUMENT IS UNLIMITED

DISCLAIMER

This report was prepared as an account of work sponsored by an agency of the United States Government. Neither the United States Government nor any agency thereof, nor Battelle Memorial Institute, nor any of their employees, makes **any warranty, expressed or implied, or assumes any legal liability or responsibility for the accuracy, completeness, or usefulness of any information, apparatus, product, or process disclosed, or represents that its use would not infringe privately owned rights.** Reference herein to any specific commercial product, process, or service by trade name, trademark, manufacturer, or otherwise does not necessarily constitute or imply its endorsement, recommendation, or favoring by the United States Government or any agency thereof, or Battelle Memorial Institute. The views and opinions of authors expressed herein do not necessarily state or reflect those of the United States Government or any agency thereof.

PACIFIC NORTHWEST LABORATORY
operated by
BATTELLE MEMORIAL INSTITUTE
for the
UNITED STATES DEPARTMENT OF ENERGY
under Contract DE-AC06-76RLO 1830

Printed in the United States of America

Available to DOE and DOE contractors from the
Office of Scientific and Technical Information, P.O. Box 62, Oak Ridge, TN 37831;
prices available from (615) 576-8401. FTS 626-8401.

Available to the public from the National Technical Information Service,
U.S. Department of Commerce, 5285 Port Royal Rd., Springfield, VA 22161.

PNL--7975

DE92 008204

MODEL ASSESSMENT OF PROTECTIVE
BARRIERS: PART III

Status of FY 1990 Work

M. J. Fayer
M. L. Rockhold
D. J. Holford

February 1992

Prepared for
the U.S. Department of Energy
under Contract DE-AC06-76RLO 1830

Pacific Northwest Laboratory
Richland, Washington 99352

MASTER

EP

PREFACE

Protective barriers are being considered for use at the Hanford Site to enhance the isolation of radioactive wastes from water, plant, and animal intrusion. This study is part of an ongoing effort to assess the effectiveness of protective barriers for isolation of wastes from water. Part I of this study was the original modeling assessment by Pacific Northwest Laboratory (PNL)^(a) of various protective barrier designs (e.g., soil type, vegetation). In Part II of this study, additional barrier designs were reviewed and several barrier modeling assumptions were tested. A test plan was then produced that detailed the requirements for hydrologic modeling of protective barriers. This report (Part III) summarizes the status of protective barrier modeling in FY 1990. The report contains a comparison of the UNSAT2, TOUGH, and PORFLO-3 code solutions to the barrier edge problem, verification tests of PORFLO-3 operating in the axisymmetric mode for use in simulating infiltration into animal burrows and root channels, an analysis of drainage from small-tube lysimeters using the TOUGH code, and a comparison of field data and simulation results from the UNSAT-H computer code. Some of the TOUGH work and all of the UNSAT2 work reported here was documented in an unpublished letter report in FY 1988. Two sections from that FY 1988 letter report are included as appendixes in this report (Part III). These appendixes describe laboratory testing of the Field Lysimeter Test Facility (FLTF) soil and generation of weather parameters.

(a) Pacific Northwest Laboratory is operated by Battelle Memorial Institute for the U.S. Department of Energy under Contract DE-AC06-76RLO 1830.

ABSTRACT

In 1990, Pacific Northwest Laboratory (PNL) conducted work under the Barrier Simulation task of the Protective Barriers program, which is managed jointly by PNL and Westinghouse Hanford Company. Two-dimensional simulations of the barrier edge were conducted with the UNSAT2, TOUGH, and PORFLO-3^(a) codes. The UNSAT2 simulation, an extension of previous work, was conducted to document the run time characteristics of the UNSAT2 code and test a new grid. The new grid, which had 2% more nodes, took 6% longer to obtain a solution. The water-content contour results, however, were smoother for the new grid. The next step should be to solve the problem with progressively higher node densities until the solution does not change. Simulation of the barrier edge problem with the TOUGH and PORFLO-3 codes yielded water-content contour solutions that were much smoother than the UNSAT2 solution. Additional effort should be directed to testing with a 0.05-cm/yr flux through the barrier to demonstrate whether the differences among the codes are significant. A verification test of PORFLO-3 Version 1.1 was conducted in preparation for using the code to study infiltration into animal burrows and root channels, and axisymmetric solutions of water infiltration using PORFLO-3 were compared to generalized solutions for infiltration from a surface point source. The TOUGH code was used to test the hypothesis that temperature changes along the side walls of small-tube lysimeters could induce drainage of in situ water located beneath supposedly impermeable asphalt layers. The results imply that temperature effects on protective barriers could be significant and should be calculated. The UNSAT-H Version 2.0 model was used to simulate the water balance of eight of the eighteen lysimeters located at the Field Lysimeter Test Facility (FLTF). Comparisons between the simulation results and measurements in the lysimeters were used to document the ability of the model. Generally, the model overpredicted evaporation in the winter and underpredicted it in the summer. Sensitivity tests revealed that the hydraulic conductivity function, snow cover, and potential evaporation were important to successful modeling of

(a) PORFLO-3 is copyrighted by Analytic and Computational Research, Inc., subject to Limited Government License.

storage in a protective barrier. Results also indicate that hysteresis is important to successful modeling of drainage through protective barriers. The steady-state flux method was used to measure the hydraulic properties of the FLTF soil for use in simulations of protective barriers. The results lend credibility to the practice of using calculated conductivity values in simulations of protective barriers. A computer code for generating sequences of weather variables given the statistics was also tested for use at the Hanford Site. The statistics of the generated weather variables matched those of the measured data, verifying that the code works. This code will prove useful for constructing long sequences of weather variables for use in long-term simulations.

SUMMARY

In 1990, Pacific Northwest Laboratory (PNL) conducted work under the Barrier Simulation task of the Protective Barriers program that is managed jointly by PNL and Westinghouse Hanford Company. This work consisted of three subtasks that included 1) comparison of two-dimensional simulation results from three codes, 2) verification of the PORFLO-3^(a) code for infiltration into dry soil, and 3) use of the TOUGH code for understanding the potential causes of drainage from lysimeters.

Two-dimensional simulations of the barrier edge were conducted with the UNSAT2, TOUGH, and PORFLO-3 codes. The UNSAT2 simulation, an extension of previous work, was conducted to document the run time characteristics of the UNSAT2 code and test a new grid. The new grid, which had 2% more nodes, took 6% longer to obtain a solution. The water-content contour results, however, were smoother for the new grid. After 500 years, fluxes through the waste zone closest to the barrier edge were about 38% greater using the new grid. For both grids, about 200 years were needed before fluxes decreased below the design requirement of 0.05 cm/yr. Because the grid change noticeably affected the solution, the current node densities may be insufficient. The next step should be to solve the problem with progressively higher node densities until the solution does not change.

Simulation of the barrier edge problem with the TOUGH and PORFLO-3 codes yielded water-content contour solutions that were much smoother relative to the UNSAT2 solution. The solutions from all three codes were similar for all areas except under the barrier. At 500 years, TOUGH predicted slightly higher water contents than PORFLO-3; the UNSAT2 predictions were slightly lower than PORFLO-3. In terms of flux moving through the waste zone at 500 years, the predictions were 0.05, 0.016, and 0.014 cm/yr for TOUGH, UNSAT2, and PORFLO-3, respectively. All of these values are at or below the proposed barrier

(a) PORFLO-3 is copyrighted by Analytic and Computational Research, Inc., subject to Limited Government License.

standard of 0.05 cm/yr. Additional effort should be directed to testing with a 0.05-cm/yr flux through the barrier to demonstrate whether the differences among the codes are significant.

A verification test of PORFLO-3 Version 1.1 was conducted in preparation for using the code to study infiltration into animal burrows and root channels. Axisymmetric solutions of water infiltration using PORFLO-3 were compared to generalized solutions for infiltration from a surface point source. Comparisons of the two solutions were qualitative, given that some of the particulars (e.g., node density and arrangement, internodal conductance calculation, surface boundary description) were not identical. Despite the differences in how the problem was solved, the comparisons showed that PORFLO-3 predicted wetting front positions that were comparable to those predicted using the generalized solutions. For a more quantitative benchmark of PORFLO-3, the TOUGH code should be used to solve this problem. Some of the difficulties in the comparisons reported here (e.g., node density and arrangement, internodal conductance calculation) can then be eliminated. Cumulative mass balance errors for PORFLO-3 were 1.4% after 0.15 h of infiltration into sand and 0.73% after 2.5 h of infiltration into silt loam. This level of error is acceptable for conducting sensitivity tests of infiltration into animal burrows and root channels.

The TOUGH code was used to test the hypothesis that temperature changes along the side walls of small-tube lysimeters could induce drainage of in situ water located beneath supposedly impermeable asphalt layers. Drainage from the lysimeters has been observed year-round and the peak occurs during the summer. The proposed mechanism for producing drainage of in situ water is redistribution of water in the liquid and vapor phases in response to temperature gradients. Using mean monthly soil temperatures measured at a nearby site, TOUGH predicted that some of the in situ water would drain and that the peak would occur during the summer, just as the measurements indicate. The results imply that any lysimeter that has below-ground surfaces exposed to uneven temperature changes may be subject to the same effect. The results also imply that temperature effects on protective barriers could be significant and should be calculated.

The UNSAT-H Version 2.0 model was used to simulate the water balance of eight of the eighteen lysimeters located at the Field Lysimeter Test Facility (FLTF). Comparisons between the simulation results and measurements in the lysimeters were used to document the ability of the model. Ambient precipitation, 2x average precipitation, and precipitation to breakthrough (i.e., drainage) treatments were simulated. Differences between measured and simulated water contents ranged as high as $0.023 \text{ cm}^3/\text{cm}^3$ for the ambient treatment and $0.089 \text{ cm}^3/\text{cm}^3$ near the soil-sand interface for the breakthrough treatment. Simulated storage followed the trend in the measured values, although differences of as much as 5 cm were observed at certain times. Generally, the model overpredicted evaporation in the winter and underpredicted it in the summer. Root-mean-square errors were 1.47 and 2.21 cm for the ambient and 2x average treatments, respectively. Sensitivity tests revealed that the hydraulic conductivity function, snow cover, and potential evaporation were important to successful modeling of storage in a protective barrier. When the above parameters and processes were adjusted (though not optimized), the root-mean-square error for the 2x average treatment was reduced 63% to 0.81 cm. For the breakthrough treatment, simulated drainage was obtained only by using field-measured sorption and saturated conductivity data. This result indicates that hysteresis is important to successful modeling of drainage through protective barriers.

The steady-state flux method was used to measure the hydraulic properties of the FLTF soil for use in simulations of protective barriers. The water retention results of the experiment indicated higher water contents (in the matric potential range of -100 to 0 cm) than previously measured. The unsaturated conductivity results are very similar to the values calculated using the van Genuchten retention function fit to previously measured retention data and the Mualem conductivity model. This result lends credibility to the practice of using calculated conductivity values in simulations of protective barriers.

WGEN, a computer code for generating sequences of weather variables given the statistics, was tested for use at the Hanford Site. The companion code, WGENPAR, was used to derive statistics for a 30-year record of weather

data collected at the Hanford Meteorological Station. These statistics were then used in the WGEN code to generate a 30-year sequence of weather variables. The statistics of the generated weather variables matched those of the measured data, providing verification that the code is functioning. The WGEN code will prove useful for constructing much longer sequences of weather variables for use in long-term simulations.

CONTENTS

PREFACE	iii
ABSTRACT	v
SUMMARY	vii
1.0 INTRODUCTION	1.1
2.0 CODE SOLUTIONS TO THE BARRIER EDGE PROBLEM	2.1
2.1 PROBLEM DESCRIPTION	2.1
2.2 UNSAT2 SOLUTION	2.3
2.3 TOUGH SOLUTION	2.12
2.4 PORFLO-3 SOLUTION	2.15
2.5 COMPARISON OF CODE SOLUTIONS	2.16
2.5.1 Total Head Solutions	2.16
2.5.2 Water Content Solutions	2.18
2.5.3 Matric Potential Solutions	2.18
2.5.4 Flux-Past-the-Waste Solutions	2.18
3.0 VERIFICATION OF AXISYMMETRIC SOLUTION USING PORFLO-3	3.1
3.1 GENERALIZED SOLUTION USED TO VERIFY PORFLO-3	3.1
3.1.1 Problem Description	3.2
3.1.2 Verification Results	3.6
4.0 TEMPERATURE EFFECTS ON LYSIMETER DRAINAGE	4.1
4.1 DESCRIPTION OF LYSIMETER DESIGN AND DATA	4.1
4.2 PROBLEM DESCRIPTION	4.4
4.3 SIMULATION RESULTS	4.6
5.0 COMPARISON OF FIELD DATA AND UNSAT-H SIMULATION RESULTS	5.1
5.1 MODEL DESCRIPTION	5.1

5.2	METHOD	5.2
5.2.1	Barrier Representation	5.4
5.2.2	Soil Properties	5.4
5.2.3	Initial Conditions	5.6
5.2.4	Boundary Conditions	5.7
5.2.5	Simulation Controls	5.11
5.3	RESULTS	5.12
5.3.1	Ambient Precipitation Treatment	5.12
5.3.2	2x Average Precipitation Treatment	5.14
5.3.3	Precipitation to Breakthrough Treatment	5.22
5.4	DISCUSSION AND SUMMARY	5.25
6.0	REFERENCES	6.1
	APPENDIX A - DETERMINATION OF FLTF SOIL HYDRAULIC PROPERTIES	A.1
	APPENDIX B - GENERATION OF LONG-TERM WEATHER VARIABLES	B.1
	APPENDIX C - GENERALIZED SOLUTION TO INFILTRATION FROM A SURFACE POINT SOURCE	C.1

FIGURES

2.1	Barrier Conceptualization for Two-Dimensional Modeling	2.2
2.2	Comparison of Methods for Describing Soil Hydraulic Properties	2.5
2.3	Finite-Element Grids for UNSAT2	2.6
2.4	UNSAT2 Results, after 500 Years, Original Grid	2.8
2.5	UNSAT2 Results, after 500 Years, New Grid	2.9
2.6	UNSAT2 Results after 500 Years, Matric Potential	2.10
2.7	Estimated Flux Past the Bottom-Left Corner of the Waste Zone Versus Time, UNSAT2 Cases 2a and 2b	2.11
2.8	Finite-Difference Grid for TOUGH and PORFLO-3	2.14
2.9	TOUGH Head and Water Content Results	2.15
2.10	PORFLO-3 Results after 500 Years	2.17
2.11	Simulation Results after 500 Years, Matric Potential	2.19
2.12	Estimated Flux Past the Bottom-Left Corner of the Waste Zone Versus Time, UNSAT2, TOUGH, and PORFLO-3 Solutions	2.20
3.1	Soil Hydraulic Properties for Verification Test of PORFLO-3	3.3
3.2	PORFLO-3 and GSIPS Solutions to Infiltration into a Sand from a Surface Point Source for Three Times	3.7
3.3	PORFLO-3 and GSIPS Solutions to Infiltration into a Silt Loam from a Surface Point Source for Three Times	3.11
4.1	Cross Section of Lysimeter	4.2
4.2	Drainage from Lysimeter No. 9 Compared with Average Monthly Precipitation and Soil Temperature at the 1.3-cm Depth	4.3
4.3	Drainage from Lysimeter No. 2 Compared with Average Monthly Precipitation and Soil Temperature at the 1.3-cm Depth	4.4
4.4	Cross Section of Radial Grid	4.5
4.5	Comparison of Drainage Predicted by Constant-Temperature and Variable-Temperature Simulations	4.7

4.6	Comparison of Drainage Predicted by Variable-Temperature Model and Measured from an Asphalt Barrier Lysimeter	4.8
4.7	Simulated Liquid Velocities	4.9
4.8	Simulated Temperatures	4.10
4.9	Simulated Vapor Pressures	4.11
4.10	Simulated Water Contents	4.13
5.1	Lysimeter Design and Conceptual Model	5.3
5.2	Soil Hydraulic Properties: Water Retention and Hydraulic Conductivity	5.8
5.3	Initial Water Contents for All Lysimeters	5.9
5.4	Cumulative Precipitation for Each of the Three Precipitation Treatments	5.11
5.5	Cumulative Potential Evaporation for the Ambient and 2x Average Precipitation Treatments Without and With a Snow Cover and the Precipitation to Breakthrough Treatment	5.12
5.6	Measured and Simulated Water Contents for the Ambient Precipitation Treatment on 2 November 1988 and 14 March 1989	5.13
5.7	Measured and Simulated Storage for the Ambient Precipitation Treatment, Lysimeter W2	5.14
5.8	Measured and Simulated Water Contents for the 2x Average Precipitation Treatment on 2 November 1988 and 14 March 1989	5.15
5.9	Measured and Simulated Storage for the 2x Average Precipitation Treatment, Lysimeter W4	5.16
5.10	Measured and Simulated Storage for the 2x Average Precipitation Treatment, Lysimeter W4, Showing the Effects of 95% Confidence Intervals, $\ell = 0$, Snow Cover, and 0.7 PE	5.18
5.11	Measured and Simulated Storage for the 2x Average Precipitation Treatment, Lysimeter W4	5.23
5.12	Measured and Simulated Water Contents for the Precipitation to Breakthrough Treatment on 18 May 1988 and 29 June 1988	5.24
5.13	Measured and Simulated Drainage for the Precipitation to Breakthrough Treatment Using the Silt Loam Desorption Curve	5.26

A.1	Steady-State Flux Apparatus	A.2
A.2	Measured Water Retention Data and van Genuchten Function Fit for FLTF Soil	A.6
A.3	Measured Hydraulic Conductivity Data and van Genuchten Function Fit for FLTF Soil	A.7
B.1	Comparison of Observed and Generated Mean Monthly Precipitation	B.5
B.2	Comparison of Observed and Generated Mean Monthly Maximum and Minimum Air Temperatures	B.5
B.3	Comparison of Observed and Generated Mean Monthly Solar Radiation	B.6
C.1	Example Input File for the GSIPS Code	C.6
C.2	Example Output File from the GSIPS Code	C.6

TABLES

2.1	AP-1 Soil Properties Used by UNSAT2	2.4
2.2	UNSAT2 Simulation Summary	2.13
3.1	Parameters for Describing Soil Hydraulic Properties Using the van Genuchten Retention Function and Mualem Conductivity Model	3.4
3.2	Cumulative Mass Balance Errors for the PORFLO-3 Simulations of Infiltration into Sand from a Surface Point Source	3.10
4.1	Parameters for Describing Hydraulic Properties with the van Genuchten-Burdine Functions	4.6
5.1	Lysimeter Descriptions, Identifiers, and Simulation Dates for Each Treatment	5.4
5.2	Simulation Node Depths	5.5
5.3	Parameters for Describing Hydraulic Properties with the van Genuchten and Mualem Functions	5.7
5.4	Periods of Extended Snow Cover and Mean Daily Air Temperature Equal to or Below 0°C	5.21
5.5	Summary of Water Balance Parameters for Each Simulation	5.27
A.1	Soil Hydraulic Properties Determined with the Steady-State Flux Technique for a Composite of Selected FLTF Soil Samples	A.4
B.1	Weather-Generation Parameters Generated with WGENPAR Using Hanford Meteorological Station Data from the Period 1958-1987	B.3
B.2	Comparison of Observed and Generated Weather Variables for the Hanford Meteorological Station from the Period 1958-1987	B.4
C.1	Coefficient Matrix Used by the GSIPS Code	C.6

1.0 INTRODUCTION

Radioactive waste exists at the U.S. Department of Energy's (DOE's) Hanford Site in a variety of locations, including subsurface grout and tank farms, solid waste burial grounds, and contaminated soil sites. Some of these waste sites may need to be isolated from percolating water to minimize the potential for transport of the waste to the ground water, which eventually discharges to the Columbia River. Multilayer protective barriers have been proposed as a means of limiting the flow of water through the waste sites (DOE 1987). A multiyear research program [managed jointly by Pacific Northwest Laboratory (PNL)^(a) and Westinghouse Hanford Company for the DOE] is aimed at assessing the performance of these barriers (Adams and Wing 1986). One aspect of this program involves the use of computer models to predict barrier performance. Three modeling studies have already been conducted (Lu, Phillips, and Adams 1982; Fayer et al. 1985; Fayer 1987) and a test plan was produced (Fayer 1990). The simulation work reported here was conducted by PNL and extends the previous modeling work.

The purposes of this report are to understand phenomena that have been observed in the field and to provide information that can be used to improve hydrologic modeling of the protective barrier. An improved modeling capability results in better estimates of barrier performance. Better estimates can be used to improve the design of barriers and the assessment of their long-term performance.

Four topics related to protective barriers were studied: 1) subbarrier flow that originates beyond the edge of the barrier, 2) infiltration into animal burrows and root channels, 3) drainage beneath an asphalt layer in small-tube lysimeters, and 4) validity of a near-surface water balance model. The first topic, subbarrier flow, was studied using the multidimensional codes UNSAT2, TOUGH, and PORFLO-3^(b). The objectives were to 1) establish the run-time parameters of the UNSAT2 code for solving Case 2 from Fayer (1987)

(a) Pacific Northwest Laboratory is operated by Battelle Memorial Institute for DOE under Contract DE-AC06-76RLO 1830.

(b) PORFLO-3 is copyrighted by Analytic and Computational Research, Inc., subject to Limited Government License.

for use in future code benchmarking, 2) study the effect of using an improved grid design in solving Case 2 with the UNSAT2 code, and 3) solve the same problem using the TOUGH and PORFLO-3 codes for comparison with the UNSAT2 solution.

The second topic related to protective barriers, that of animal burrows and root channels, was studied using the PORFLO-3 code. Point infiltration problems were simulated using PORFLO-3 in the axisymmetric mode. The PORFLO-3 results were compared with published solutions. The objective was to verify the ability of PORFLO-3 to solve such a problem before using the code to study infiltration in animal burrows and root channels.

The third topic related to protective barriers, that of drainage beneath asphalt layers, was studied using the TOUGH code. TOUGH was run in the axisymmetric mode with a nonisothermal domain and an active air phase. The objective was to determine whether annual fluctuations in air temperature at the edge of the lysimeters could induce vapor redistribution and eventually drainage of in situ water located beneath the asphalt layers.

The fourth topic related to protective barriers, that of the validity of a near-surface water balance model, was studied using the UNSAT-H code. Eight lysimeters located at the Field Lysimeter Test Facility (FLTF) were simulated for durations up to 1.5 years. The predicted water balance parameters were compared with the measured values. The objective was to document the ability of the model to make such predictions.

Section 2.0 describes the results of simulating subbarrier flow using the UNSAT2, TOUGH, and PORFLO-3 codes. Section 3.0 describes the verification test of PORFLO-3 for infiltration into dry soil from a surface point source. Section 4.0 describes the TOUGH simulations of water redistribution beneath asphalt layers in lysimeters in response to temperature gradients. Section 5.0 describes the validation testing of the UNSAT-H computer code.

Three appendixes are included. Appendix A provides measurements of unsaturated conductivities of the FLTF soil for use in future simulations. Appendix B provides a verification test of a weather generation code that will be used to generate sequences of weather variables for long-term simulations of the protective barrier. Appendix C describes the derivation of the

generalized solution to infiltration from a surface point source that was compared with solutions generated with the PORFLO-3 code.

2.0 CODE SOLUTIONS TO THE BARRIER EDGE PROBLEM

One area of concern for hydrologic modeling of protective barriers is characterizing the flow of water from outside the barrier toward the waste zone beneath the barrier, the so-called barrier edge problem. Solutions to this problem can be used to optimize the size of the barrier and predict contaminant migration. Since the previous study (Fayer 1987) was conducted, a question arose concerning the grid design used in the two-dimensional simulations with the UNSAT2 code (Davis and Neuman 1983). In this section, another grid design is tested to see if the results differ. Also reported in this section are applications of the TOUGH code (Pruess 1987) and the PORFLO-3 code (Runchal and Sagar 1989) to the same barrier edge problem. TOUGH and PORFLO-3 differ from UNSAT2 in a number of ways, including numerical implementation and soil hydraulic property description. The objective of applying these codes to the barrier edge problem is to verify the original UNSAT2 solution and establish a measure of each code's ability to solve the problem.

2.1 PROBLEM DESCRIPTION

The problem used for testing throughout this section is Case 2 from Fayer (1987). Figure 2.1 shows how the problem (i.e., Case 2) was conceptualized for the simulations. The soil type is a loamy sand (sampled from the AP Tank Farm in the 200-East Area of the Hanford Site) known as AP-1 soil. The soil is considered homogeneous throughout the model domain. The stippled area marked "Waste" indicates where waste could be located and does not represent an actual obstacle that affects flow. Yearly variations in the recharge rate are assumed to be damped with depth. Thus, the values used for recharge are treated as fluxes along the upper boundary that remain constant through time. Initially, the model domain is in equilibrium with a recharge flux of 5 cm/yr. At time zero, the barrier is emplaced and the flux beneath it becomes zero. For the 2-m area adjacent to the barrier, the recharge flux is increased to 15 cm/yr to simulate runoff from the barrier.

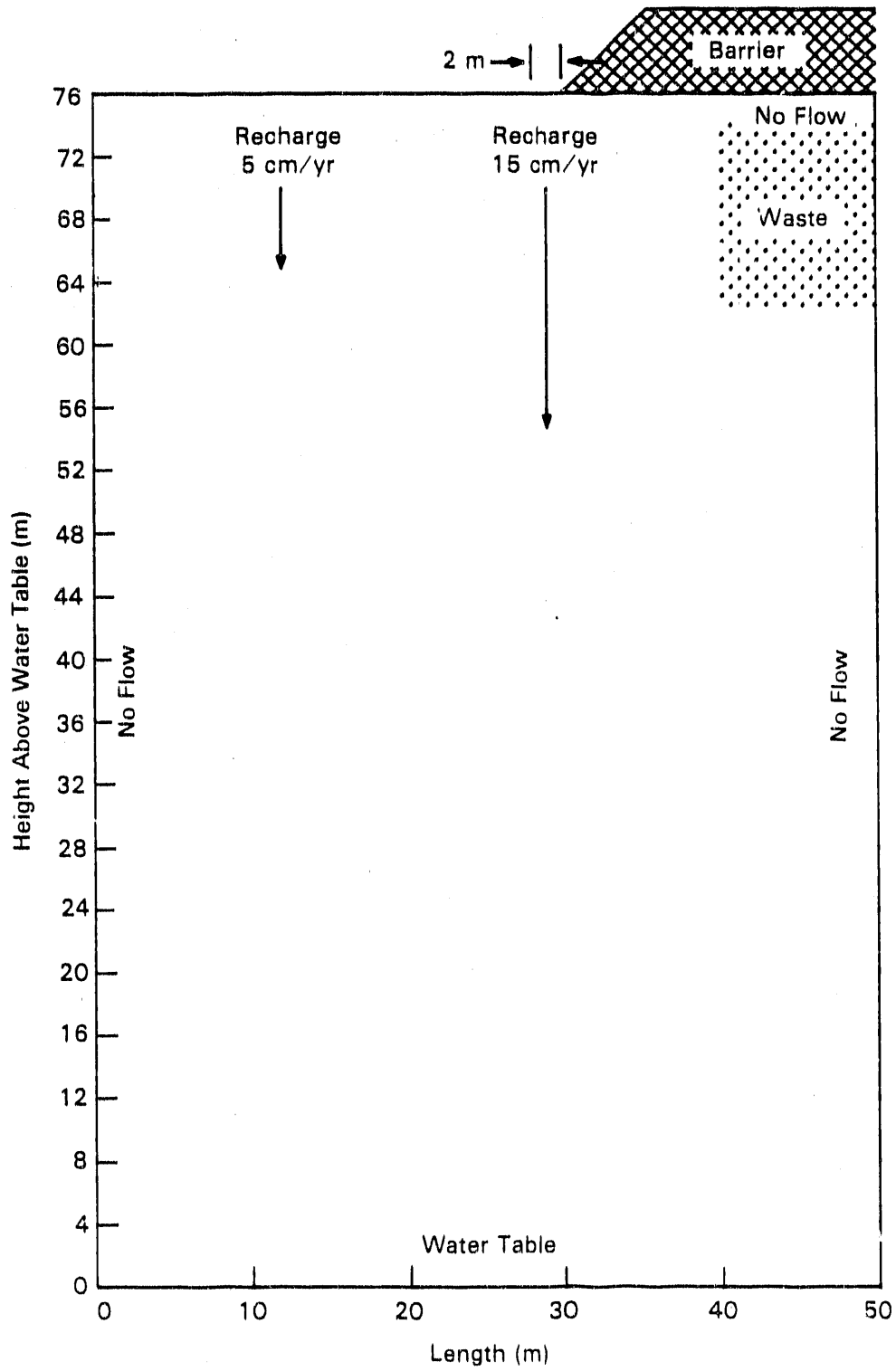


FIGURE 2.1. Barrier Conceptualization for Two-Dimensional Modeling

In addition to differences in numerical implementation, two areas that may affect the code comparison are grid design and the calculation of soil hydraulic properties. The grid used for each simulation is discussed in the separate code sections. For soil hydraulic properties, UNSAT2 uses tabular values and linearly interpolates between the values. The values used in the reported simulations are listed in Table 2.1. The soil hydraulic properties are described in the TOUGH (with modified subroutines PCAP and RELP) and PORFLO-3 codes using the Brooks and Corey functions (Campbell 1985):

$$\theta = (\theta_s - \theta_r)(h_e/h)^{1/b} + \theta_r \quad (2.1)$$

$$K = K_s(h_e/h)^{2+3/b} \quad (2.2)$$

where θ_s = saturated water content
 θ_r = residual water content
 h = matric potential
 h_e = matric potential at air entry
 K_s = saturated hydraulic conductivity and
 b = curve-fitting parameter.

Both the UNSAT2 values and the hydraulic functions are plotted in Figure 2.2. Visually, there appears to be no significant difference for water contents less than $0.3 \text{ m}^3/\text{m}^3$ (the simulation range), and thus the different hydraulic property descriptions should not significantly obscure the code comparisons.

2.2 UNSAT2 SOLUTION

Fayer et al. (1985; Fayer 1987) describe UNSAT2 and its previous use on the barrier edge problem. The grid used for those reports is shown in Figure 2.3a. The number of elements to which interior nodes are connected alternates between four and eight. This variation in element connections could contribute to the irregularity previously observed in the water content contours, such as contours that did not change smoothly or that indicated pockets of increased water content 1 to 2 m above the water table. These

TABLE 2.1. AP-1 Soil Properties Used by UNSAT2
(saturated conductivity is 8.472 m/d)

<u>Water Content (m³/m³)</u>	<u>Matric Potential (m)</u>	<u>Relative Conductivity</u>
0.0185	443.8	3.13 x 10 ⁻¹⁶
0.0200	22.04	4.18 x 10 ⁻¹³
0.0300	2.580	1.16 x 10 ⁻⁸
0.0400	1.320	2.84 x 10 ⁻⁷
0.0500	0.872	2.05 x 10 ⁻⁶
0.0600	0.647	8.52 x 10 ⁻⁶
0.0800	0.423	6.47 x 10 ⁻⁵
0.1200	0.246	8.59 x 10 ⁻⁴
0.1600	0.172	4.73 x 10 ⁻³
0.2000	0.131	1.74 x 10 ⁻²
0.2400	0.106	4.76 x 10 ⁻²
0.2800	0.088	1.16 x 10 ⁻¹
0.3200	0.076	2.33 x 10 ⁻¹
0.3600	0.066	4.57 x 10 ⁻¹
0.4050	0.040	8.86 x 10 ⁻¹
0.4140	0.020	9.71 x 10 ⁻¹
0.4170	0.000	1.00

observations can be seen in Figures 5.3, 5.5, 5.6, and 5.8 of Fayer (1987). A new grid, shown in Figure 2.3b, uses node-element connections in which all interior nodes are connected to six elements. This design should provide a better solution to the problem (i.e., smoother water content contours) with less computer time.

Two simulations were performed. The first simulation used the original grid and is nearly an exact repeat of Case 2 from Fayer (1987). This simulation was repeated to document the exact amount of computer time used, as well as the time step information, which was not done originally. Such information will prove useful for future code testing and benchmarking. The second simulation used the new grid design. Because of the design, the number of nodes

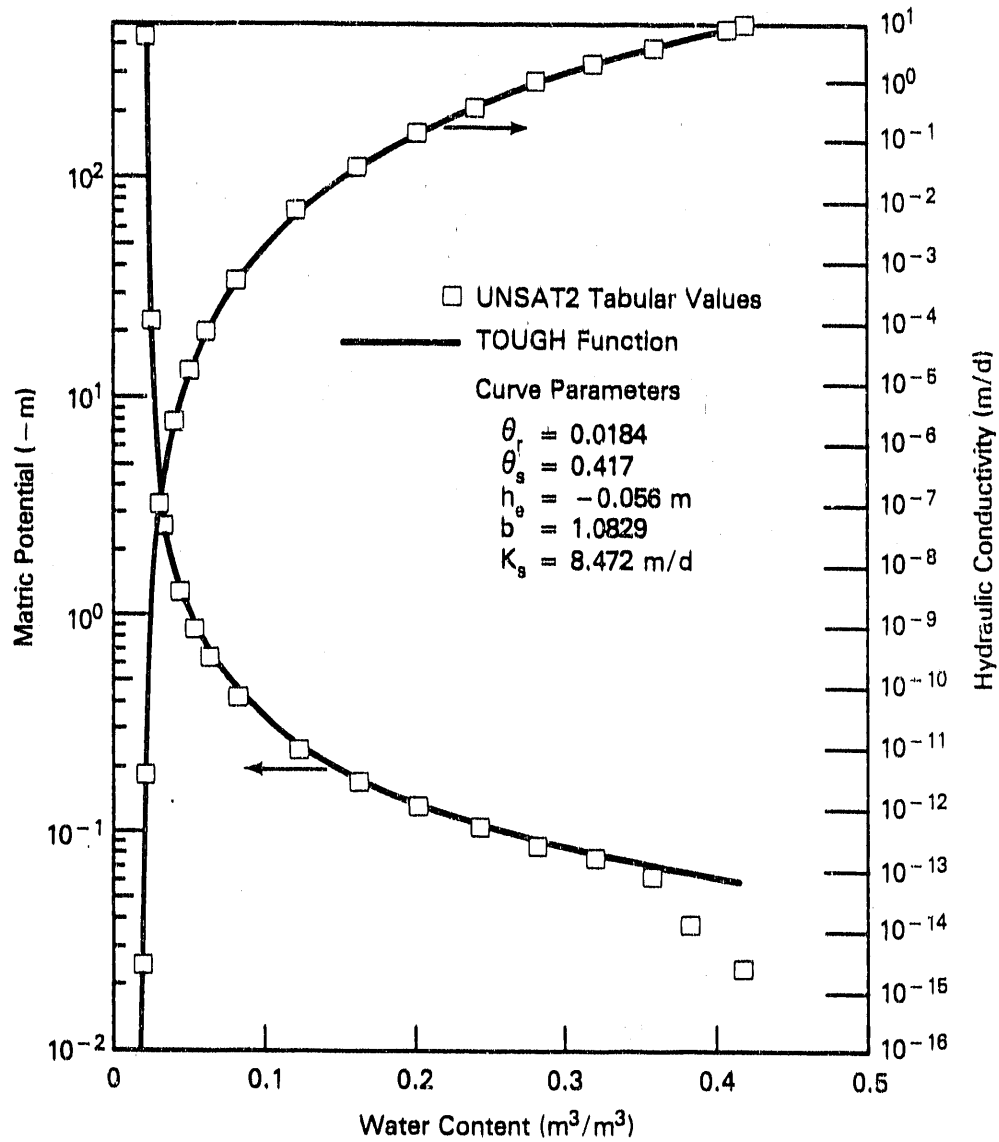
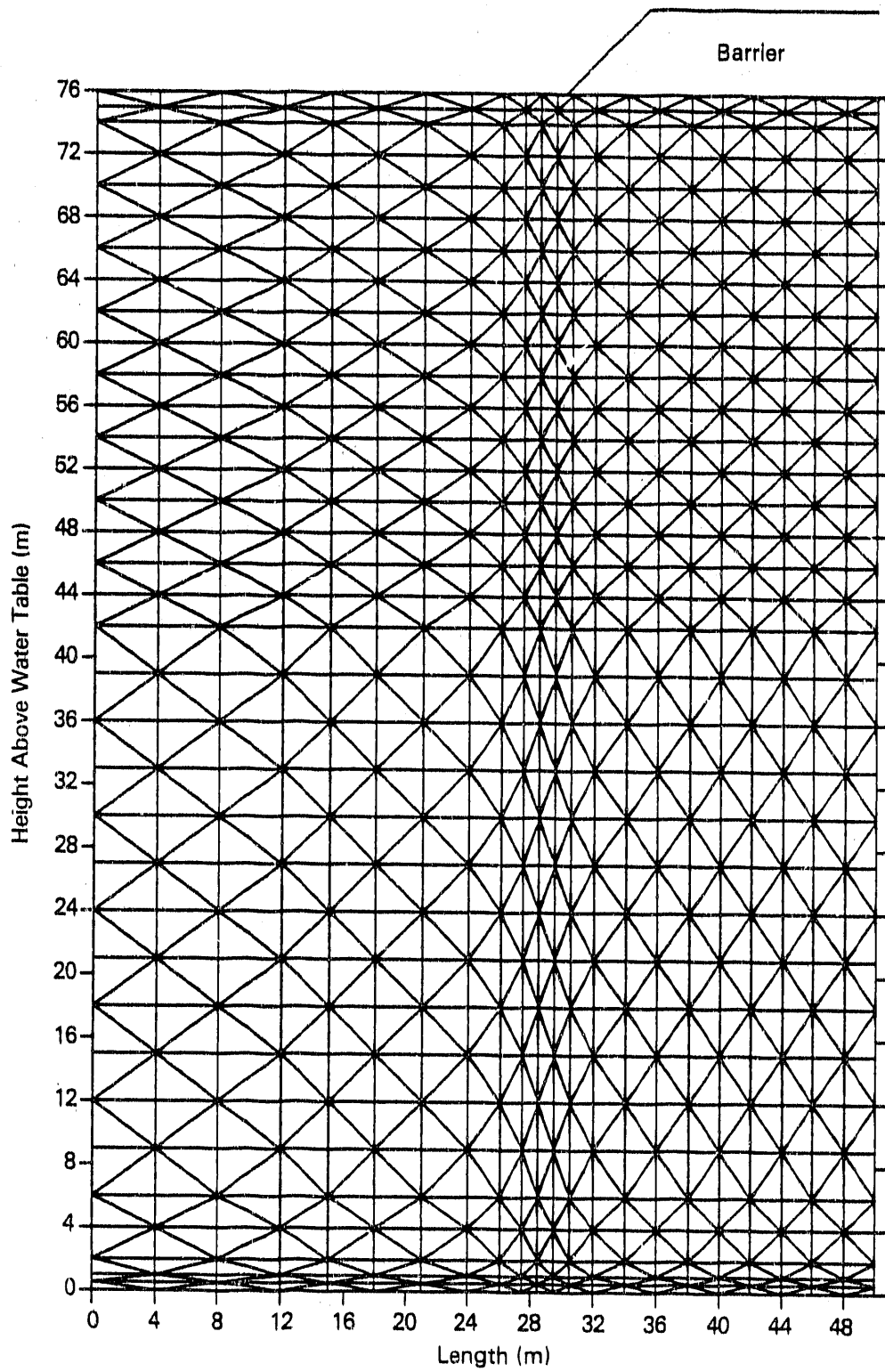


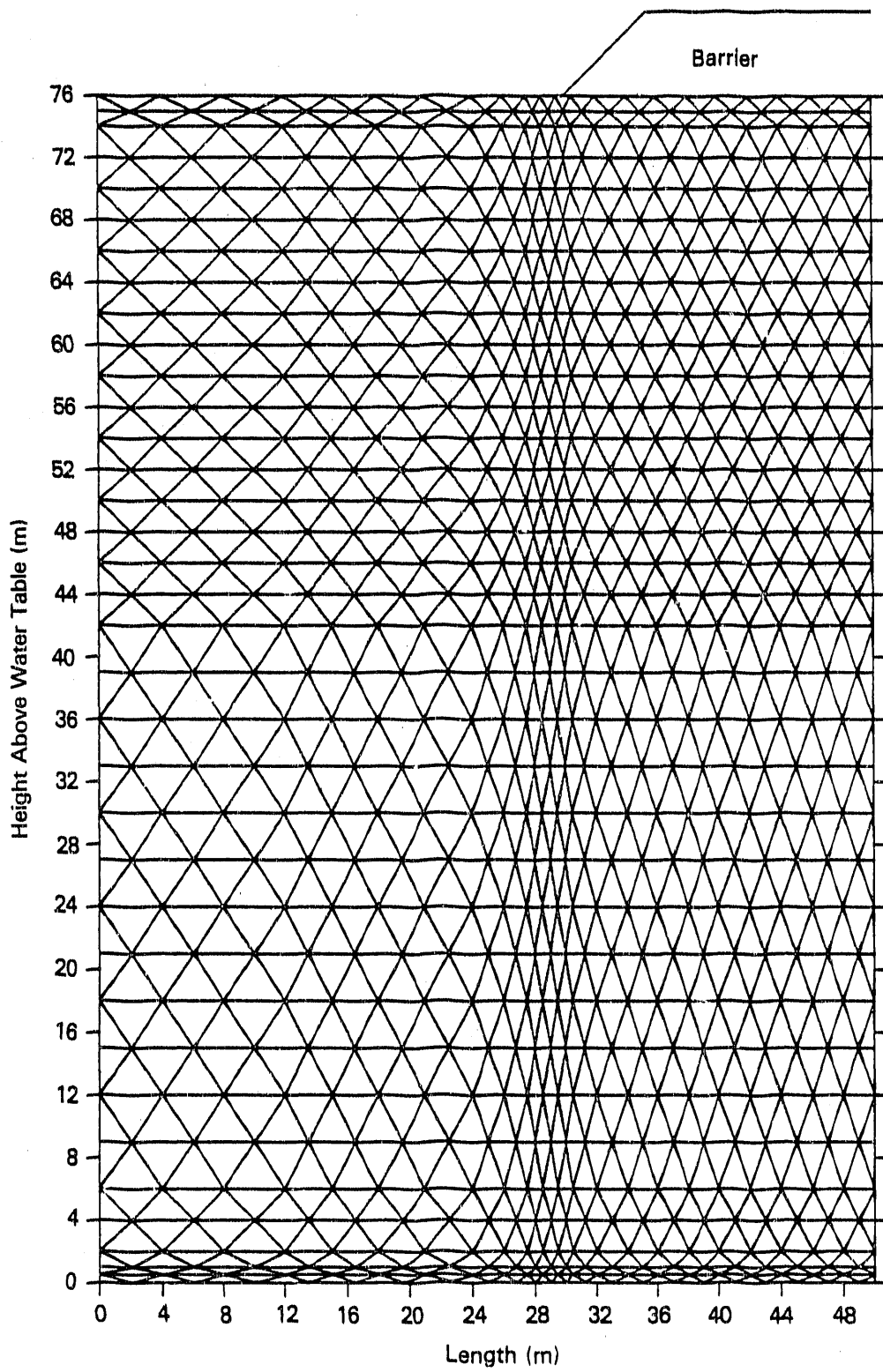
FIGURE 2.2. Comparison of Methods for Describing Soil Hydraulic Properties

and elements in the new grid is slightly larger than in the original grid (846 versus 828 nodes and 1575 versus 1540 elements, respectively). Otherwise, the only difference between both of these simulations and the original Case 2 is that these simulations used a backward-difference approximation of the time derivative rather than a central-difference approximation.



a) Original Grid

FIGURE 2.3. Finite-Element Grids for UNSAT2



b) New Grid

FIGURE 2.3. (contd)

The results of the two simulations, in the form of contour plots of total head and water content, are displayed in Figures 2.4 and 2.5, respectively. The results using the original grid are identical to the results of Case 2 in Fayer (1987), even in the vicinity of the water table. This result implies that changing the time integration scheme had no noticeable effect on the solution.

Comparing the total head contours of the UNSAT2 results reported here shows no noticeable differences between the two simulations. Comparing the water content contours indicates general agreement on the location of the contour levels but disagreement on the smoothness of the contours and on the

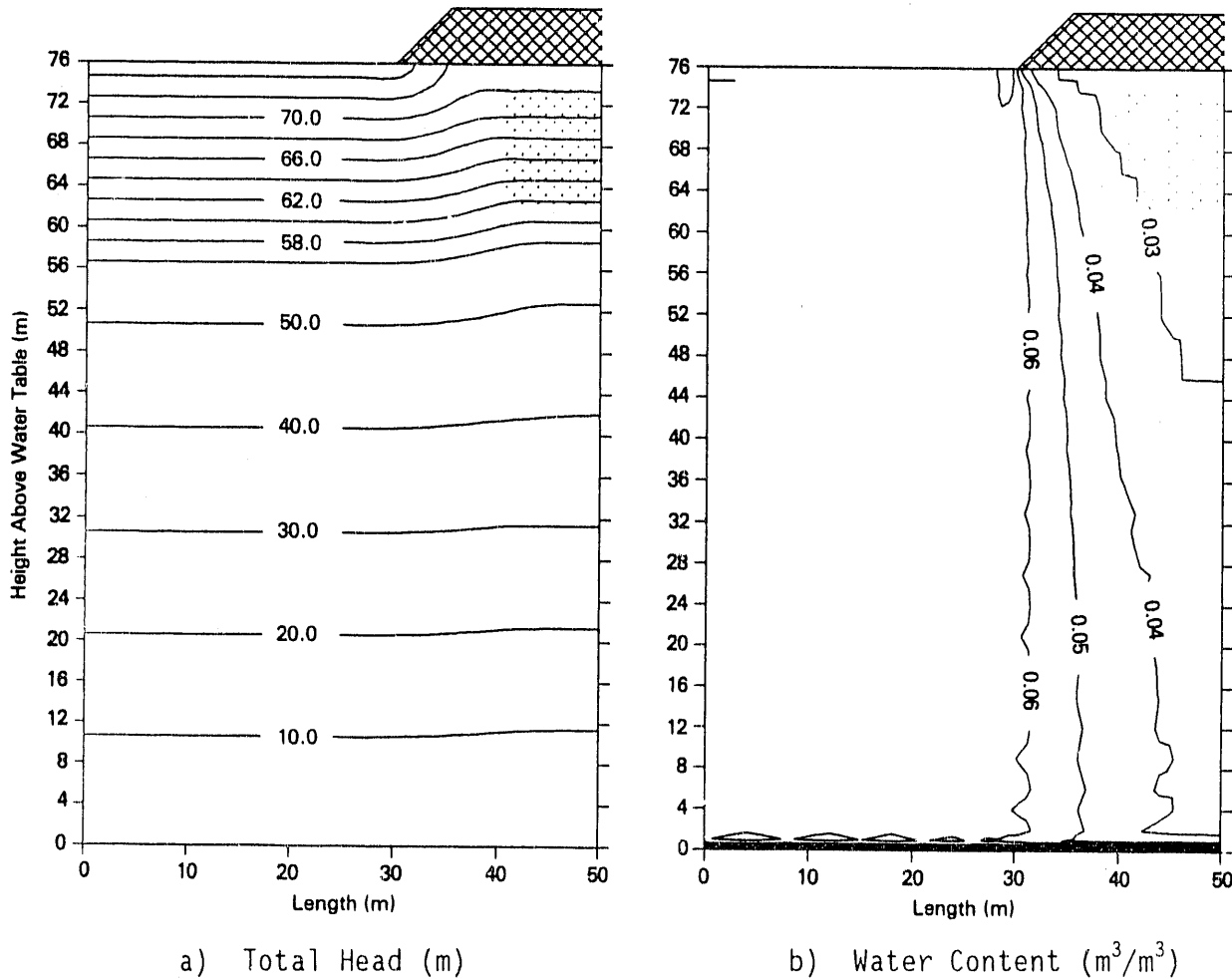


FIGURE 2.4. UNSAT2 Results, after 500 Years, Original Grid

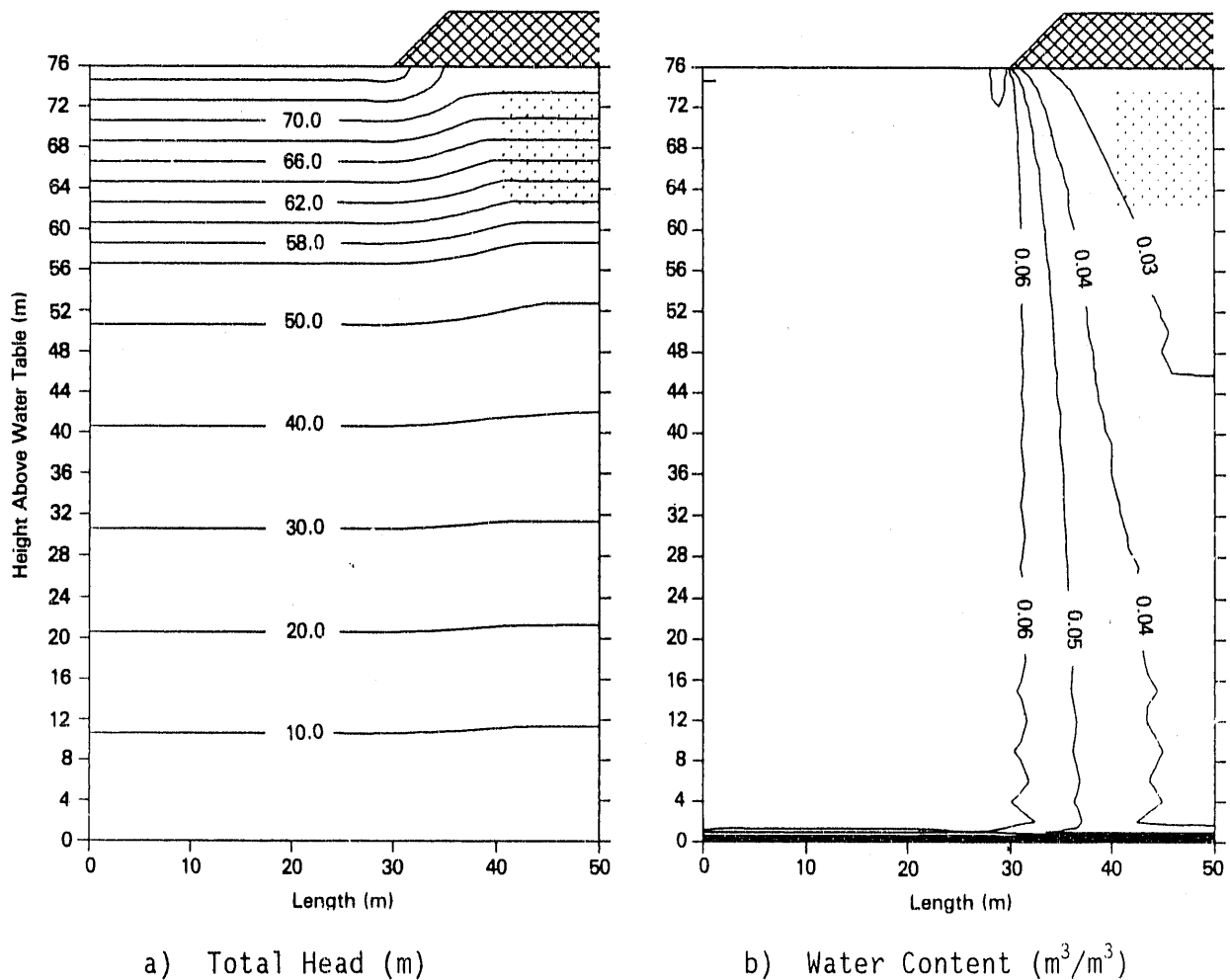


FIGURE 2.5. UNSAT2 Results, after 500 Years, New Grid

solution near the water table. With the new grid, water content contours above 20 m are much smoother, especially the 0.03 cm^3/cm^3 contour in the vicinity of the waste form. Below 20 m, the contours are slightly smoother, but still irregular. The irregularities are not a result of inappropriate contouring but represent the actual UNSAT2 solution. The second area of difference is near the water table, where the new grid design appears to have eliminated the presence of "islands" of higher water content.

Another type of comparison in the 1987 study was to look at fluxes moving past the bottom-left corner of the waste area (located at $x = 40$ m and $z = 62$ m in Figure 2.1 of this report). A gradient of 1.0 m/m was assumed to be

operating at this point, such that the water content could be used to calculate the conductivity value and thus the flux. The error in assuming a gradient of 1.0 m/m was estimated at 10%. To check that assumption, the matric potential profile for each simulation at 500 years has been plotted in Figure 2.6. For both simulations, the matric potential gradient at the bottom-left corner of the waste zone is approximately 0.28 m/m, directed to the right and 18° above horizontal. Together with the gravity gradient (1 m/m downward), the total gradient is 0.95 m/m directed downward, about 16° to the right of vertical. The assumption of a gradient of 1.0 m/m in both simulations was within 5% of actual and is therefore considered acceptable for the entire 500 years.

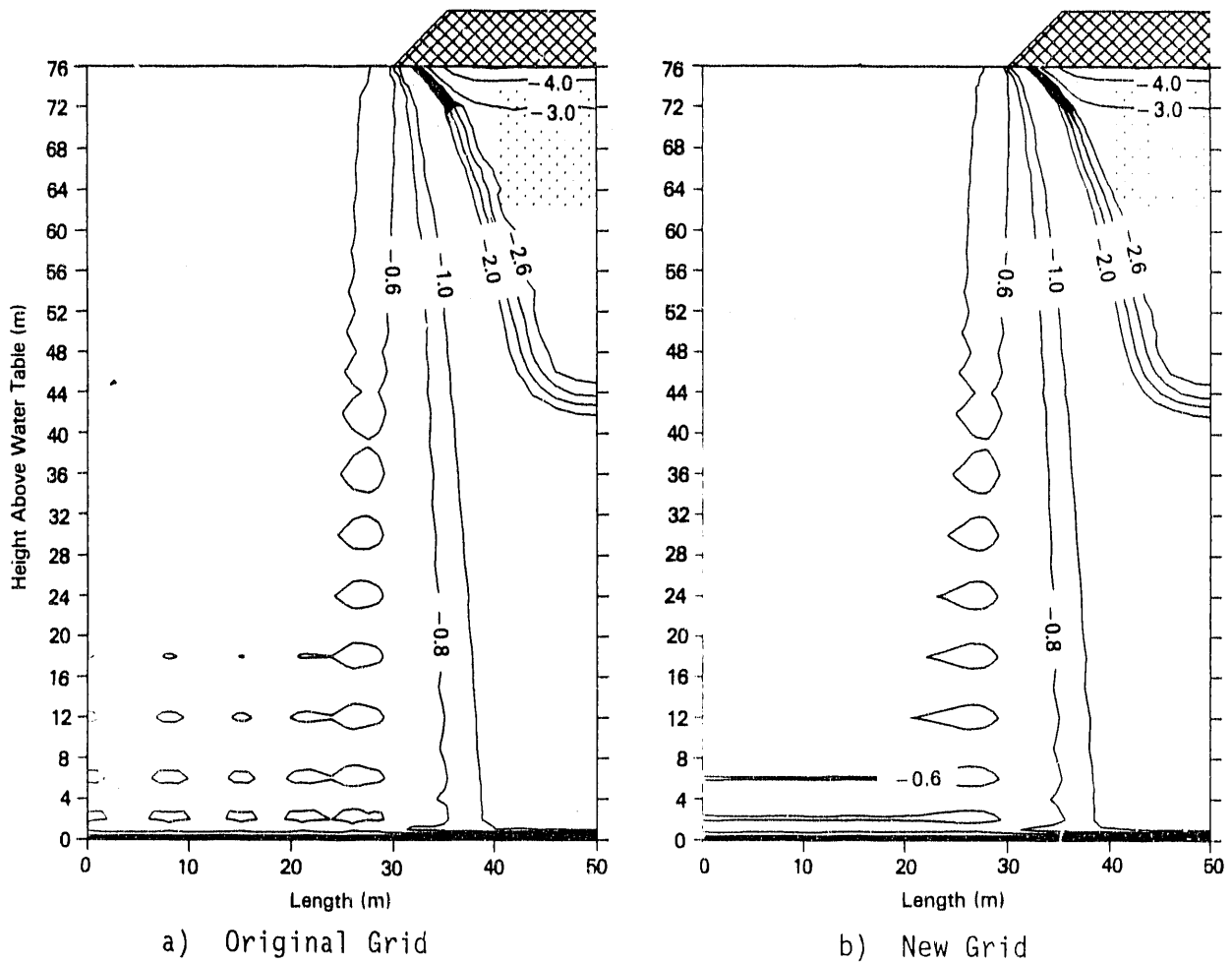


FIGURE 2.6. UNSAT2 Results after 500 Years, Matric Potential (m)

Figure 2.7 shows the flux past the waste for all solutions. Again, the results using the original grid are identical to those of the previous study (Fayer 1987). The results using the new grid are identical for the first 250 years, after which the new grid yields a flux that is higher. By 300 years, the difference appears to have stabilized with flux for the new grid 38% higher than that for the original grid.

Relatively minor changes in grid design are accompanied by noticeable differences in the simulation results, which calls into question the adequateness of the grid resolution. An additional test with an increased node density should be conducted to see if the solution changes. The expectation is that above some level of node density, the solution should not change, thereby

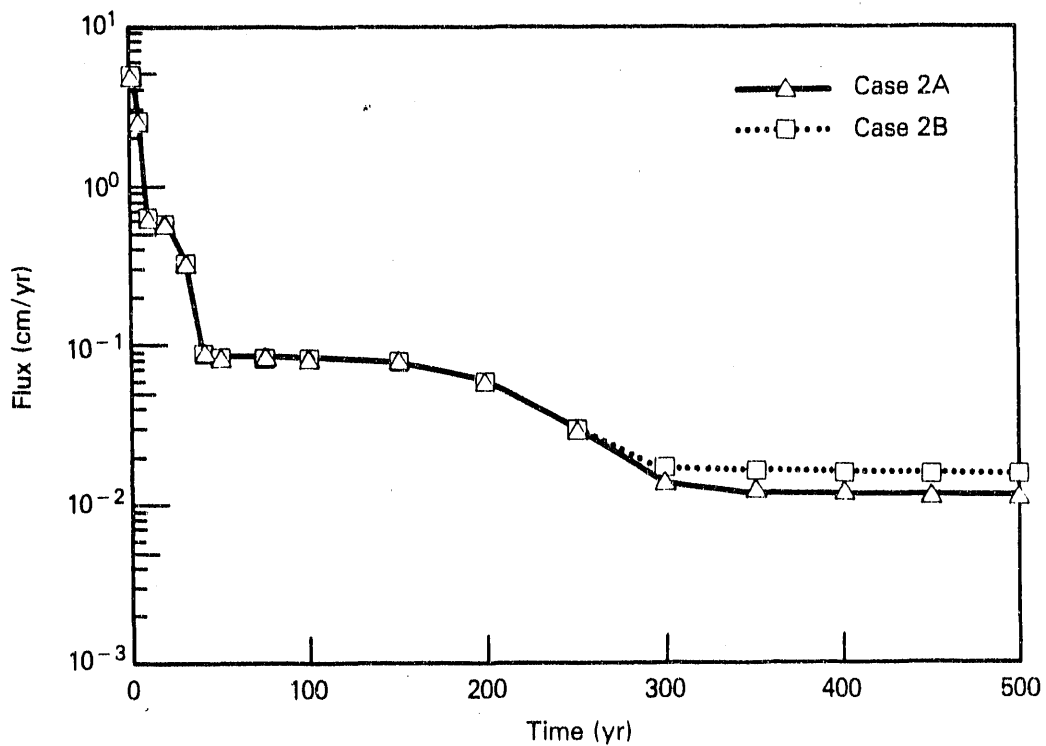


FIGURE 2.7. Estimated Flux Past the Bottom-Left Corner of the Waste Zone Versus Time, UNSAT2 Cases 2A and 2B

suggesting that a correct solution has been obtained. Conducting this test will require some modifications to the code to enable handling more nodes.

A summary of the simulation parameters is given in Table 2.2. Both simulations used the same number of time steps (2117), although there is no record of the number of iterations required for each. Using the new grid resulted in about 6% more time, but the increased time is partly the result of the increased number of nodes (about 2%). In all subsequent code comparisons, reference to the UNSAT2 solution will refer to the solution generated using the new grid.

2.3 TOUGH SOLUTION

The TOUGH code (Pruess 1987) is a multidimensional code that solves for the flow of water, vapor, air, and heat in porous and fractured media. TOUGH uses an integrated finite-difference method to discretize the flow equations in space and solves the system of equations using Newton-Raphson iteration. TOUGH is written in standard FORTRAN 77 and runs on the Hanford Cray XM-P^(a) computer.

Because TOUGH solves three simultaneous equations for the flow of 1) water, 2) gas, and 3) heat, care must be taken to ensure that no gas or heat flows, so that a direct comparison can be made with the other codes. The requirement for no heat flow was enforced by assigning a constant temperature of 20°C to all water initially in the system and a specific enthalpy of 8.38×10^4 J/kg (enthalpy of water at 20°C) to the recharge water. The requirement for no air flow was enforced by placing large constant-pressure boundary elements (containing nearly dry gravel) at the top of the model where recharge was occurring. These large elements maintained a constant air pressure in the system but did not prevent air from flowing into the system to replace the water draining out beneath the barrier.

(a) Cray XM-P is a product of Cray Research, Inc. Mendota Heights, Minnesota. Reference to this computer should not be regarded as an endorsement.

TABLE 2.2. UNSAT2 Simulation Summary

Run Number	Final Time (d)	Initial Time Step (d)	Maximum Time Step (d)	Number of Time Steps (d)	MicroVAX ^(a) CPU (h:min:s)		
					Grid		
					Original	New	
1	365.25	0.01	12	95	00:37:06	00:38:41	
2	730.5	10	15	26	00:10:56	00:11:22	
3	1826.25	15	25	46	00:19:41	00:20:29	
4	7305.0	25	30	184	01:18:43	01:22:45	
5	18262.5	25	100	118	00:58:10	00:59:41	
6 ^(b)	36525.0	80	100	184	01:28:46	01:34:43	
7 ^(b)	182625.0	100	100	<u>1464</u>	<u>11:48:29</u>	<u>12:32:48</u>	
				Total =	2117	16.7 h	17.7 h

(a) MicroVAX is a product of the Digital Equipment Corporation, Maynard, Massachusetts. Reference to this computer should not be regarded as an endorsement.

(b) Attempts to increase the maximum time step size above 100 days resulted in nonconvergence of the solution.

Figure 2.8 shows the TOUGH (and PORFLO-3) finite-difference grid. A total of 770 nodes were used (9% less than UNSAT2). An attempt was made to have higher node densities in the same area of the flow domain as in the UNSAT2 simulations. Internodal conductivities were calculated using an arithmetic mean (an option for using a geometric mean was not available in TOUGH).

The initial time step size was 1 s. If the number of iterations needed to solve for a given time step was less than four, the next step size would be double. If a solution was obtained with anywhere from four to nine iterations, the next step size would be the same. If the code did not converge to a solution after nine iterations, the current time step size was reduced by a factor of four and the solution attempt repeated. The default value for convergence was used.

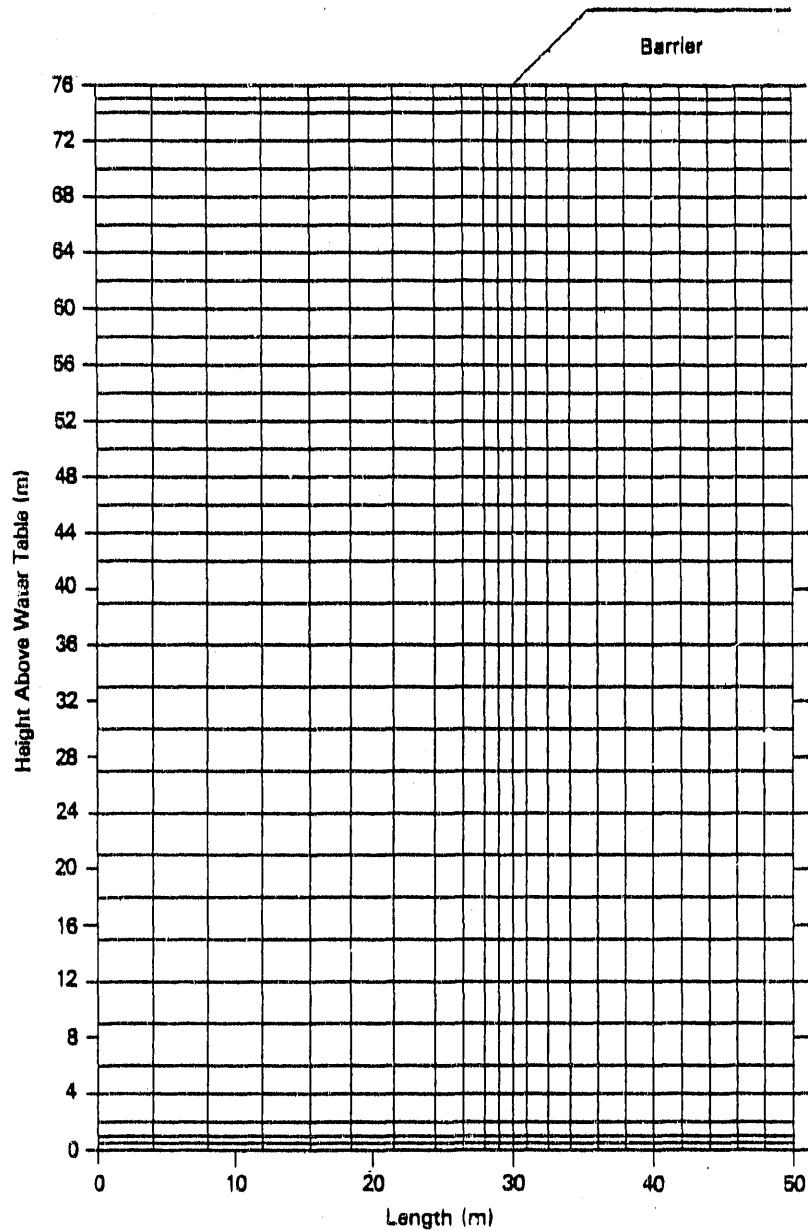


FIGURE 2.8. Finite-Difference Grid for TOUGH and PORFLO-3

The TOUGH results, converted to total head and water content profiles, are displayed in Figure 2.9. TOUGH used 36 time steps to solve this problem in 2.05 h on a Sun-4^(a) computer. A rough estimate of comparable Cray computer time is 0.12 h. The number of time steps used is significantly less than the 2117 steps used by UNSAT2.

(a) Sun-4 computer is a product of Sun Microsystem, Inc., Mountain View, California. Reference to this computer should not be regarded as an endorsement.

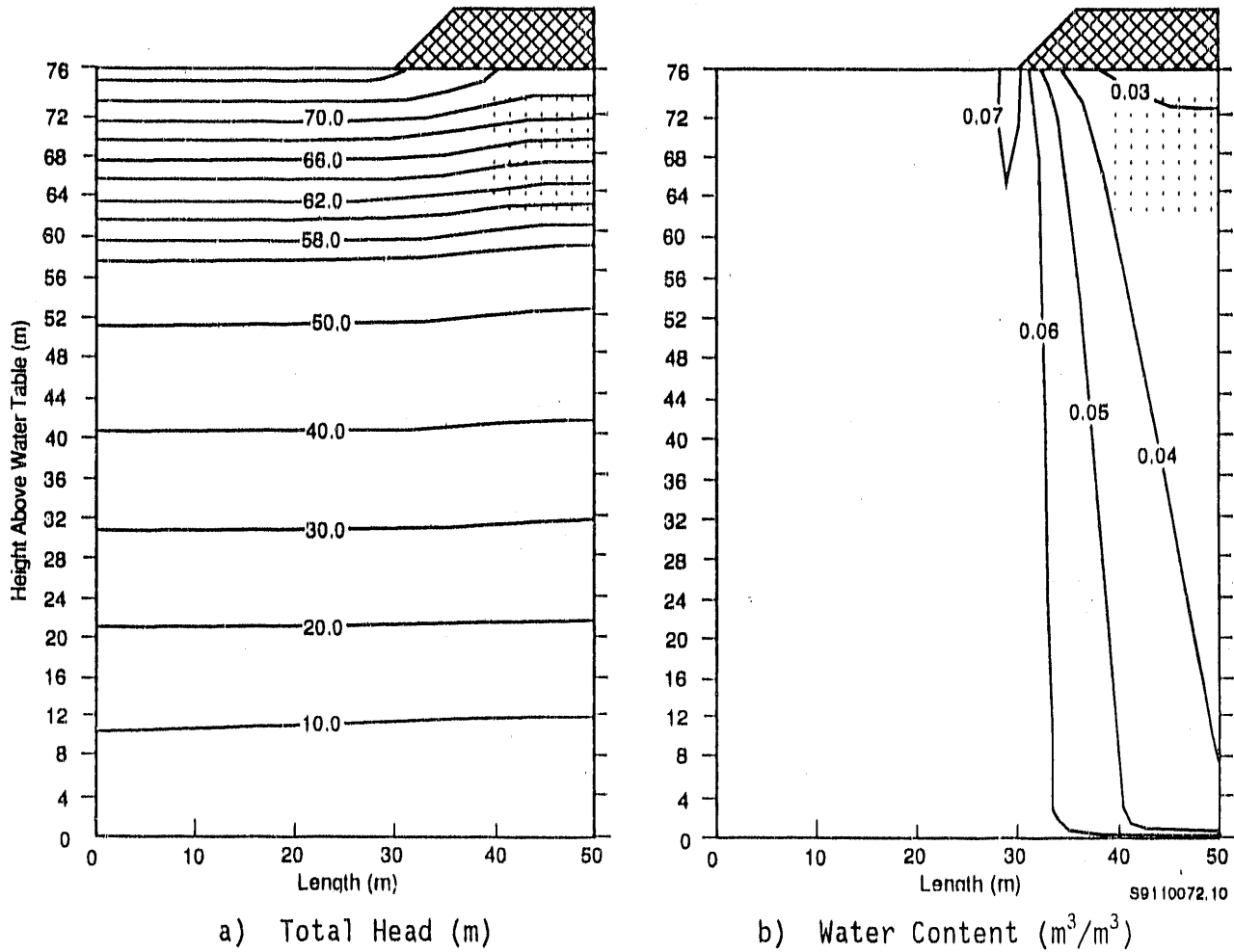


FIGURE 2.9. TOUGH Head and Water Content Results

2.4 PORFLO-3 SOLUTION

PORFLO-3 Version 1.1, an enhanced version of the original PORFLO-3 Version 1.0 code (Runchal and Sagar 1989), was chosen to analyze the barrier edge problem. The PORFLO-3 code is a multidimensional code that simulates fluid flow, heat transfer, and mass transport in variably saturated geologic media. PORFLO-3 uses the nodal point integration method to discretize the flow equations in space. The code user can choose from several options for solving the system of equations. PORFLO-3 is written in standard FORTRAN 77 and runs on the Hanford Cray computer.

The important new feature of PORFLO-3 Version 1.1 is automatic time step reduction. This feature allows the code to reduce the size of the time step (whenever the code encounters difficulty in solving for a particular time step) rather than terminating the simulation with an incomplete solution. The time step reduction feature is valuable for solving problems involving water infiltration into initially dry soils where steep hydraulic gradients can develop that necessitate the use of very small time steps for a correct solution.

The PORFLO-3 finite-difference grid is identical to the TOUGH grid in Figure 2.8 except that boundary nodes are located outside the domain displayed. A total of 770 nodes were used (the same as for TOUGH). Internodal conductivities were calculated using a geometric mean (an option for using an arithmetic mean did not appear to be functioning).

The initial time step size was 1 s. The time step size was doubled whenever the code converged to a solution using 30 iterations or less. Otherwise, the time step was reduced by half and the solution attempt repeated.

The PORFLO-3 results, converted to total head and water content profiles at 500 years, are displayed in Figure 2.10. PORFLO-3 used 3700 time steps to solve this problem in 0.65 h on the Hanford Cray computer. The number of time steps used is double the number used by UNSAT2 and 100 times the number used by TOUGH.

2.5 COMPARISON OF CODE SOLUTIONS

Solutions to the barrier edge problem have been obtained using the codes UNSAT2, TOUGH, and PORFLO-3. The results from these three codes are compared by contrasting the total head, water content, matric potential, and flux-past-the-waste solutions.

2.5.1 Total Head Solutions

Over the lower half of the domain, the total head contours of all three solutions are similar. On the upper left quarter of the domain, the PORFLO-3 and UNSAT2 results are similar; TOUGH predicted slightly lower total

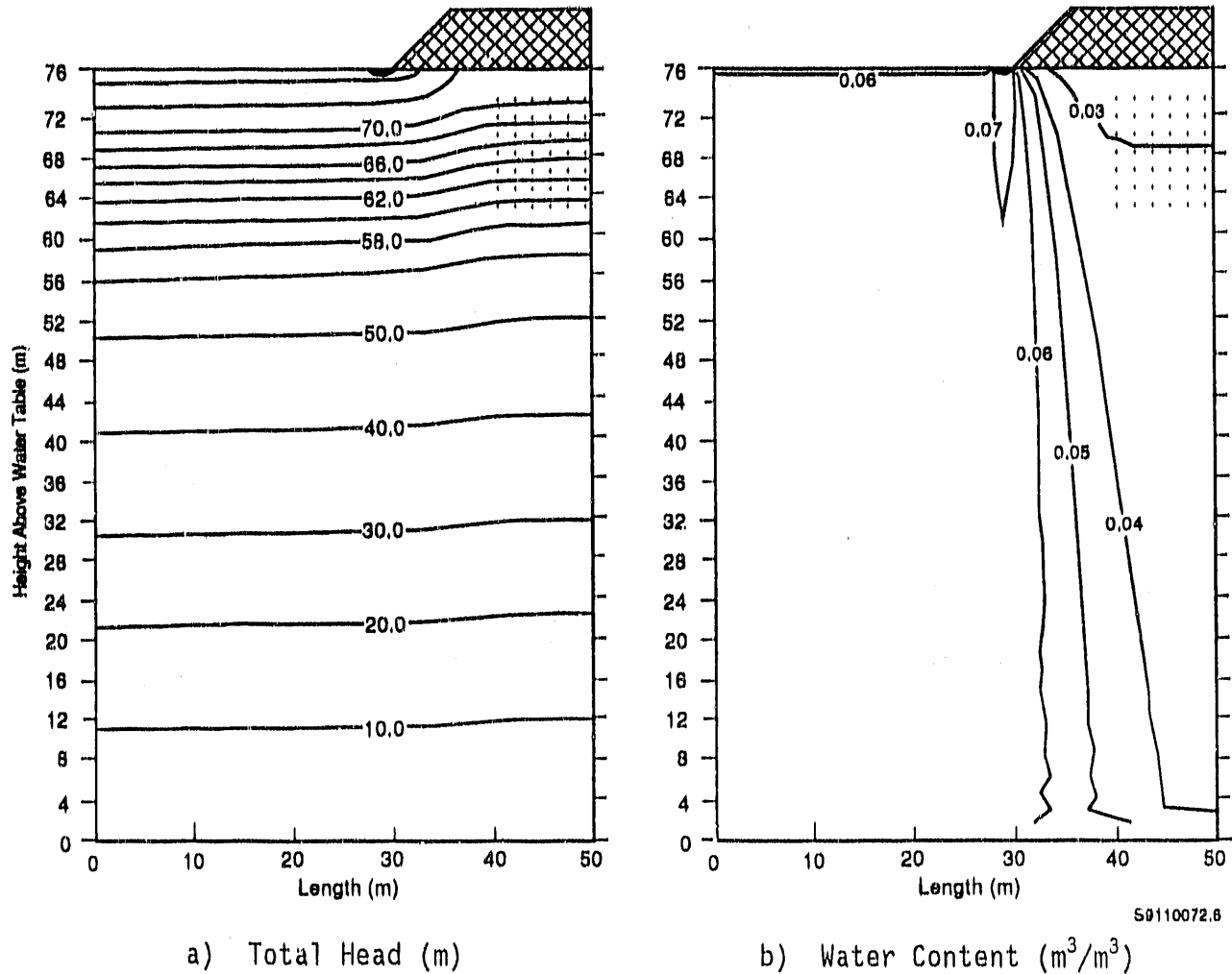


FIGURE 2.10. PORFLO-3 Results after 500 Years

heads at a given elevation. Such a result implies slightly drier conditions than the other codes. For the point located at $x = 0$ m and $z = 72$ m, the TOUGH solution indicates a total head value of roughly 70.5 m, which translates to a matric potential value of 1.5 m. This area of the domain should be operating at or near a gradient of 1.0 m/m, which would correspond to a matric potential value of approximately 0.56 m.

In the upper right half of the domain, the change in total head predicted with TOUGH is more gradual than that predicted with the other codes as the

contours are followed from left to right. The total head contours predicted by TOUGH have a distinct horizontal component after 500 years, a result not seen in the other solutions.

2.5.2 Water Content Solutions

The most striking aspect of the results is the smoothness of the water content contours predicted with TOUGH and PORFLO-3 versus those predicted with UNSAT2. None of the unevenness seen in the UNSAT2 solution is present. Another notable result is that the location of the water content contours, most notably the location of the $0.03\text{-m}^3/\text{m}^3$ contour, is different. TOUGH predicted that the $0.03\text{-m}^3/\text{m}^3$ contour would be near the top of the waste form, whereas UNSAT2 predicted it would be 16 m below the waste form. PORFLO-3 predicted that the $0.03\text{-m}^3/\text{m}^3$ contour would pass through the middle of the waste form.

The 0.04- and $0.05\text{-m}^3/\text{m}^3$ contours are similar for UNSAT2 and PORFLO-3; TOUGH shows them being slightly to the right. The $0.06\text{-m}^3/\text{m}^3$ contour is similar for all three codes. The $0.07\text{-m}^3/\text{m}^3$ contour, indicating the zone beneath the 15-cm/yr recharge area, extends downward 4 m using UNSAT2, 12 m using TOUGH, and 16 m using PORFLO-3.

2.5.3 Matric Potential Solutions

Figure 2.11 is a plot of matric potential contours for TOUGH and PORFLO-3. The matric potential plot for UNSAT2 was shown in Figure 2.6. Just as for the water content contours, UNSAT2 predicted matric potential contours with large irregularities. All three code solutions show the same general trend, which is that matric potential decreases going from the center to the upper right of the domain (i.e., toward the waste). This result is in accord with the water content results. For the location $x = 0$ m and $z = 72$ m, TOUGH-predicted contours do not indicate the presence of the low matric potential (-1.5 m) that was discussed in Section 2.5.1.

2.5.4 Flux-Past-the-Waste Solutions

As reported in Section 2.2, for UNSAT2, flux moving past the bottom-left corner of the waste area (located at $x = 40$ m and $z = 62$ m in Figure 2.1) was calculated using the water content at that point and assuming a gradient of

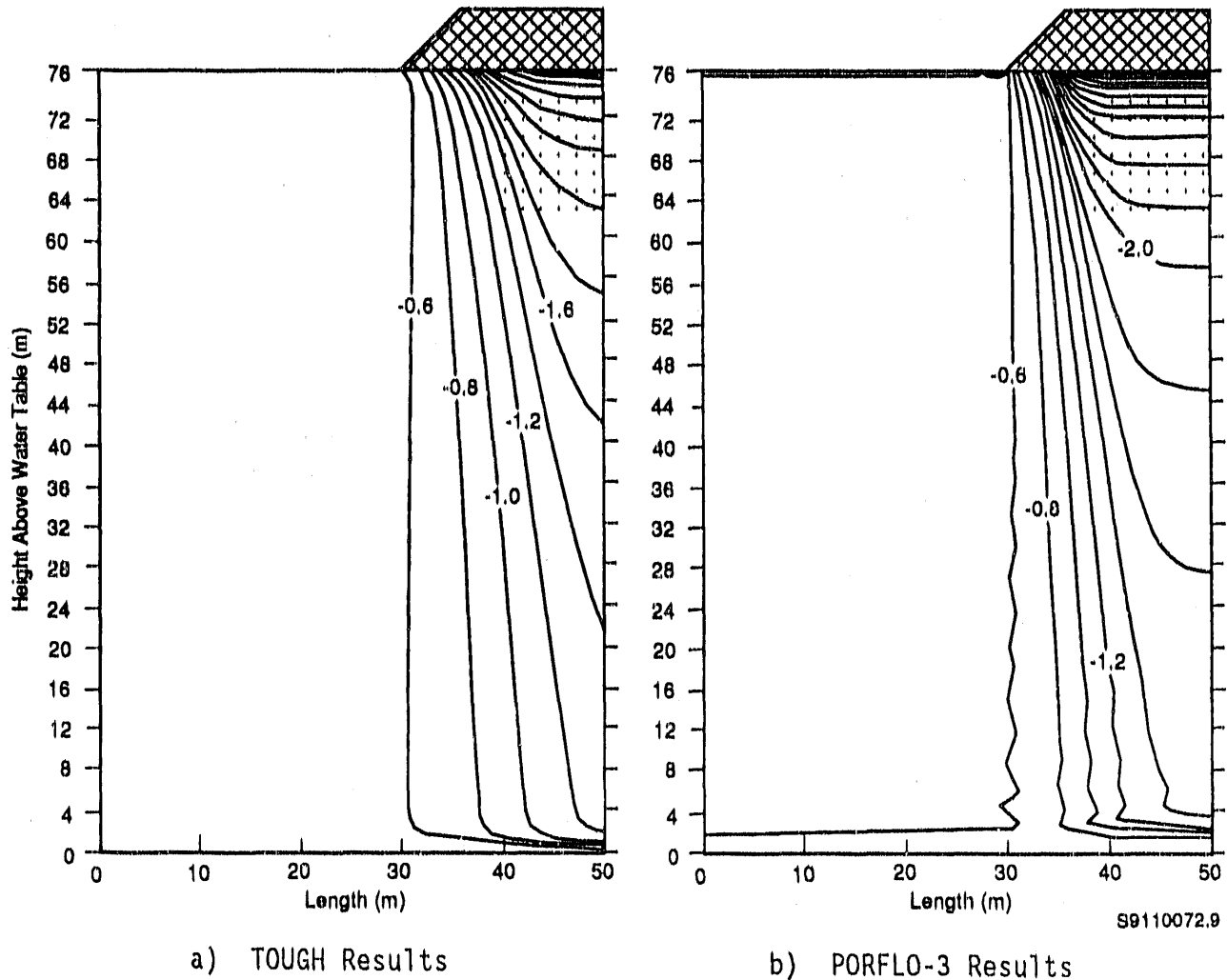


FIGURE 2.11. Simulation Results after 500 Years, Matric Potential (m)

1.0 m/m. The PORFLO-3 and TOUGH codes, however, provide fluxes. For both TOUGH and PORFLO-3, the fluxes were averaged to yield the flux moving past the lower-left corner of the waste zone. These values are shown in Figure 2.12.

For both the TOUGH and PORFLO-3 solutions, the relationship between flux and time varies smoothly. In contrast, the UNSAT2 solution is uneven and reflects the use of a table of hydraulic property values that are linearly interpolated. Such interpolation does not provide values that exactly match those provided by the functional representation used in the other codes. This problem is exacerbated by the fact that the area around the waste is dry and

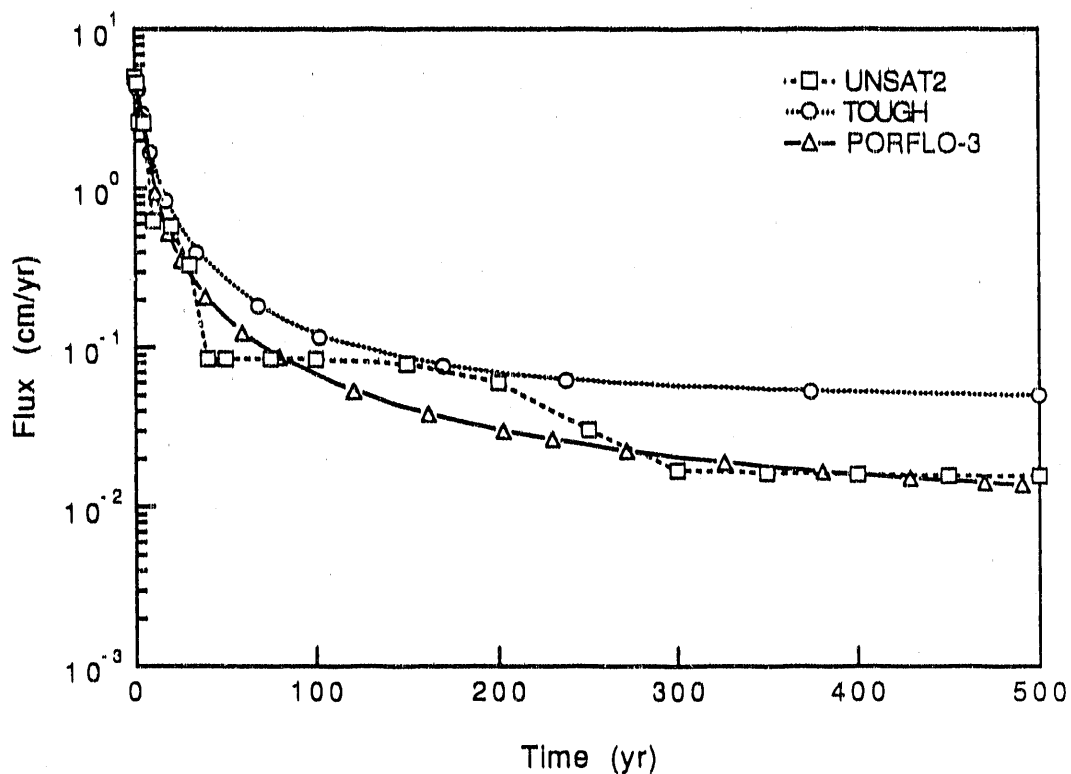


FIGURE 2.12. Estimated Flux Past the Bottom-Left Corner of the Waste Zone Versus Time, UNSAT2, TOUGH, and PORFLO-3 Solutions

changes in hydraulic properties are increasingly non-linear. This result indicates that the comparison between the UNSAT2 solution and the other solutions is not direct. Such a restriction also holds for the comparison of total heads, water contents, and matric potentials. Despite this restriction, treating the tabular values as representing a slightly different sediment indicates one possible variation to be expected.

The fluxes predicted by TOUGH and PORFLO-3 are similar in the early years, but begin to diverge after 100 years, with PORFLO-3 indicating increasingly lower fluxes. By 500 years, the flux predicted with PORFLO-3 is about 28% of that predicted with TOUGH. This result is in accord with the lower water contents predicted by PORFLO-3 near the waste. One reason for the difference may be the use of different methods for calculating internodal conductivities. For the TOUGH simulation, internodal conductivities were

calculated using an arithmetic mean; for PORFLO-3, a geometric mean was used. In the future, one of the codes should be modified to give the code user the option of calculating internodal conductivities using either the arithmetic or the geometric mean so that a more direct comparison could be made.

At 500 years, the flux predicted with UNSAT2 most nearly matches the PORFLO-3 prediction. The variations between UNSAT2 predictions and those of the other codes might be accounted for by the difference in hydraulic property description. One way to eliminate this question is to modify UNSAT2 to accept the Brooks-Corey function describing hydraulic properties and re-solve the problem.

An analytic solution to the barrier edge problem does not exist. Therefore, the determination of a reasonable solution depends on obtaining similar solutions with different computer codes. The three codes that were used have provided similar water-content solutions but significantly different flux solutions (0.05, 0.016, and 0.014 cm/yr for the TOUGH, UNSAT2, and PORFLO-3 codes, respectively). The results of the water content and flux comparisons are not surprising given the non-linear relationship between water content and conductivity. The predicted flux values are all at or below the current protective barrier standard of 0.05 cm/yr. For simulations beyond 500 years, further testing with a 0.05-cm/yr flux beneath the barrier would demonstrate whether the differences among the codes are significant.

For times less than 500 years and for situations in which the flux through the barrier is desired to be less than 0.05 cm/yr, the flux solution should be more precise because it controls convective contaminant transport. Because it does not provide a flux solution, the UNSAT2 code will not be included in future analyses. For the PORFLO-3 and TOUGH codes, differences in the flux solution may be reducible by addressing concerns such as the method of interpolating properties between nodes and the time density. In addition to addressing these concerns, a further prudent move might be to bring another code, such as TRACR3D (Travis 1984), to bear on the problem. One of the goals of future two-dimensional modeling should be to determine the most reasonable

solution to this particular barrier problem. Once a common flux solution is known, these and other codes can be more effectively evaluated so that future code applications will be more credible.

3.0 VERIFICATION OF AXISYMMETRIC INFILTRATION SOLUTION USING PORFLO-3

The test plan for hydrologic modeling of protective barriers (Fayer 1990) discusses the need to simulate the effect of infiltration into animal burrows and root channels on drainage through the barrier. PORFLO-3 Version 1.1 (described in Section 2.4) was chosen for this purpose. Before addressing infiltration into burrows and channels, the code was tested to demonstrate that, in the axisymmetric mode, it can predict infiltration into dry soil. This section describes a verification test of Version 1.1 of the PORFLO-3 code that supplements the earlier testing of PORFLO-3 Version 1.0 (Magnusen, Baca, and Sondrup 1990).

3.1 GENERALIZED SOLUTION USED TO VERIFY PORFLO-3

Healy and Warrick (1988) developed a generalized solution to infiltration from a surface point source that allows for estimation of the time-varying extent of the wetting front and wetted volume that develop. The method is based on numerical finite-difference solutions of a dimensionless form of Richard's equation for axially symmetric flow using an extension to the VS2D computer code (Lappala, Healy, and Weeks 1987; Healy 1987). The numerical solutions for a variety of soils and source strengths are summarized in the form of empirical equations, the coefficients of which are part of the generalized solution method.

Though less accurate than actual numerical solutions, the general solutions provide rapid qualitative verification. Hence, they will not be considered as "exact" solutions, but will be used as reference standards for comparison. The generalized solution method allows more realistic problems to be solved, relative to most analytical solution methods, because actual soil hydraulic properties can be used. Thus, some limitations of analytical techniques such as steady flow (Wooding 1968) or constant diffusivity (Warrick 1974) are eliminated.

The program called Generalized Solution to Infiltration from a Surface Point Source (GSIPS) was written to incorporate the generalized solution equations, coefficients, and scaling factors developed by Healy and Warrick (1988)

into a table look-up and interpolation algorithm. This program was used to generate solutions to the PORFLO-3 verification problems. Details of the theory underlying Healy and Warrick's (1988) generalized solution are contained in Appendix C. The input and output files used for verification test of PORFLO-3, as well as a listing of the GSIPS program, are also contained in Appendix C.

3.1.1 Problem Description

The PORFLO-3 code was configured to simulate an axially-symmetric quarter-cylinder, with dimensions of 20 cm in the radial direction and 30 cm in the vertical direction. Two soils, a sand and a silt loam, were used in the verification testing. For the sand simulations, two additional variables were included: spatial discretization and internodal conductance. The combination of these variables that produced the best match to the GSIPS solution was used for the silt loam simulation.

For the sand simulations, two different grids were used to test code consistency and the effects of spatial discretization on the simulation results. Uniform node spacings of 0.5 and 1.0 cm were used in both the radial and vertical directions for a total of 600 and 2400 nodes in the active computational domains for the coarse and fine grids, respectively. The computational time increases as the number of nodes is increased. Therefore, no simulations were conducted with the finer grid used by Healy and Warrick (1988) and described in Appendix C. Their grid had 4224 nodes that were variably, rather than uniformly, spaced.

The sides and bottom of the domain were specified as no-flow boundaries. A uniform flux of $100 \text{ cm}^3/\text{h}$ was applied for 0.15 h to an area 2 cm in radius in the upper left corner of the model domain. The remainder of the top boundary was specified as a no-flow boundary. An aspect of the VS2D solutions (Healy and Warrick 1988) that cannot be duplicated using PORFLO-3 is the changing area of infiltration. The VS2D code allows the surface flux to be spread over the minimum area needed to achieve complete infiltration. Thus, during the initial phase, infiltration can occur over a smaller area than is needed later. With PORFLO-3, the needed area was specified a priori and not adjusted during the course of the simulation.

The hydraulic properties used for the verification problems are shown in Figure 3.1. The properties for the sand are from Rockhold, Fayer, and Gee (1988). The properties for the silt loam were provided by PNL staff and represent field-measured sorption (i.e., the wetting curve). The curves in Figure 3.1 correspond to the van Genuchten (1978) water retention function and the Mualem conductivity model using the parameters listed in Table 3.1. A uniform effective saturation of 0.01 was specified as an initial condition. This condition yielded initial matric potential values of -59.3 and -2.38×10^5 cm for the sand and silt loam, respectively. For the silt loam, this value of matric potential is an order of magnitude lower than values measured at depth in the field by PNL staff.

For the sand simulations, the two options used for calculating inter-nodal conductances were geometric mean and upstream weighting. The geometric mean was selected because it yielded the closest match between analytical solutions of one-dimensional infiltration and solutions using Version 1.0 of

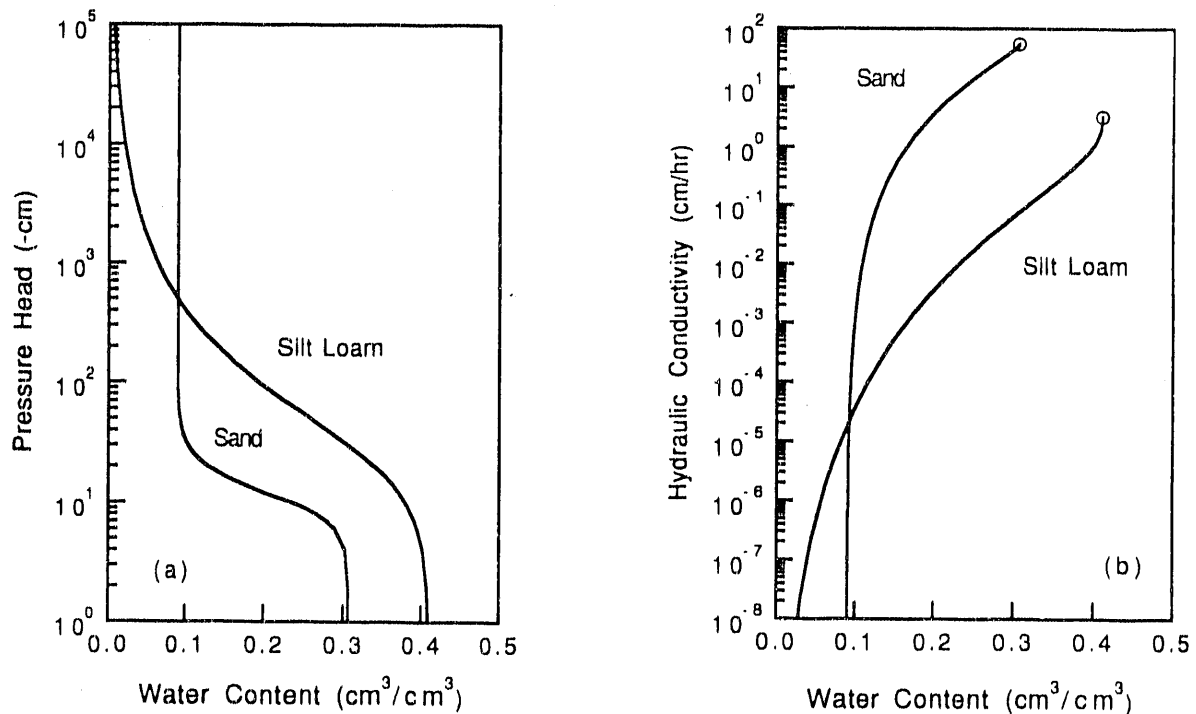


FIGURE 3.1. Soil Hydraulic Properties for Verification Test of PORFLO-3

TABLE 3.1. Parameters for Describing Soil Hydraulic Properties Using the van Genuchten Retention Function and Mualem Conductivity Model

<u>Soil Type</u>	<u>θ_s</u>	<u>θ_r</u>	<u>α</u> <u>(1/cm)</u>	<u>n</u>	<u>K_s</u> <u>(cm/h)</u>
Sand	0.307	0.09	0.093	3.693	55.44
Silt Loam	0.411	0.0	0.042	1.5	3.24

the PORFLO-3 code (Magnusen, Baca, and Sondrup 1990). The upstream weighting option was used because Brutsaert (1971) showed that, in the case of sharp wetting fronts advancing into an initially dry medium, it is often necessary to use the relative hydraulic conductivity for the cell from which water is flowing to obtain reasonable results and minimize numerical oscillations. The method used in the GSIPS formulation is suspected to be either upstream weighting or arithmetic mean.

For the simulations with the coarse grid, an initial time step of 10^{-5} h was used. Simulations with the fine grid required the initial time step to be 10^{-6} h, the same value used by Healy and Warrick (1988). Following the successful solution of a time step, the next step size was increased by the factor 1.03, with a maximum time step of 10^{-4} h compared with the value of 0.1 used by Healy and Warrick (1988). For all simulations, if convergence was not attained for a given time step, the time step was automatically reduced by half.

In the PORFLO-3 code, successful convergence to the solution of a given time step is judged by the criterion:

$$R = \max (1 - h_{r,z}^{n+1} / h_{r,z}^n) \leq c \quad (3.1)$$

where R = maximum residual of all internal nodes
h = matric potential
n = index of time steps, e.g., h^n is the matric potential after n time steps

r, z = indexes denoting node numbers in the radial and vertical directions, respectively

c = user-specified convergence criterion (dimensionless).

For all simulations, the value of c was specified as 10^{-3} . This value, which is the default value provided in PORFLO-3, means that a time step solution is accepted only when the change in matric potential during an iteration is less than 1/1000 of the matric potential value, evaluated for every node.

The 0.125 contour of effective saturation (i.e., the designated wetting front) was used to compare the PORFLO-3 results and GSIPS solutions. A perfect match was not expected given the differences in such areas as discretization, internodal conductance, and surface boundary description. The degree of variability seen in the sand results will be used to judge the comparison of the wetting front solutions for infiltration into silt loam.

In addition to qualitative comparisons between the PORFLO-3 and GSIPS solutions, mass balance errors were also determined for the PORFLO-3 solutions. The mass balance error (in percent) was calculated as $100(1-MBR)$, where MBR (the mass balance ratio) was calculated as

$$MBR = \left[\sum_{r,z=2}^{r_{m-1}, z_{m-1}} (\theta_{r,z} V_{r,z}) \Big|_{t^{n+1}} - \sum_{r,z=2}^{r_{m-1}, z_{m-1}} (\theta_{r,z} V_{r,z}) \Big|_{t^0} \right] / (Q t^{n+1}) \quad (3.2)$$

where θ = volumetric water content (dimensionless)

V = volume of computational cell (L^3)

t = time (T)

Q = net flux rate (L^3T^{-1})

m = subscript indicating maximum value of associated parameter,
e.g., r_m is the maximum value of r .

This ratio is simply the change in storage divided by the net influx that was specified over a given time interval, excluding boundary nodes. Because of no-flow side and bottom boundaries, only the upper boundary flux is considered. If the $MBR = 1.0$, perfect mass balance has been maintained and the

mass balance error is 0%. Values of MBR > 1.0 and < 1.0 indicate positive and negative mass balance errors, respectively.

For the purpose of conducting sensitivity tests of infiltration into animal burrows and root channels, a mass balance error of 5% or less is considered acceptable. For actual calculations of drainage through the barrier, a more stringent criterion (e.g., 1% or less) should be considered.

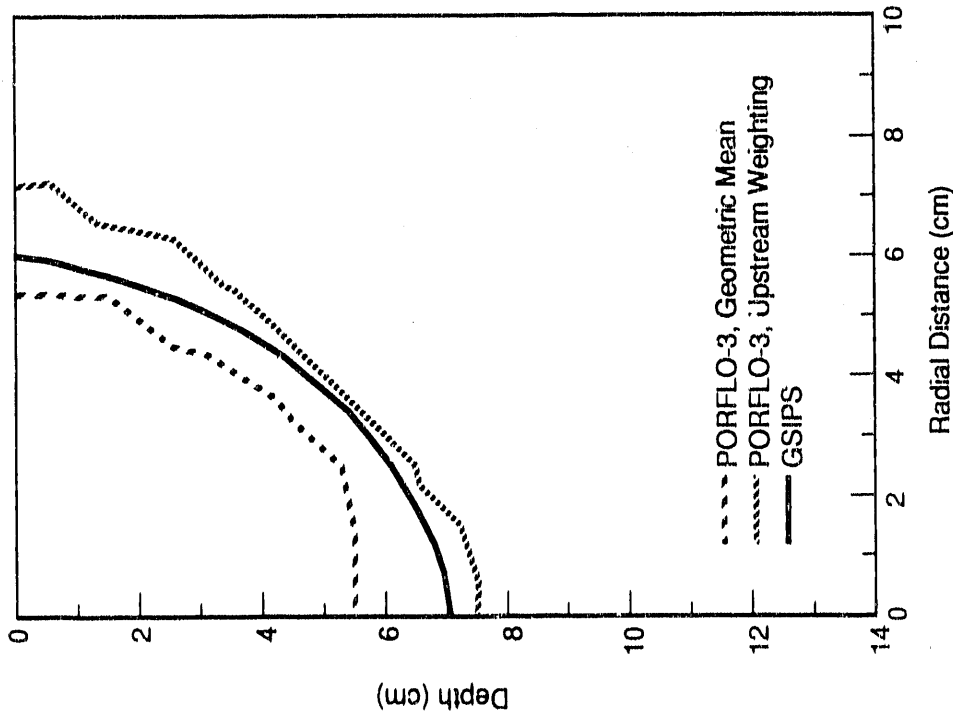
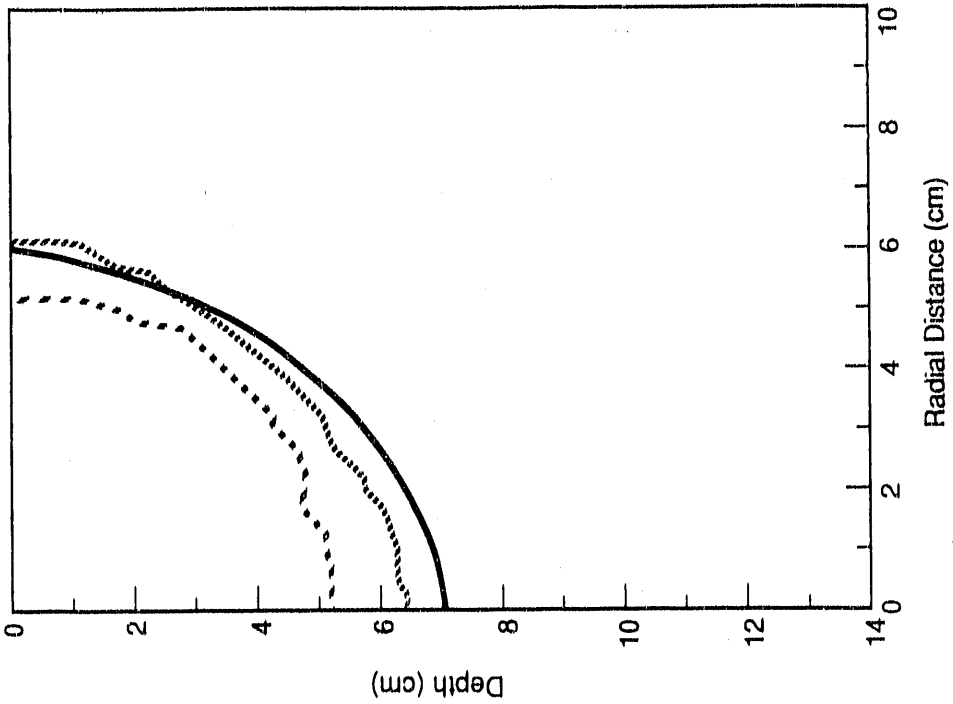
3.1.2 Verification Results

The PORFLO-3 solutions representing 0.05 h of infiltration into the sand are plotted with the GSIPS solution in Figure 3.2a. The wetting front simulated by PORFLO-3 does not extend as deep or as far horizontally as the wetting front predicted using GSIPS, if either the coarse or fine grid is used with the geometric mean. When the upstream weighting option is used, results using both the coarse and fine grids match the GSIPS solution more closely, with the closest match obtained using the fine grid. The mass balance errors are listed in Table 3.2. The upstream weighting and coarse grid combination yielded the lowest error (0.54%) after 0.05 h, while the geometric mean and fine grid yielded the highest (2.30%).

The PORFLO-3 solutions representing 0.10 h of infiltration are shown in Figure 3.2b. As for the earlier time, the PORFLO-3 solutions from both grids using the geometric mean result in wetting fronts that do not extend as deep or spread as far horizontally as the wetting front predicted using GSIPS. The solutions for both grids using upstream weighting resulted in closer matches to the GSIPS solution. The mass balance error after 0.10 h of simulation is less than for the initial time period (see Table 3.2); the relationships among options remain the same.

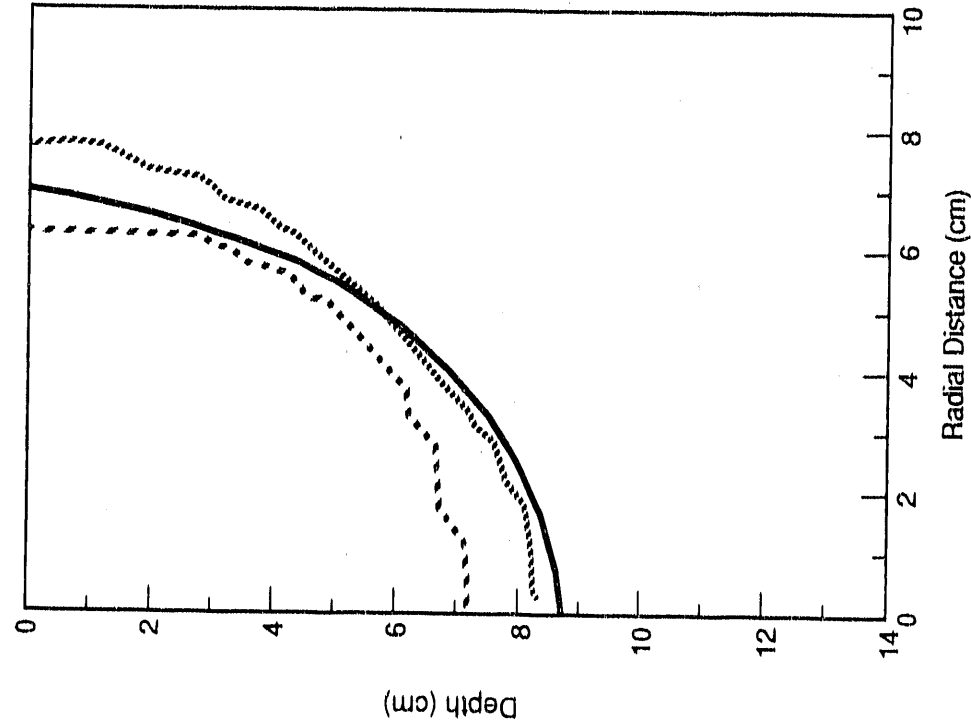
The PORFLO-3 and GSIPS solutions representing 0.15 h of infiltration are shown in Figure 3.2c. Again, the use of the geometric mean option results in underprediction of the extent of the wetting front. The mass balance error after 0.15 h of simulation is lower than after 0.1 h for the fine grid, but higher for the coarse grid (see Table 3.2).

For all three times, the differences in the predicted location of the wetting front using geometric mean and upstream weighting were approximately 1



a) 0.05 h

FIGURE 3.2. PORFLO-3 and GSIPS Solutions to Infiltration into a Sand from a Surface Point Source for Three Times. PORFLO-3 simulations with coarse grid are on the left, fine grid on the right.



S9110072.2

b) 0.10 h

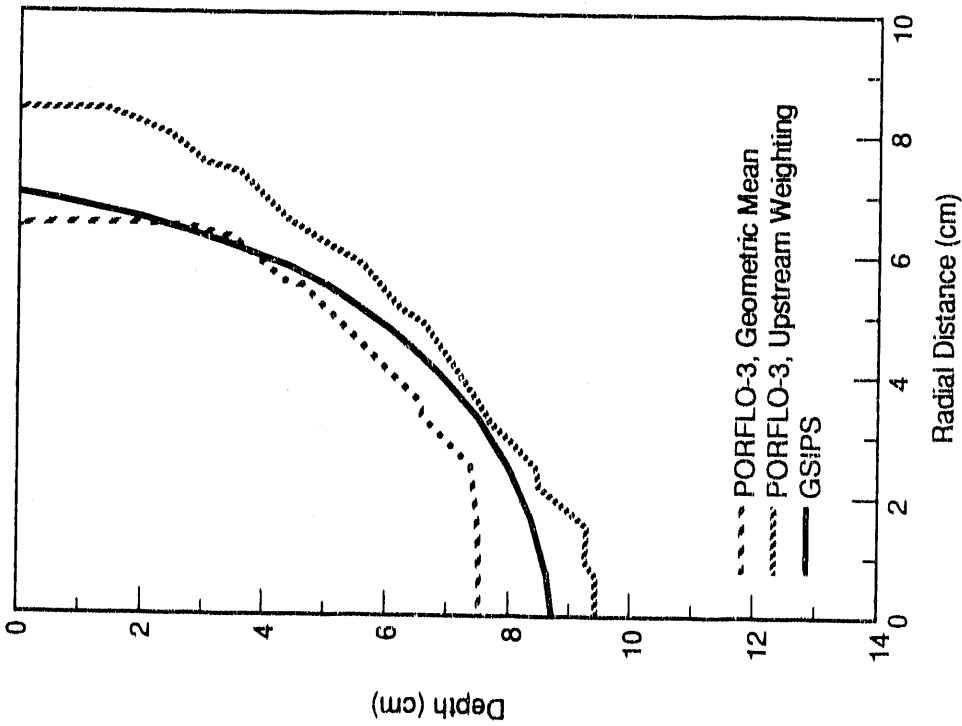
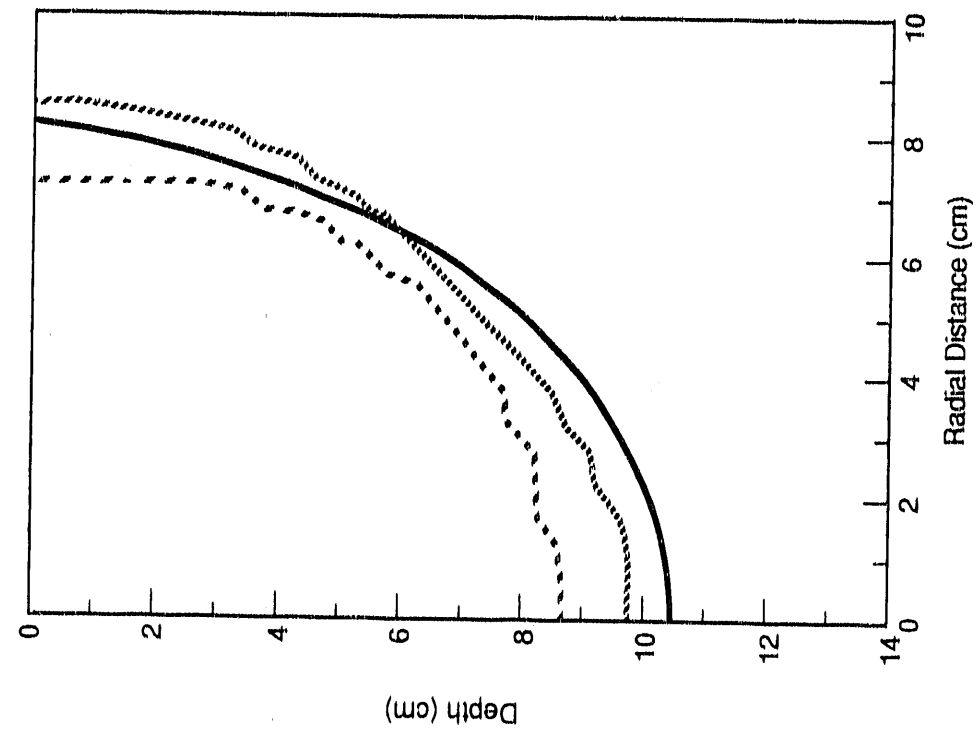
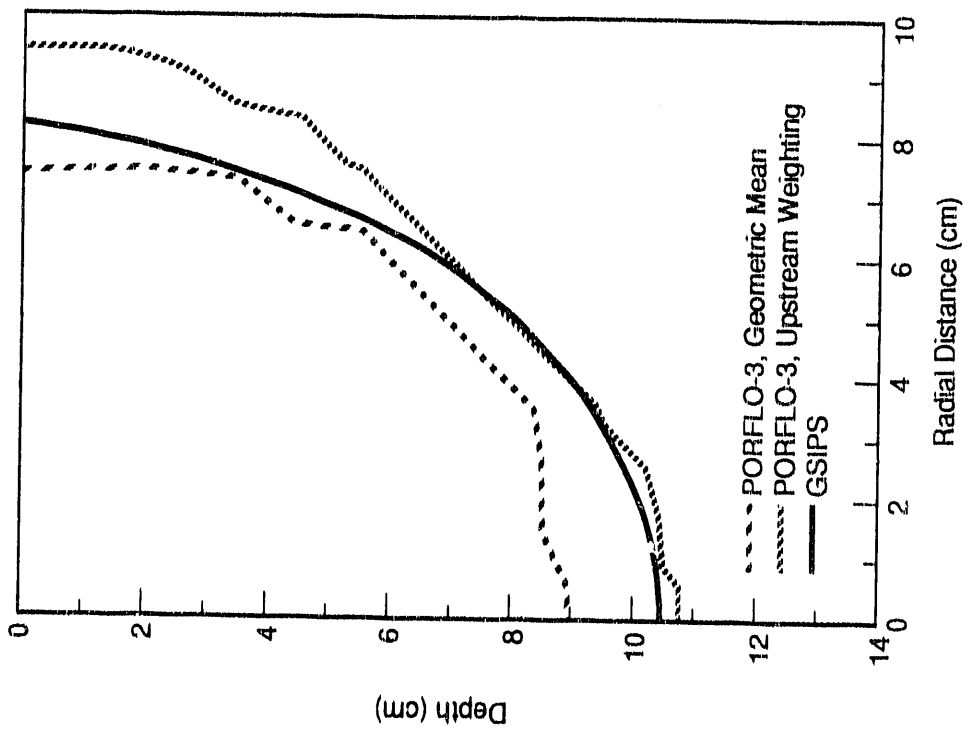


FIGURE 3.2. (contd)



S91100723



c) 0.15 h

FIGURE 3.2. (contd)

TABLE 3.2. Cumulative Mass Balance Errors for the PORFLO-3 Simulations of Infiltration into Sand from a Surface Point Source

Simulated Time (h)	Option for Internodal Conductance	Cumulative Error (%)	
		Coarse	Fine
0.05	Upstream Weighting	0.54	0.80
	Geometric Mean	0.82	2.30
0.10	Upstream Weighting	0.37	0.54
	Geometric Mean	0.73	1.56
0.15	Upstream Weighting	0.56	0.41
	Geometric Mean	1.41	1.21

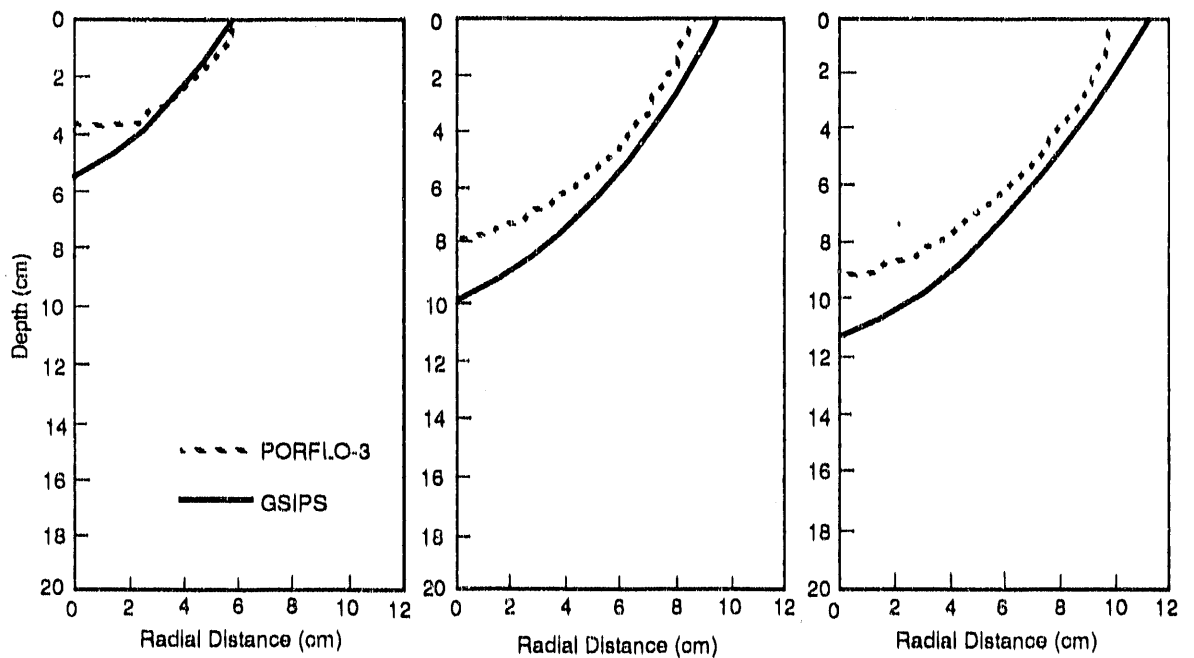
to 2 cm for the fine and coarse grids, respectively. For all three times, using the fine grid slightly reduced the distance between the wetting front and the source. The reductions were about 0.5 cm when using the geometric mean and 1.0 cm when using upstream weighting.

The slightly lower cumulative mass balance error obtained using the fine grid relative to the coarse grid after 0.15 h of simulation reflects positively on code consistency. Errors associated with the finite-difference approximations should be reduced as the node spacing is reduced. However, because the size of the initial time step differed, and because the size of the time step was halved every time convergence was not obtained, the time steps were not the same for both grids during the simulations. The difference in time steps may account for the observation that the mass balance error after 0.05 and 0.10 h of simulation, using the fine grid, was actually higher than for the coarse grid, regardless of weighting option. Therefore, a more rigorous test of code consistency would be to fix the size of the time steps at a sufficiently small value so that convergence was always assured and there would be no reduction in the size of the time step.

In terms of both mass balance error and matching the GSIPS solutions, the best results were obtained using a fine grid in combination with the upstream weighting option. Based on these results, the silt loam simulation was set up with 1) the fine grid, 2) an initial time step size of 10^{-6} h, and 3) upstream weighting. Because of the low saturated conductivity of the silt loam, the input flux was lowered to $10 \text{ cm}^3/\text{h}$ over a radius of 3.5 cm.

The PORFLO-3 solutions representing 0.3, 1.5, and 2.5 h of infiltration are plotted with the corresponding GSIPS solutions in Figure 3.3. At 0.3 h, the wetting front predicted by PORFLO-3 matches the lateral location of the GSIPS front but not the vertical extent. This result reflects the PORFLO-3 use of a larger area for infiltration. Such differences should decrease over time as the size of the input area decreases relative to the overall wetted volume.

At 1.5 h, the PORFLO-3 solution has the general shape of the GSIPS solution, but lags it by 1 to 2.5 cm. The largest discrepancy occurs directly under the source. At 2.5 h, the same relationship is observed. The cumulative mass balance errors for the three time periods are 0.34, 0.58, and 0.73%, respectively. Although they are under 1%, the error is accumulating despite



S9110072.4

a) 0.3 h

b) 1.5 h

c) 2.5 h

FIGURE 3.3. PORFLO-3 and GSIPS Solutions to Infiltration into a Silt Loam from a Surface Point Source for Three Times

using the fine grid and smaller initial time step. The accumulation of error may be caused by the very low matric potentials in this simulation. Such low matric potentials lead to very large gradients near the wetting front, and these gradients provide an opportunity for more error. The accumulation of error may also be the result of using a convergence criterion of 0.001 (the default), which may have been too high for this problem. With initial potentials of -2.38×10^5 cm, the criterion would be met even if the potential was changing by as much as 230 cm per iteration. Further testing should include a lower value for the convergence criterion than was used, or the use of a different convergence criterion.

In summary, wetting front advance in response to infiltration into initially dry soil was predicted using PORFLO-3 in the axisymmetric mode and using GSIPS, which provided generalized solutions to such problems. Comparisons of the two solutions were qualitative given that the code configurations (e.g., node density and arrangement, internodal conductance calculation, surface boundary description) were not identical. Despite the differences in how the problem was solved, the comparisons showed that PORFLO-3 predicted wetting front positions that were comparable to those generated with GSIPS. For a more quantitative benchmark of PORFLO-3, the TOUGH code should be used to solve this problem. Some of the difficulties in the comparisons reported here (e.g., node density and arrangement, internodal conductance calculation) can then be eliminated.

The results from the sand infiltration problem demonstrated the sensitivity of PORFLO-3 predictions to the node density and method of calculating internodal conductances. Depending on the options used, the wetting front position predicted with PORFLO-3 changed relative to the location of the source by from 0.5 to 2.0 cm. These changes in the position of the front are significant, given that the maximum vertical extent of the front was 10.5 cm at 0.15 h. Conclusions regarding which set of options worked best are not appropriate because the comparisons were qualitative and the PORFLO-3 solutions were shown to be significantly affected by the use of different options. Further testing should include simulations with progressively higher node densities until the solution does not change.

Cumulative mass balance errors were 1.4% after 0.15 h of infiltration into sand and 0.73% after 2.5 h of infiltration into silt loam. This level of error is acceptable for conducting sensitivity tests of infiltration into animal burrows and root channels.

4.0 TEMPERATURE EFFECTS ON LYSIMETER DRAINAGE

Eight of the lysimeters in the Small Tube Lysimeter Facility (STLF) located at the Hanford Site have an asphalt layer that was leak tested and assumed to be impermeable to water (Freeman and Gee 1989a). Freeman and Gee (1989b) report, however, that during the first year of operation, small amounts of water (14 to 232 ml) drained from these lysimeters. The TOUGH code (Pruess 1987) was used to test the hypothesis that temperature variations at the lysimeter wall induced the movement of in situ water (in both the liquid and vapor form) beneath the asphalt layer, and that this temperature-induced movement contributed to drainage. The results of this test are presented in this section.

4.1 DESCRIPTION OF LYSIMETER DESIGN AND DATA

Ten lysimeters at the STLF are being used to evaluate the performance of asphalt barrier formulations under natural environmental conditions (Freeman et al. 1989; Freeman and Gee 1989a). Eight of the lysimeters contain asphalt layers; the two that do not serve as the experiment control. Each lysimeter (Figure 4.1) was constructed from a 1.7-m length of PVC pipe that has a diameter of 30 cm. All of the lysimeters were filled with layers of gravel and coarse sand. Four of the lysimeters then received a 15-cm-thick layer of asphalt admix, four received a 1.3-cm-thick layer of rubberized asphalt, and two received no asphalt (i.e., the control lysimeters). All of the lysimeters were then filled with sand and covered with a 15-cm-thick layer of gravel. The water content of the sand and gravel placed under the asphalt barrier was not measured, but information in Freeman and Gee (1989b) indicates that at least six of the lysimeters probably contained very wet sand and gravel. The information consists of observations that two of the four rubberized asphalt layers leaked during testing and had to be resealed and that the four admix layers naturally released water during curing.

Figure 4.2 shows measured monthly water drainage from one of the control lysimeters (No. 9) for the 2-year period since the lysimeter was installed in July 1988. Also shown are the average monthly precipitation and soil

11/11/88

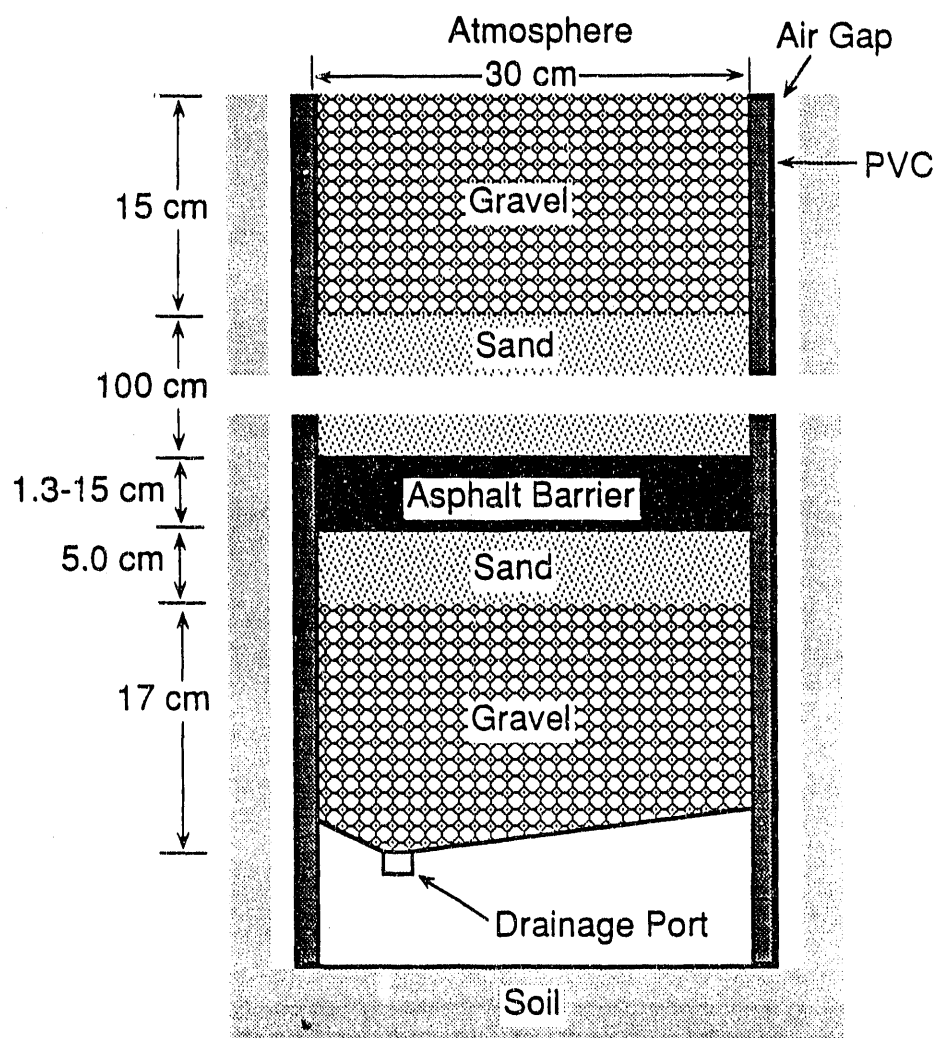


FIGURE 4.1. Cross Section of Lysimeter

temperature measured at the nearby Hanford Meteorological Station (Stone et al. 1983). Because there is no barrier to impede infiltration, drainage correlates to rainfall with a lag time of one month.

Figure 4.3 shows drainage from one of the lysimeters (No. 2) containing a rubberized asphalt layer compared with the precipitation and temperature data shown in Figure 4.2. Unlike the control lysimeter, drainage from the

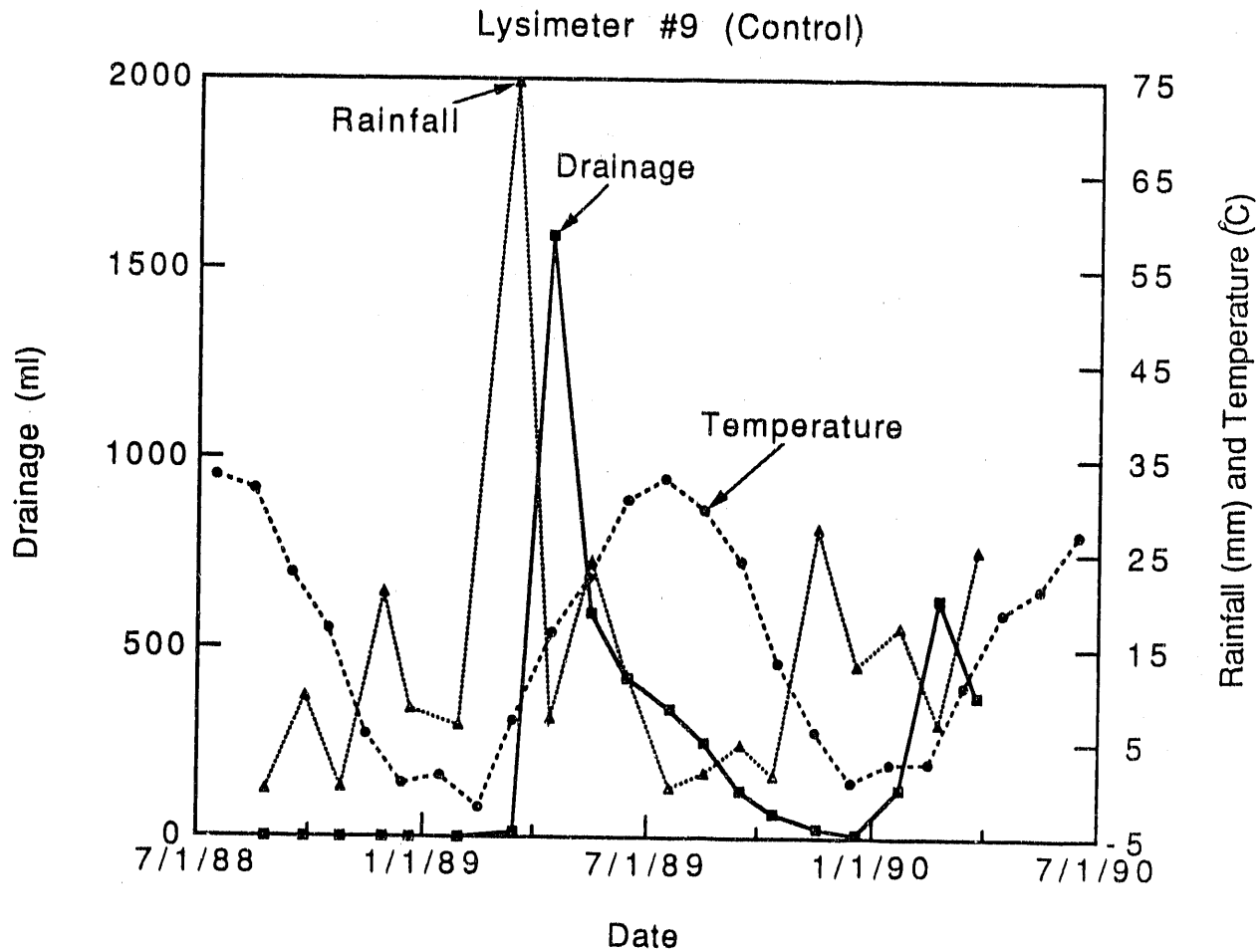


FIGURE 4.2. Drainage from Lysimeter No. 9 (control) Compared with Average Monthly Precipitation and Soil Temperature at the 1.3-cm Depth

asphalt lysimeter correlates to temperature. Also, the amount of drainage is small compared with the control lysimeter and shows no correlation with precipitation. For these reasons, the drainage water is hypothesized to be residual water from the installation of the barriers and not leakage through the barrier. This hypothesis is supported by the observation of PNL staff that salt placed above the asphalt barrier has not been detected in the drainage water.

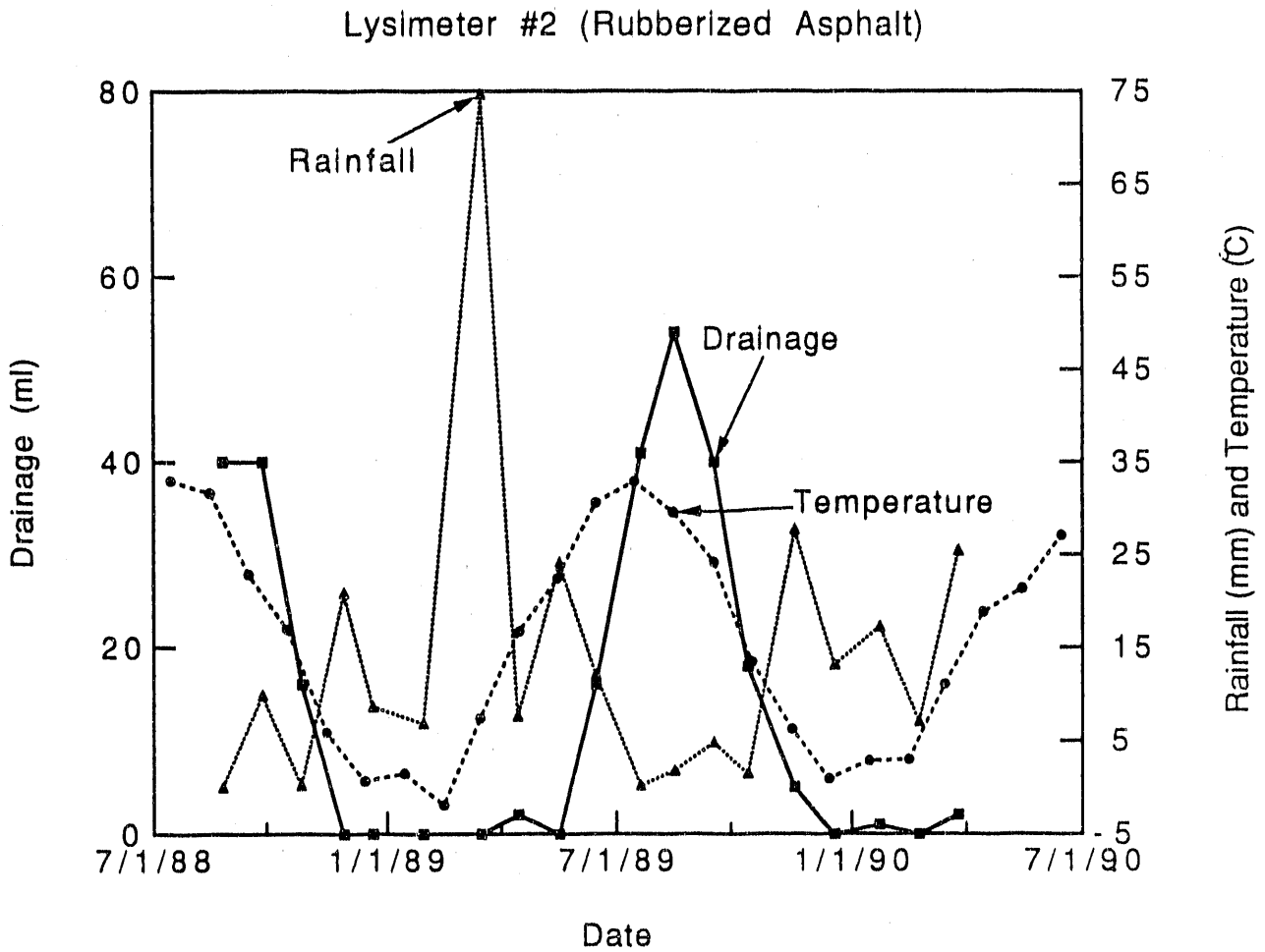


FIGURE 4.3. Drainage from Lysimeter No. 2 (rubberized asphalt barrier) Compared with Average Monthly Precipitation and Soil Temperature at the 1.3-cm Depth.

4.2 PROBLEM DESCRIPTION

The TOUGH code (Pruess 1987), which was described in Section 2.4, was used to assess the effect of temperature variations at the lysimeter walls on water and vapor movement beneath the asphalt layer. Two axisymmetric simulations of the lysimeter were conducted using the radially symmetric grid shown in Figure 4.4. In the first simulation, the lysimeter temperature was maintained at a constant temperature of 15.3°C (the yearly average soil temperature at the 91.4-cm depth). In the second simulation, the average monthly

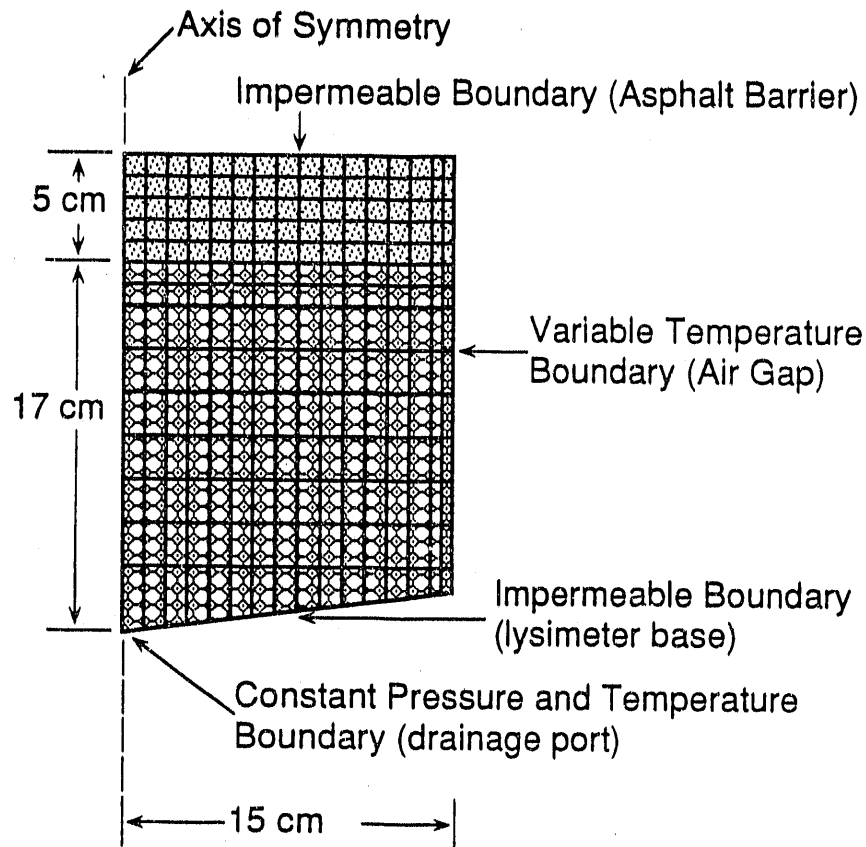


FIGURE 4.4. Cross Section of Radial Grid (scale 2x that of Figure 4.1)

temperature at the 1.3-cm depth (see Figure 4.2 or 4.3) was applied along the side boundary of the model (Figure 4.4). The drain was held at a constant temperature of 15.3°C. The initial temperature throughout the entire system was 32.9°C (the average July soil temperature). The initial water saturation was 90% for the sand layer and 10% for the gravel layer.

Thermal conductivities for saturated and dry conditions were estimated at 0.29 and 2.2 W/m°C, respectively, based on properties for average soils as reported by Hillel (1980). The specific heat of quartz (Hillel 1980) was used for the sand, and specific heat of granite (Weast 1982) was used for gravel. Nodes next to the variable temperature boundary were given a large (10^8) specific heat so that they would remain at the specified temperature.

The hydraulic properties of the coarse sand and gravel were described using the van Genuchten water retention and Burdine hydraulic conductivity

functions (van Genuchten 1978). The parameters for the functions are given in Table 4.1. The coarse sand parameters were derived by fitting the retention function to a data set containing a combination of retention data for sand (soils 4141 and 4142 from Mualem 1976a). The gravel parameters were derived by fitting the retention function to a data set containing estimated gravel properties (Fayer et al. 1985).

All variables in TOUGH were converted to double precision so that simulations could be run on a Sun-4 workstation.

4.3 SIMULATION RESULTS

Figure 4.5 shows a comparison of drainage predicted using a constant temperature throughout the model domain and using a constant temperature at the drain and a variable temperature at the lysimeter wall. The variable temperature resulted in a decrease in drainage relative to the constant-temperature simulation when temperatures are below the yearly average and an increase in drainage when temperatures are above the yearly average. However, the increase in drainage in summer is not as great as that actually observed in most of the lysimeters. For example, drainage from lysimeter No. 2 is plotted in Figure 4.6 (data provided by PNL staff). A maximum of 54 ml was collected in August 1989, whereas the simulated drainage for that month was 13 ml.

The difference between the drainage rates in winter and summer is illustrated by the simulated flow fields for February and August 1989 in Figure 4.7. Overall, flow velocities are much higher in August than in February, delivering more liquid mass to the drain in the lower left-hand corner. An interesting feature of the flow fields is the convection cell that formed in

TABLE 4.1. Parameters for Describing Hydraulic Properties with the van Genuchten-Burdine Functions

<u>Material</u>	<u>S_{1r}</u>	<u>S_{1s}</u>	<u>α (1/kPa)</u>	<u>n</u>	<u>K_s (m⁵/s)</u>
Coarse Sand	0.02247	1.00	0.741	2.80355	1.09×10^{-3}
Pea Gravel	0.01193	1.00	50.317	2.18628	3.50×10^{-3}

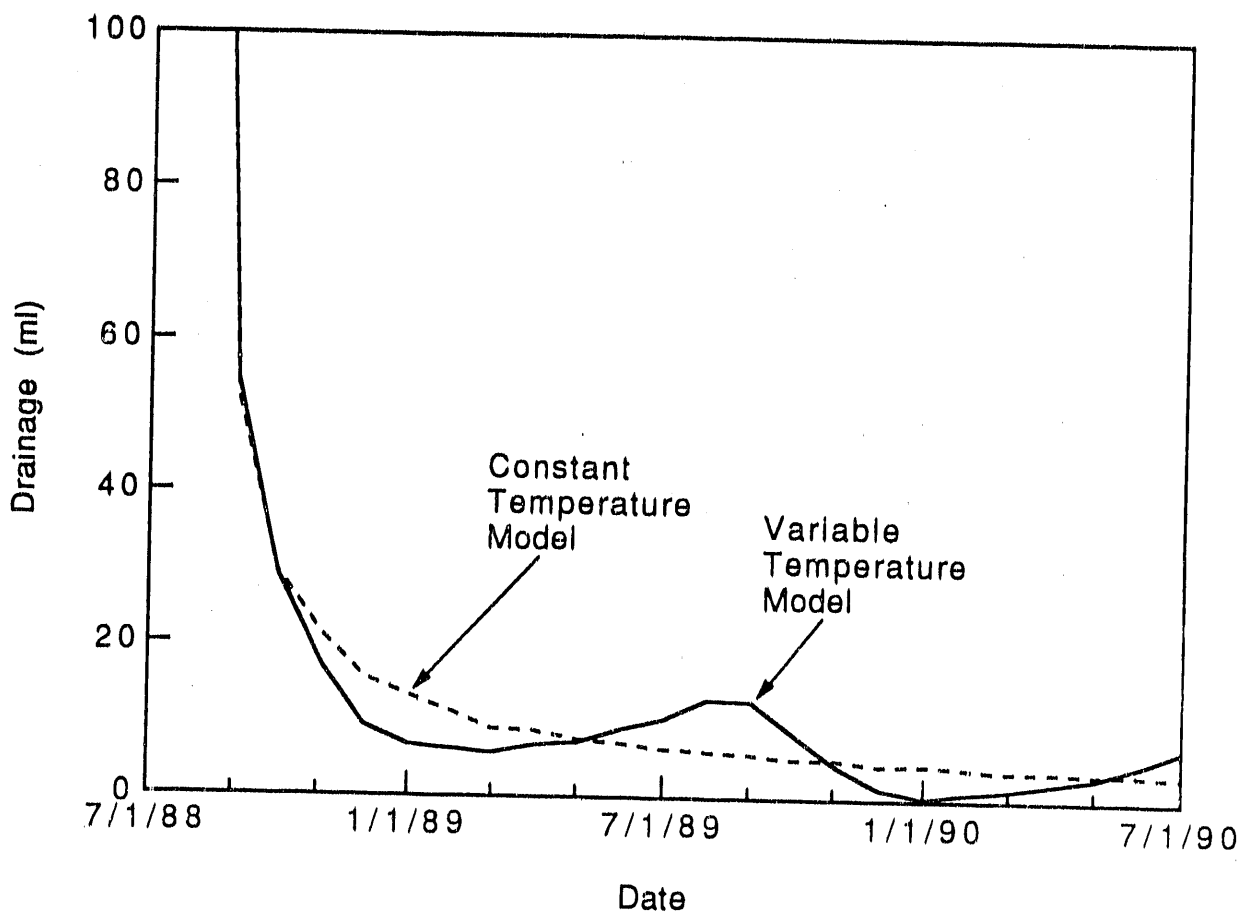


FIGURE 4.5. Comparison of Drainage Predicted by Constant-Temperature and Variable-Temperature Simulations

the wet, sandy layer. Because the gravel layer acts as a barrier to the downward flow of water, the water in the wet layer circulates in response to liquid density differences caused by the temperature gradient across the system. The temperature contours for February and August are shown in Figure 4.8. The absolute temperature is much higher in August, with the highest temperature (32.9°C) along the right-hand side and the lowest (29.4°C) at the lower left-hand corner. The convection cell operates counterclockwise from March to September and clockwise from September to March; however, during

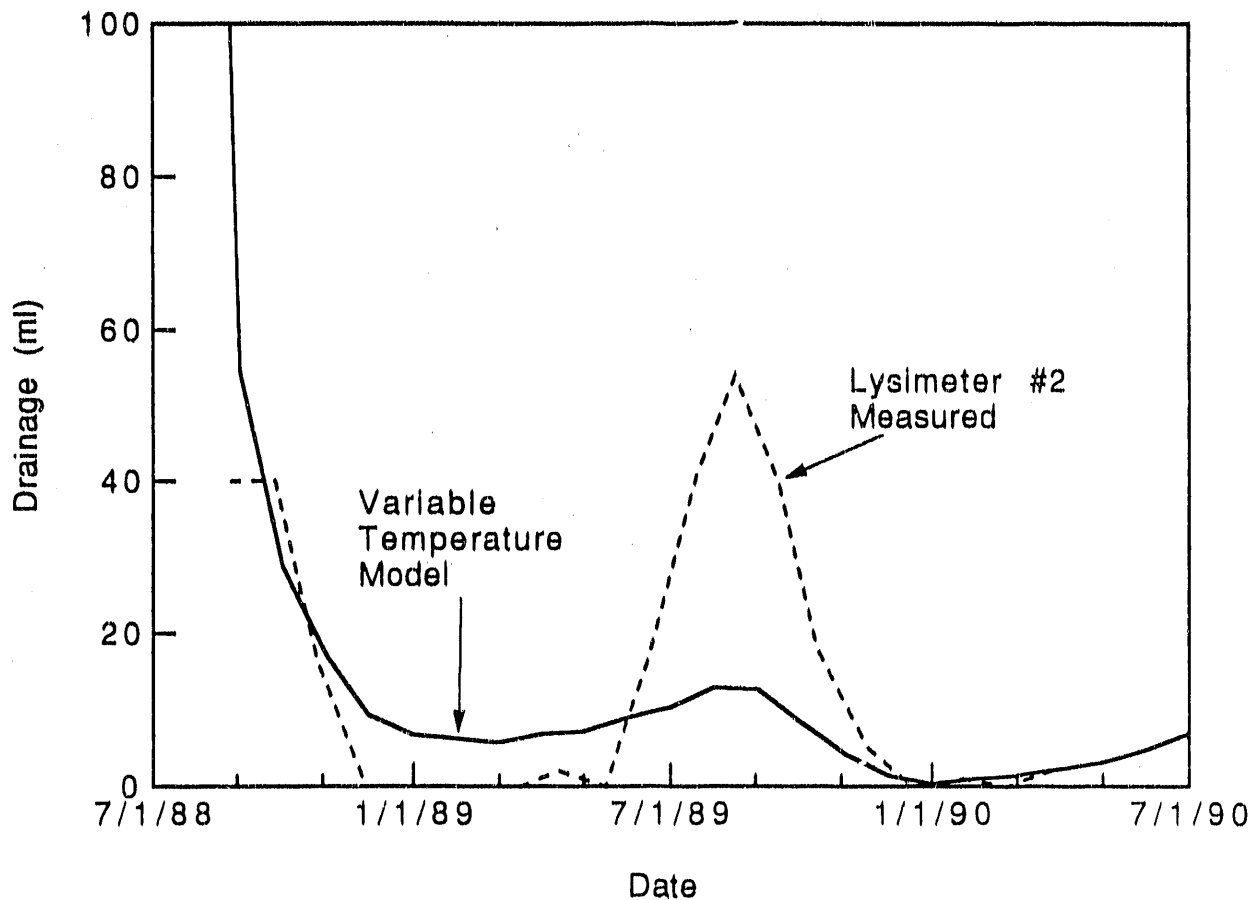


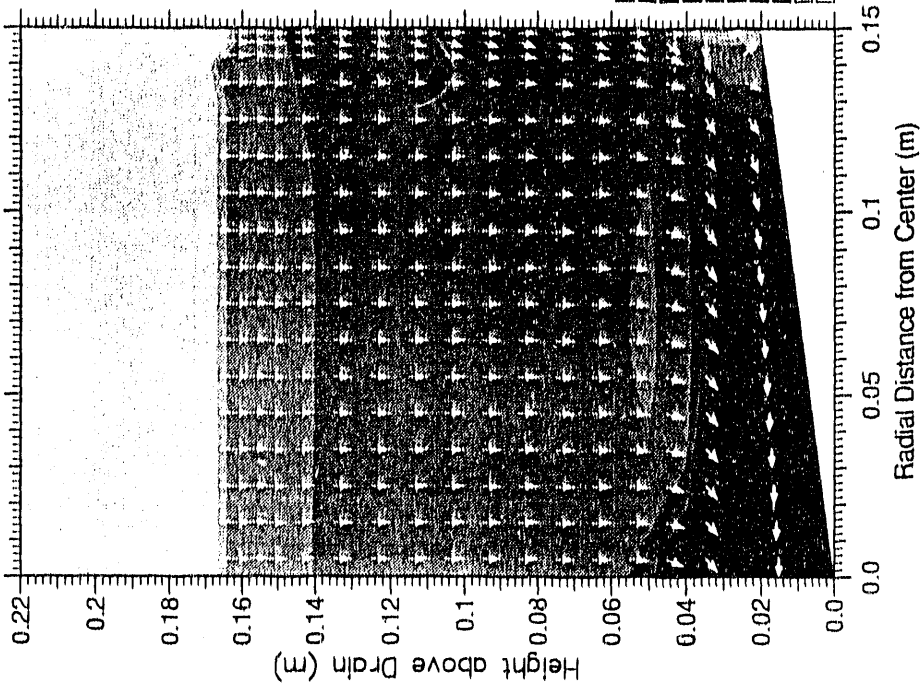
FIGURE 4.6. Comparison of Drainage Predicted by Variable-Temperature Model and Measured from an Asphalt Barrier Lysimeter

January and February the convection cell operates counterclockwise because temperatures in the column are between 1.5 and 4°C, and the density of water is highest at 4°C.

The saturated vapor pressures for February and August are shown in Figure 4.9. The pressures are much higher in August than in February, and the vapor pressure gradient is an order of magnitude higher. The vapor pressure gradient in August follows the temperature gradient (Figure 4.8) from the right-hand side to the lower left-hand side. This gradient drives water in the vapor phase from the wall to the interior of the lysimeter and toward the drain. At the lower temperatures of the lysimeter interior and drain, the

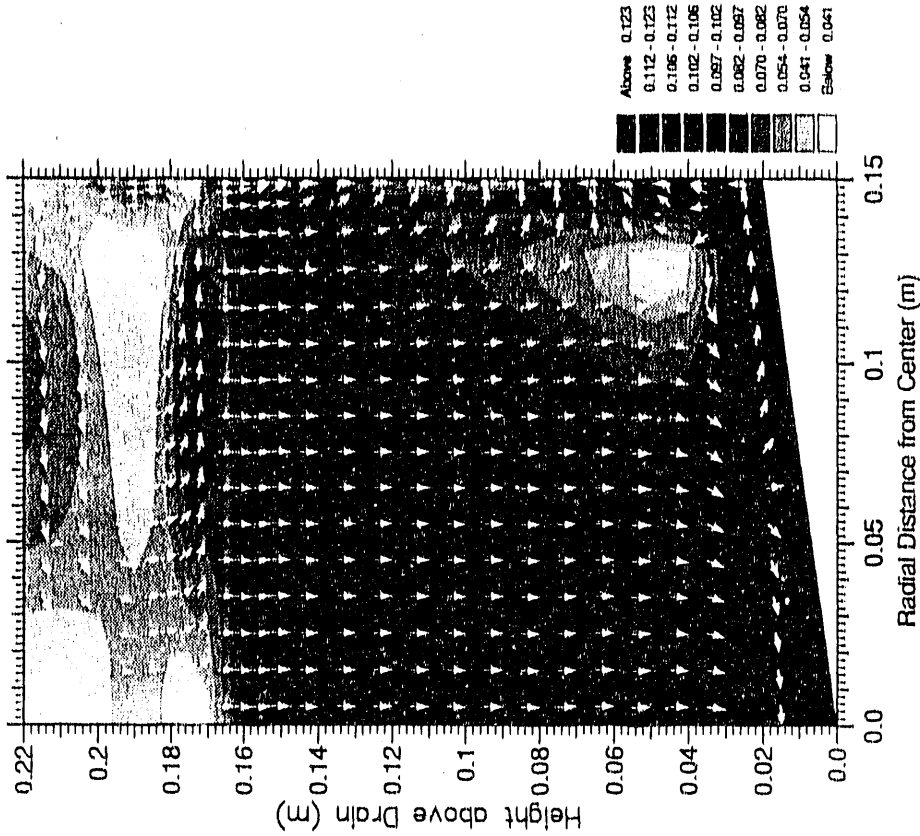
Liquid Velocities (m/yr) at 215.000 days

Minimum = 5.99219E-04 Maximum = 1.73372



Liquid Velocities (m/yr) at 396.250 days

Minimum = 9.23356E-03 Maximum = 1.28547



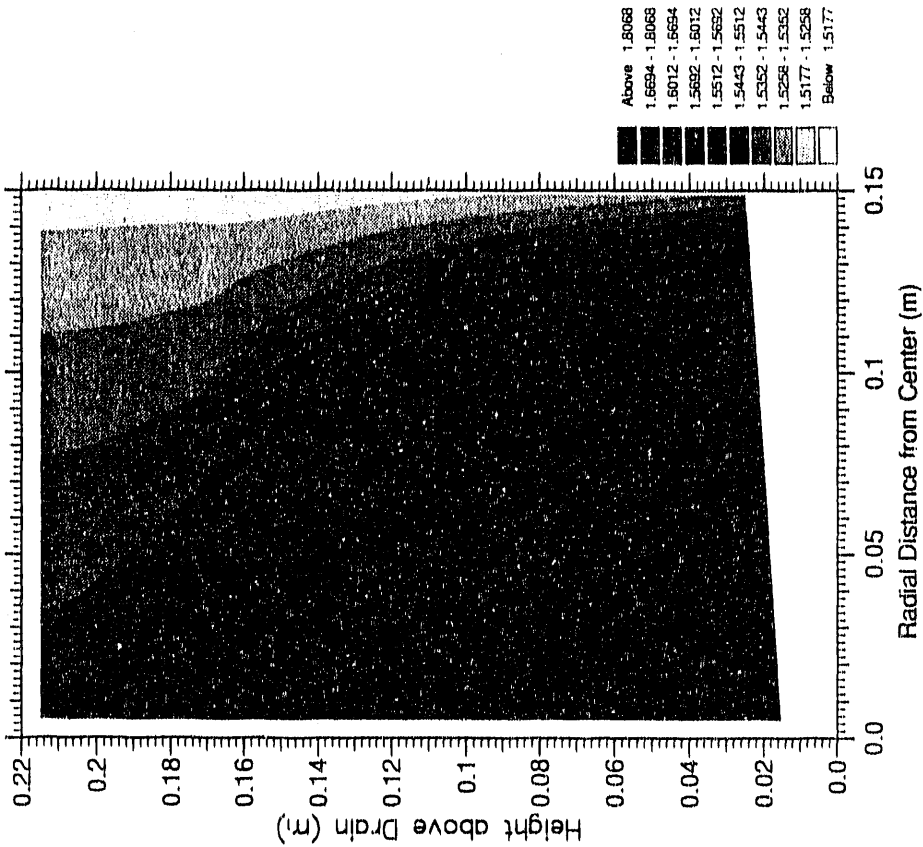
a) February 1989 (minimum = 6.0×10^{-4} m/yr, maximum = 2.8 m/yr)

b) August 1989 (minimum = 9.2×10^{-3} m/yr, maximum = 6.6 m/yr)

FIGURE 4.7. Simulated Liquid Velocities

Temperatures (°C) at 215.000 days

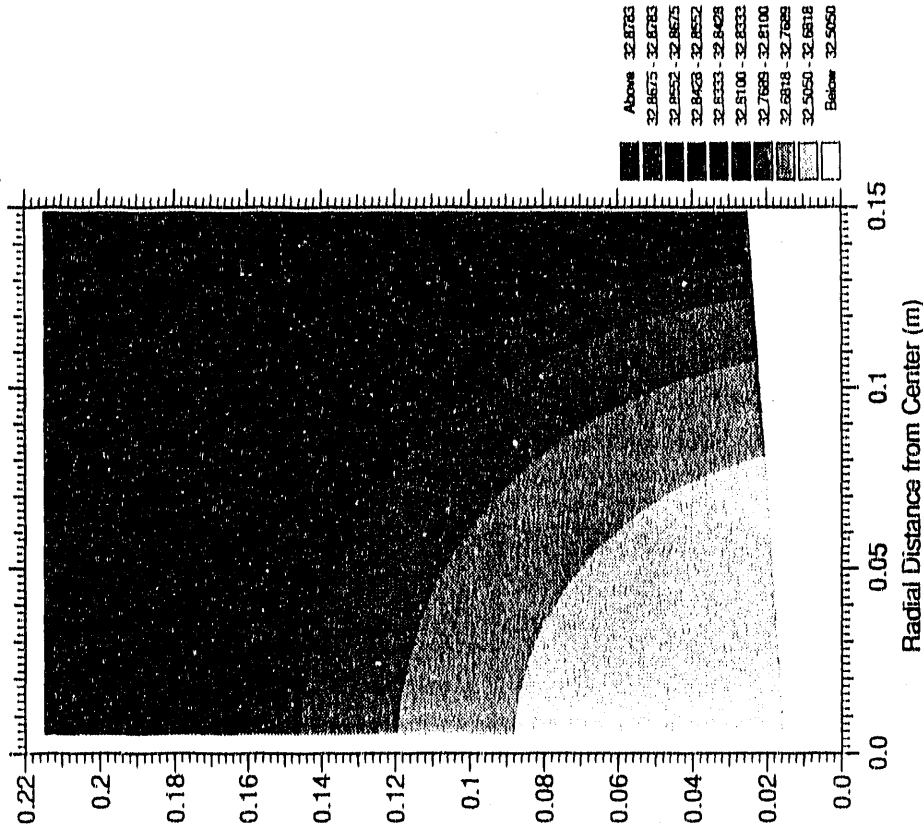
Minimum = 1.51339 Maximum = 4.25142



a) February 1989 (minimum = 1.5, maximum = 4.3°C)

Temperatures (°C) at 396.250 days

Minimum = 29.3848 Maximum = 32.8843



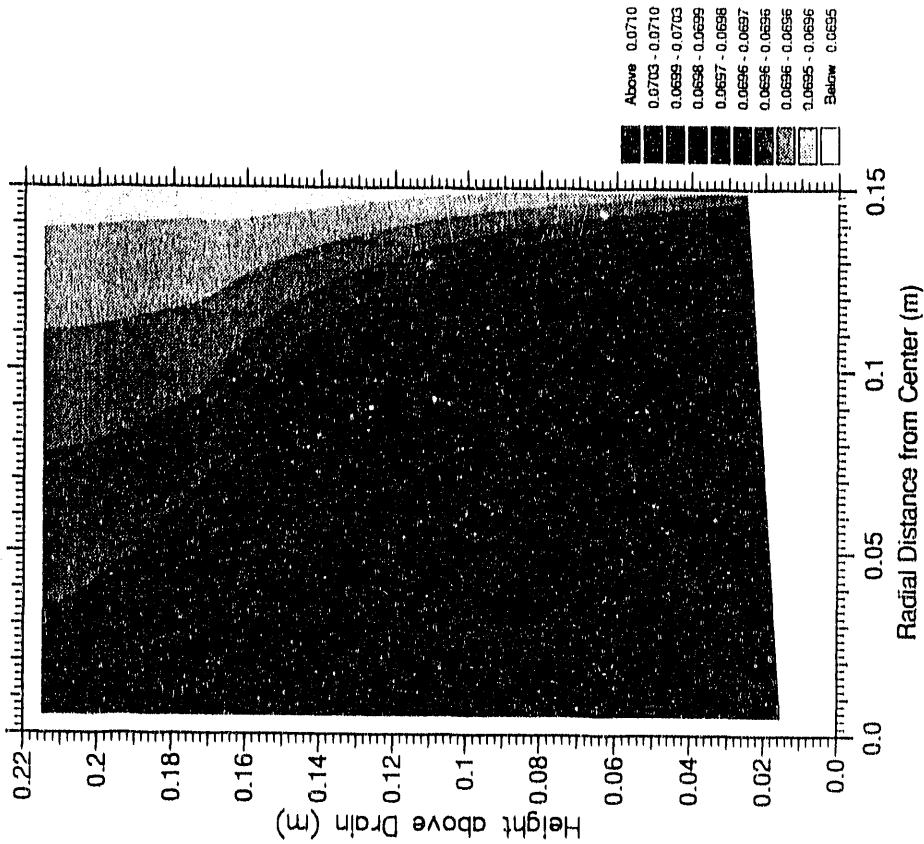
b) August 1989 (minimum = 29, maximum = 33°C)

FIGURE 4.8. Simulated Temperatures

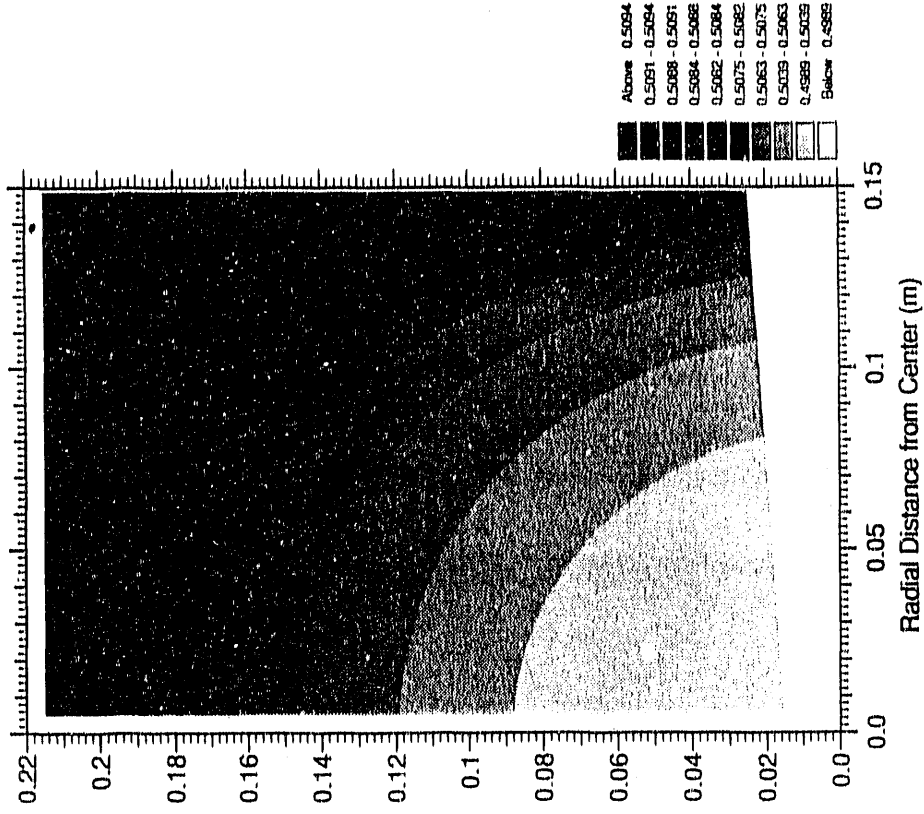
Saturated Vapor Pressures (m) at 215.000 days Saturated Vapor Pressures (m) at 396.250 days

Minimum = 6.94931E-02 Maximum = 8.43911E-02

Minimum = 0.417589 Maximum = 0.509620



a) February 1989 (minimum = 6.9×10^{-2} m, maximum = 8.4×10^{-2} m)



b) August 1989 (minimum = 0.42, maximum = 0.51 m)

FIGURE 4.9. Simulated Vapor Pressures

vapor condenses. The resulting buildup of water content leads to increased drainage, as seen indirectly in the liquid velocity profile in Figure 4.7.

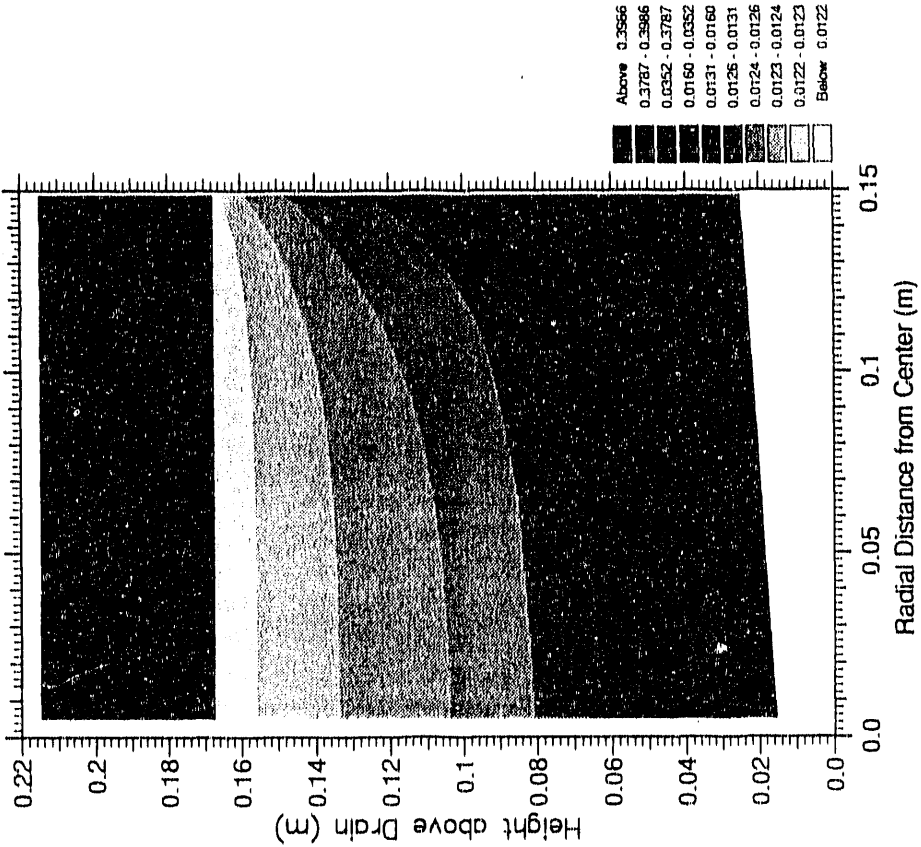
The water contents for February and August are shown in Figure 4.10. In February, the water contents are slightly higher along the right-hand side (lysimeter wall) as vapor moving there condenses. In August, the higher temperature along the right-hand side caused the column to dry out slightly as vapor was driven inward. The dry zone attracts liquid water, as evidenced by the liquid velocities directed to this zone from both above and below.

Drainage is more enhanced in the summer because of the nature of the lysimeter. In winter, vapor is driven from the core (i.e., the center of the lysimeter) to the lysimeter walls, which have a large surface area. In the summer, vapor is driven from the walls towards the core. If the same amount of vapor were transported in either direction, the location most likely to have the higher water contents necessary for increased liquid flow, and thus increased drainage, is the core. This hypothesis is borne out by the water content profiles (Figure 4.10). The water contents of the core in August are much higher than those near the wall in February.

The observed differences in drainage between February and August could be affected by the temperature dependence of the hydraulic properties of the sand and gravel (for these simulations, no effect was assumed), by diurnal and daily temperature variations (for these simulations, monthly average values were used), by the imposition of a temperature change along the lysimeter wall as has been observed in the air gap by PNL staff (for these simulations, the same temperature change was specified along the entire lysimeter wall), and by the changing temperature of the drain (for these simulations, a constant temperature was used). For example, diurnal temperature variations could enhance drainage in the summer months; freezing of soil water during the winter months would stop drainage from the column. Future simulations could address some of these concerns.

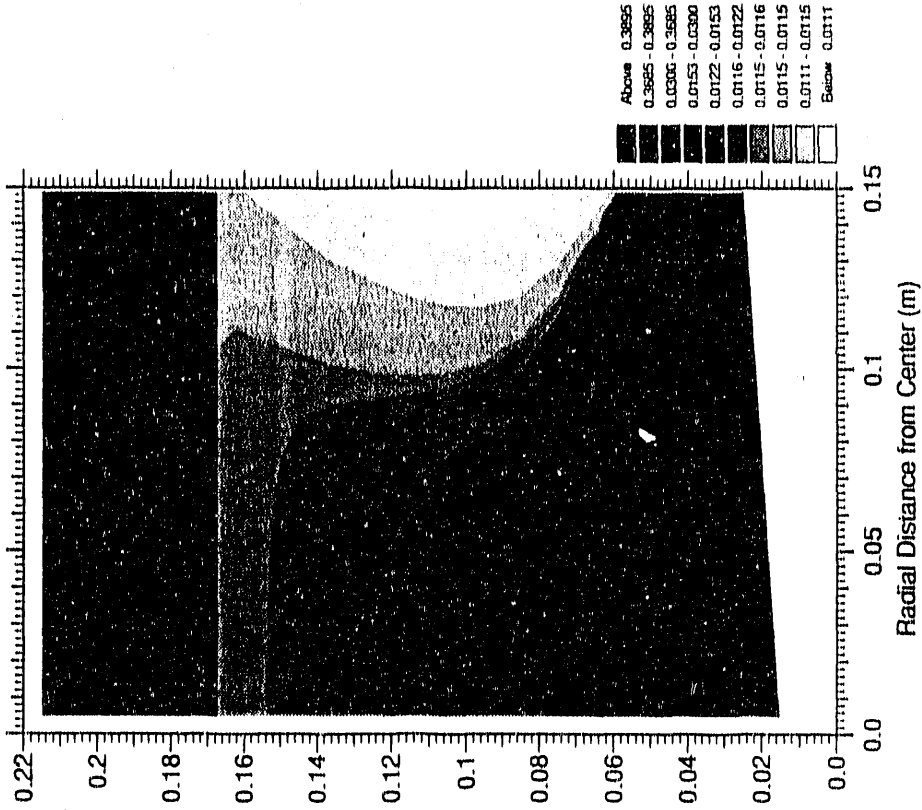
Although the simulated drainage does not match the observed drainage in magnitude, the seasonal trends are the same. The match of seasonal trends in drainage provides supporting evidence that temperature variations can affect

Water Content at 215.000 days
 Minimum = 1.22073E-02 Maximum = 0.412371



a) February 1989 (minimum = 1.2×10^{-2} , maximum = 0.412 m)

Water Content at 396.250 days
 Minimum = 7.04583E-03 Maximum = 0.404434



b) August 1989 (minimum = 7.0×10^{-3} , maximum = 0.404 m)

FIGURE 4.10. Simulated Water Contents

drainage of residual water from beneath the asphalt barrier in the lysimeters. The results imply that any lysimeter that has below-ground surfaces exposed to uneven temperature changes may be subject to the same effect.

The weighing lysimeters at the Field Lysimeter Test Facility (FLTF) are un-insulated (and thus exposed to the same temperature changes experienced by the small tube lysimeters), but no drainage has occurred. Considering the thinness (5 cm) of the gravel layer relative to its areal extent ($2.25 \times 10^4 \text{ cm}^2$), these lysimeters may not show drainage by the proposed mechanism because the sand layer above the gravel would exert more control on the vapor content in the gravel air space. In the weighing lysimeters, the sand layer is just below the silt loam soil, which keeps the sand dry relative to the sand layer beneath the asphalt barrier.

Staff at PNL report that the FLTF drainage lysimeters, which are insulated, have had some drainage. The staff suspect temperature effects; temperatures measured in several of these lysimeters show a small gradient between the inner and outer walls, as well as between the center of the riprap layer and the overlying sand and silt loam. The results from the different types of lysimeters show that temperature change must be considered when designing lysimeters to measure low annual drainage rates.

The results of the TOUGH simulation also imply that temperature effects on protective barriers could be significant. In some preliminary designs of the barrier, the subsurface riprap layer extends to the barrier sideslopes. The open pores of the riprap layer could allow significant air flow to occur. Depending on temperature and humidity of the incoming air, evaporation or condensation (and thus potential drainage) could occur. The effect of such temperature changes on drainage should be calculated.

5.0 COMPARISON OF FIELD DATA AND UNSAT-H SIMULATION RESULTS

Multilayer "protective barriers" have been proposed as a means of limiting the flow of water through the waste sites (DOE 1987). The multiyear research program outlined by Adams and Wing (1986) was designed to assess the performance of these barriers. Improved performance is defined as reducing drainage rates to the deeper vadose zone to less than 0.05 cm/yr. One aspect of this program is the use of computer models to predict the barrier's water balance, of which drainage is one component. The objective of this section is to document the ability of the UNSAT-H Version 2.0 model (Fayer and Jones 1990) to simulate the water balance of the protective barrier for durations in excess of a year without prior calibration of the model parameters. A secondary objective is to provide information that can be used to improve the water balance model, thus allowing for better predictions of long-term drainage rates through the barrier.

5.1 MODEL DESCRIPTION

UNSAT-H Version 2.0 is a one-dimensional unsaturated soil-water and heat-flow model (Fayer and Jones 1990). Because we are still testing the heat-flow component and did not initially have detailed information on thermal processes affecting evaporation at our lysimeter site, we performed the simulations without directly including heat flow.

The flow of water is calculated using the Richards equation for liquid water flow in response to gravitational and matric potential gradients and Fick's law for diffusive vapor flow. The flow equations are solved using a finite-difference scheme with variable time step sizes.

For this section, infiltration is described as a flux of either precipitation or irrigation, with no runoff. Evaporation is described as either a flux or a fixed-head condition (Gupta et al. 1978). The condition depends on the value of h_s , the suction head at the surface node, relative to the limit, h_{max} . If h_s is less than h_{max} , evaporation is set equal to the potential evaporation rate, which is calculated from meteorologic parameters. If h_s is predicted to be greater than h_{max} at the end of a time step, that

particular time step is repeated with the h_s prediction fixed at the value of h_{max} , i.e., a fixed-head condition. The evaporation rate is then a function of the net flux to the surface node from the node below. During this stage, the soil conductivity significantly affects the evaporation rate.

5.2 METHOD

The method used to document the performance of UNSAT-H Version 2.0 was to simulate the water balance behavior of eight non-vegetated lysimeters located in the FLTF described by Gee et al. (1989) and to compare the simulation results (i.e., water contents, storage, and drainage) to measurements. Although they are an integral part of the protective barrier, plants were not included in this analysis to simplify testing of the other components of the model.

None of the parameters used in the simulations reported here were calibrated. Instead, the parameters were determined independent of the simulations using standard methods to illustrate how well the model could perform without calibration.

Six of the eight lysimeters are cylinders with bottoms that are sealed except for a drain (Fig. 5.1a). These drainage lysimeters comprise two replicates of three precipitation treatments: ambient (i.e., natural precipitation), 2x average (water added to achieve twice the average precipitation received from 1955 and 1980), and breakthrough (i.e., water added until drainage occurred).

The remaining two lysimeters are rectangles 152 cm on a side and 170 cm deep. The bottoms are sealed except for a drain. These lysimeters also contain the layering sequence shown in Fig. 5.1a, except that the lowest layer is the 0.01-m-diameter gravel. These two lysimeters rest on platform scales; hence, their designation as "weighing" lysimeters. Calibration of the scales indicates an accuracy in measuring storage changes of ± 0.03 cm. The weighing lysimeters are replicates of the ambient and 2x average treatments.

All of the lysimeters were monitored biweekly with a neutron probe. Based on calibration data, the accuracy of the probe is ± 0.01 cm³/cm³. The

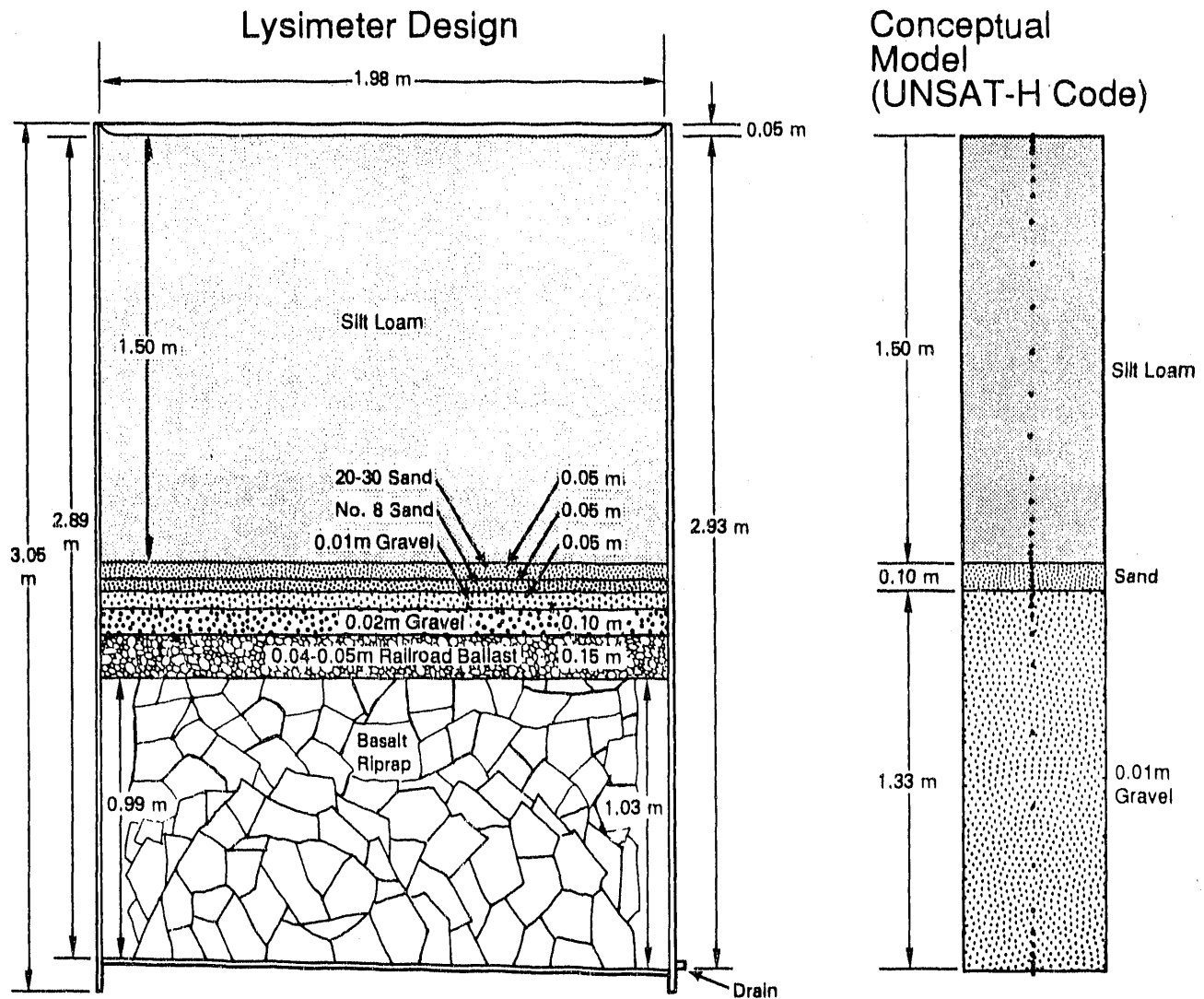


FIGURE 5.1. Lysimeter Design and Conceptual Model

lysimeters were also monitored biweekly for drainage. Collected drainage water was weighed to the nearest gram and expressed as volume per surface area of the lysimeters.

Table 5.1 lists the lysimeter descriptions, identifiers, and simulation dates for each treatment. Lysimeters D9 and D11 were covered on 14 March 1988 to eliminate evaporation and promote breakthrough. Subsequent weekly irrigations eventually saturated the silt loam; as a result, the soil surfaces subsided approximately 10 cm sometime in July 1988. Therefore, we chose to

TABLE 5.1. Lysimeter Descriptions, Identifiers, and Simulation Dates for Each Treatment

<u>Treatment Description</u>	<u>Lysimeter ID</u>		<u>Simulation Dates</u>	
	<u>Drainage</u>	<u>Weighing</u>	<u>First</u>	<u>Last</u>
Ambient	D1, D8	W2	5 Nov 1987	30 Apr 1989
2x Average	D10, D12	W4	5 Nov 1987	30 Apr 1989
Breakthrough	D9, D11	--	5 Nov 1987	30 Jun 1988

simulate the water balance of these lysimeters for the period ending 30 June 1988 rather than 30 April 1989 as was done for the other lysimeters.

5.2.1 Barrier Representation

In the conceptual model of the drainage lysimeters (Fig. 5.1b), the two sand layers were treated as a single sand layer and the various gravel sizes were treated as gravel with an average diameter of 0.01 m. The bottoms of the lysimeters have a slope of 2% from the 2.89-m depth to the drain located at 2.93 m. The simulations were made using a uniform depth of 2.93 m and assuming that the slight slope at the bottom would have a negligible effect on the annual flow of water. Simulation node spacing (Fig. 5.1b) ranged from 0.2 cm at the surface, to 2.0 cm at material interfaces, to a high of 25 cm in the middle of the gravel. Halving the spacing (i.e., doubling the number of nodes) did not change the simulation results appreciably except for the breakthrough treatment, for which the spacing in the gravel was reduced to 2 cm.

The conceptual model of the two weighing lysimeters is identical to that of the drainage lysimeters, except that the bottom of the weighing lysimeters is at 165 cm rather than at 293 cm. Therefore, below 153 cm, the node spacing is uniformly 2 cm down to 165 cm, which represents the bottom of the weighing lysimeter. For all simulations, node depths within the silt loam layer were the same (Table 5.2).

5.2.2 Soil Properties

The silt loam material was excavated from a 5-m-thick sediment deposit located about 10 km west of the lysimeter facility. The weathered portions of the sediments are generally classified as coarse-silty, mixed, mesic Xerollic

TABLE 5.2. Simulation Node Depths

Node No.	Depth (cm)						
1	0.0	12	21.0	23	144.0	34	187.0
2	0.2	13	30.0	24	147.0	35	210.0
3	0.4	14	45.0	25	149.0	36	235.0
4	0.7	15	60.0	26	151.0	37	259.0
5	1.2	16	75.0	27	153.0	38	272.0
6	2.0	17	90.0	28	157.0	39	279.0
7	3.0	18	105.0	29	159.0	40	284.0
8	4.5	19	120.0	30	161.0	41	288.0
9	7.0	20	129.0	31	163.0	42	291.0
10	10.5	21	135.0	32	167.0	43	293.0
11	15.0	22	140.0	33	175.0	--	--

Camborthids. The sands are commercially available materials. More than 90% of the particles of No. 8 sand fall between sieve sizes of 1 and 2 mm. More than 90% of the particles of 20/30 sand fall between sieve sizes of 0.25 and 1.0 mm.

Soil water retention was described using the van Genuchten (1978) model

$$\theta = \theta_r + (\theta_s - \theta_r) [1 + (\alpha h)^n]^{-m} \quad (5.1)$$

where the subscripts s and r refer to the saturated and residual values and α , n, and m are curve-fitting parameters. The parameter m was assumed to equal $1 - 1/n$. Hydraulic conductivity was described using Equation (5.1) and the Mualem (1976b) conductivity model

$$K = K_s \{1 - (\alpha h)^{n-1} [1 + (\alpha h)^n]^{-m}\}^2 [1 + (\alpha h)^n]^{-2m} \quad (5.2)$$

where ℓ is the pore interaction term, which was assumed to equal 0.5.

The silt loam parameters were fitted to laboratory desorption data determined for this soil using the hanging water column, pressure plate, and

vapor adsorption methods (Gee et al. 1989). The predicted conductivities agreed reasonably with values measured in the suction range from 0 to 200 cm using the steady-state flux control method (Klute and Dirksen 1986).

Hydraulic data for the sand and gravel were unavailable. Because preliminary simulations revealed that the model was relatively insensitive to their hydraulic properties, we described the sand and gravel using proxy data. Sand parameters were fitted to a combination of retention and conductivity data for two sand separates that were numbered 4141 and 4142 in Mualem (1976a). The particle sizes of the sand separates ranged from 0.5 to 1.0 mm and 0.25 to 0.5 mm in diameter, respectively. The gravel parameters were fitted to the estimated gravel properties reported by Fayer et al. (1985), whose predicted gravel conductivities were similar to measured values reported by Miller and Bungler (1963). All fitting was conducted with the RETC computer program (van Genuchten 1985).

The parameters used to describe the desorption properties of each material are listed in Table 5.3. Unless noted, all simulations were conducted with the desorption properties. Included in Table 5.3 are sorption parameters for the silt loam. These parameters were determined using a set of retention data that were collected as lysimeters D9 and D11 were wetted until breakthrough occurred. All of the hydraulic property functions are shown in Figure 5.2. In the simulations, values for internodal conductivities were calculated using the geometric mean.

5.2.3 Initial Conditions

The lysimeters were completely filled during June 1987 and covered with plastic until 4 November 1987. The first day simulated was 5 November.

The initial water contents of nodes representing the silt loam layer in each lysimeter were derived from neutron probe readings taken on 4 November 1987 at 15-cm depth intervals from 15 to 135 cm below the soil surface. Water contents above the 15-cm depth were set equal to the neutron probe reading at the 15-cm depth. Water contents below the 135-cm depth were set equal to the neutron probe reading at the 135-cm depth. Measurement error above 15 cm and below 135 cm was considered negligible because the water content profiles

TABLE 5.3. Parameters for Describing Hydraulic Properties with the van Genuchten and Mualem Functions
($m = 1-1/n$; $l = 0.5$)

Material	θ_r (cm^3/cm^3)	θ_s (cm^3/cm^3)	α ($1/\text{cm}$)	n	K_s (cm/h)
Silt loam:					
lab desorption	0.00	0.49600	0.01778	1.34411	4.032 ^(a)
field sorption	0.00	0.41144	0.04189	1.28772	3.240 ^(b)
Coarse sand	0.010	0.445	0.07255	2.80355	394.0
Pea gravel	0.005	0.419	4.93301	2.18628	1260.0

(a) Best-fitted value of saturated conductivity.

(b) Average of values determined in the field with a Guelph permeameter (Rockhold, Fayer, and Gee 1988).

measured between these two depths were fairly uniform and the surface of the lysimeters had been covered, preventing significant drying of the surface.

Water contents for nodes located between any two neutron probe readings were linearly interpolated. Given the initial water content at each node, the initial suction head value (relative to atmospheric datum) was determined using the soil water retention curves (Fig. 5.2a).

Water contents were not measured in the sand and gravel layers. To assign initial conditions for these layers, we simulated the redistribution of water in the lysimeters from early June 1987, when the sand and gravel layers were saturated and drained, till 4 November 1987. Initial water contents for all eight lysimeters are shown in Fig. 5.3.

5.2.4 Boundary Conditions

For modeling purposes, the two boundaries requiring specification are the bottom of the lysimeters and the soil surface. The bottom of the drainage lysimeters was 1.4 m below the silt loam layer. This distance was judged sufficient to represent this boundary as a unit gradient. In contrast, the bottom of the weighing lysimeters was only 0.2 m below the silt loam layer, too close to use a unit gradient boundary. Therefore, the bottom boundary of

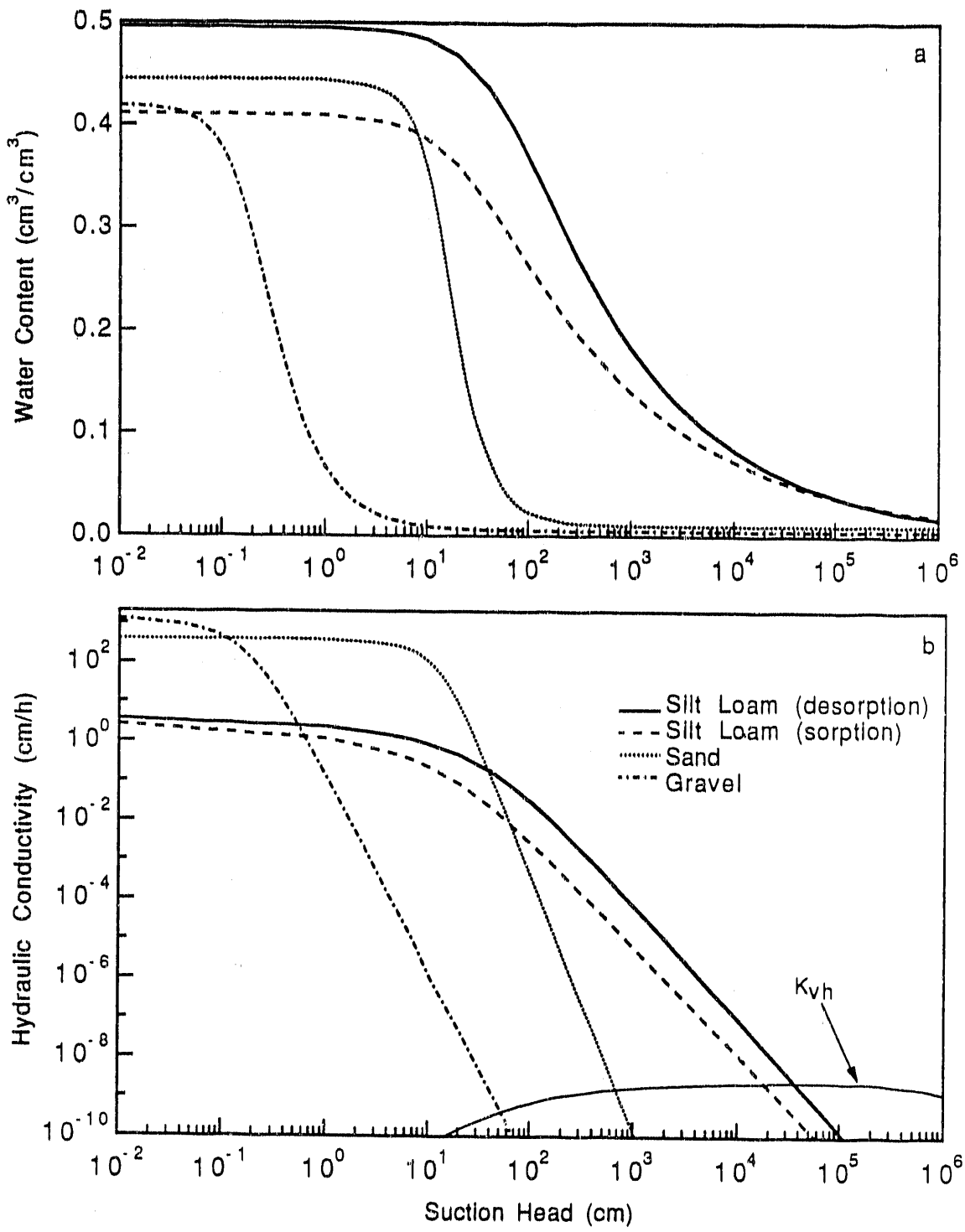


FIGURE 5.2. Soil Hydraulic Properties: Water Retention and Hydraulic Conductivity. The K_{vh} values for the silt loam at 15.3°C are included for comparison.

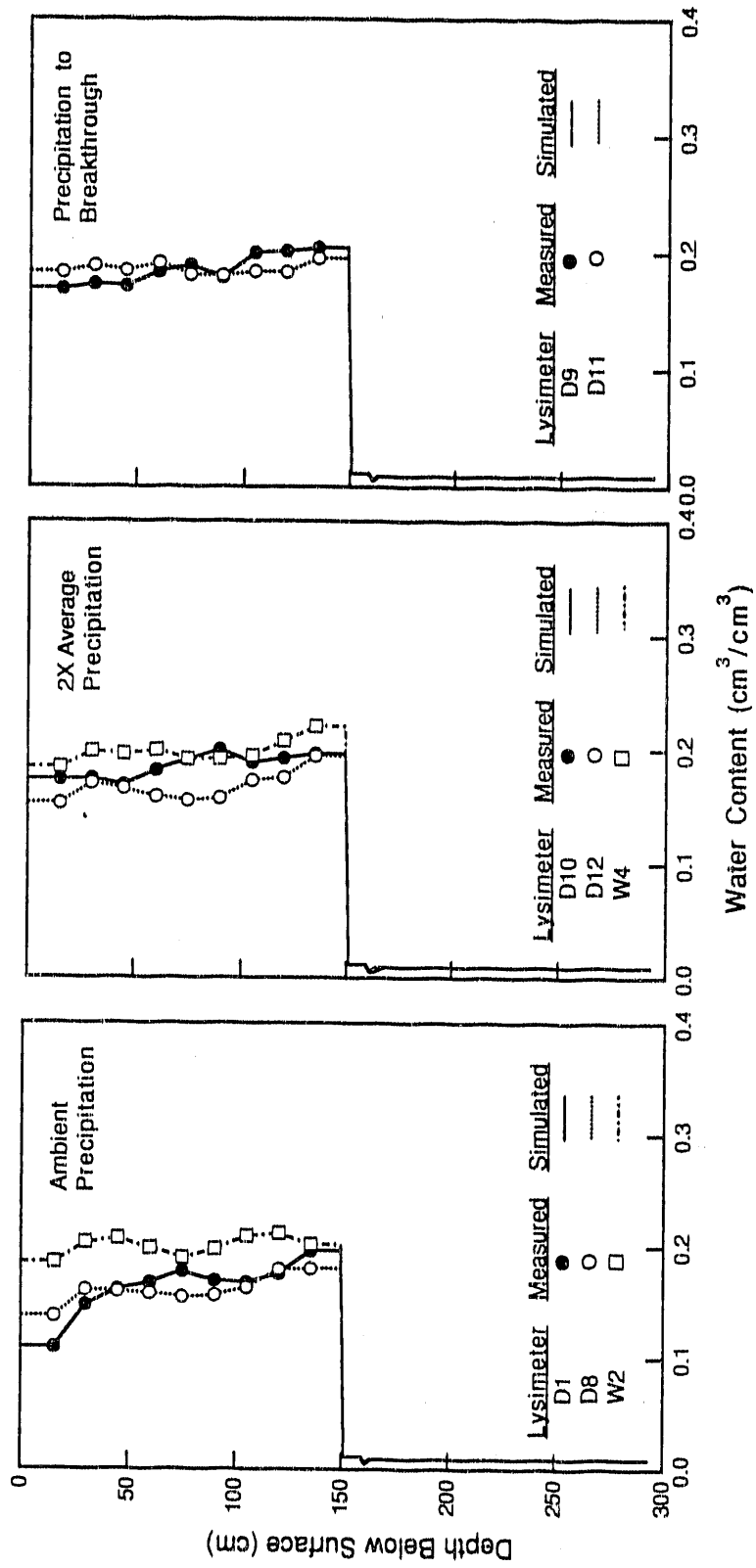


FIGURE 5.3. Initial Water Contents for All Lysimeters

the weighing lysimeters was represented as a zero-flux condition. This condition was appropriate for the weighing lysimeters because the simulated suction head of the bottom node never decreased to near zero, a condition necessary for drainage to occur.

The boundary at the soil surface was a function of the weather and irrigation treatment. The source of the weather data was the Hanford Meteorological Station (Stone et al. 1983), which is located about 200 m west of the lysimeter facility. Hourly precipitation data were used in the simulations (snow was assumed to melt immediately). In addition to natural precipitation, Columbia River water was added to the 2x average and breakthrough treatments using a rainulator. The rainulator consisted of a spray bar with six nozzles mounted on a carriage assembly that moved back and forth over the lysimeters. The nozzles dispersed water in a long, narrow elliptic pattern on the soil surface with 50% overlap (Gee et al. 1989). The addition of water was started at 0700 hours on the day of application at a rate (nominally 0.4 cm/h) less than the saturated conductivity. Cumulative precipitation for each of the three precipitation treatments is displayed in Fig. 5.4. The lysimeter design prevented runoff; thus, all precipitation and irrigation infiltrated.

Daily averages of the hourly meteorological data were converted to daily potential evapotranspiration values using the Penman equation of Doorenbos and Pruitt (1977). With no plants present, daily potential evaporation (PE) values were assumed to equal the daily potential evapotranspiration values. For the time when lysimeters D9 and D11 were covered (i.e., starting on 14 March 1988), the PE values were set to zero so that no evaporation occurred. Cumulative PE is displayed in Fig. 5.5 for the ambient and 2x average precipitation treatments, with and without a snow cover (explained in Section 5.3, Results) and for the precipitation to breakthrough treatment.

The daily PE value was distributed over the 24 hours of the day in the following manner. For the hours from 0600 to 1800, 88% of the daily PE value was assigned in proportion to the average annual receipt of solar radiation during each of those hours. For the 12 night hours, the remaining 12% of the daily PE value was distributed evenly. The value of h_{\max} was specified as 10^6 cm of water.

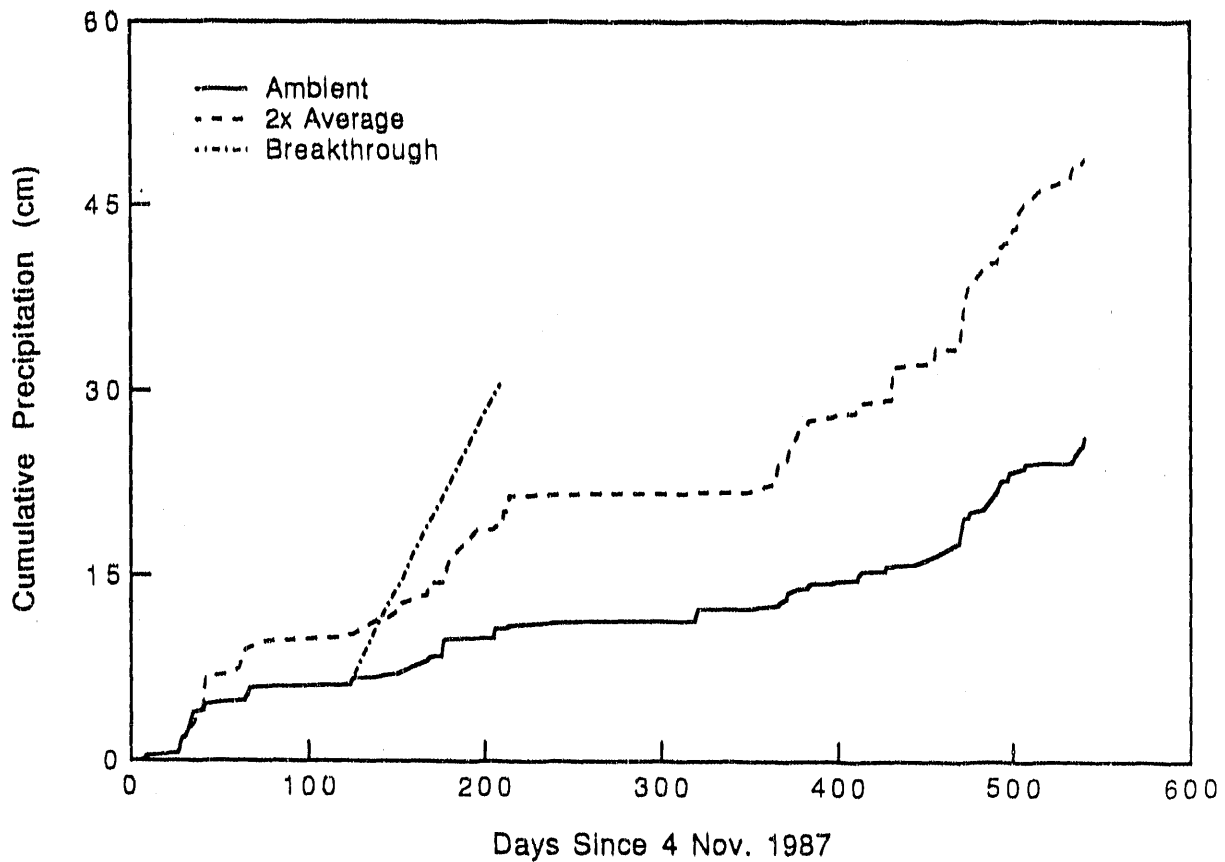


FIGURE 5.4. Cumulative Precipitation for Each of the Three Precipitation Treatments

5.2.5 Simulation Controls

The maximum size of the time steps was specified as 1.0 h to match the hourly precipitation data. Time steps were permitted to vary between 10^{-8} and 1.0 h, depending on the mass balance error. The mass balance error was calculated as the difference between the change in storage of water within the soil minus the net flux of water into the profile. If the error was less than the limit of 10^{-4} cm, the size of the next time step was increased by up to a factor of 2.0. If the error was greater than the limit, the time step was reduced by a factor of no less than 0.5. On average, the simulations required 44 steps per day. The majority of days required only 24 steps; days with precipitation required as many as 350 steps.

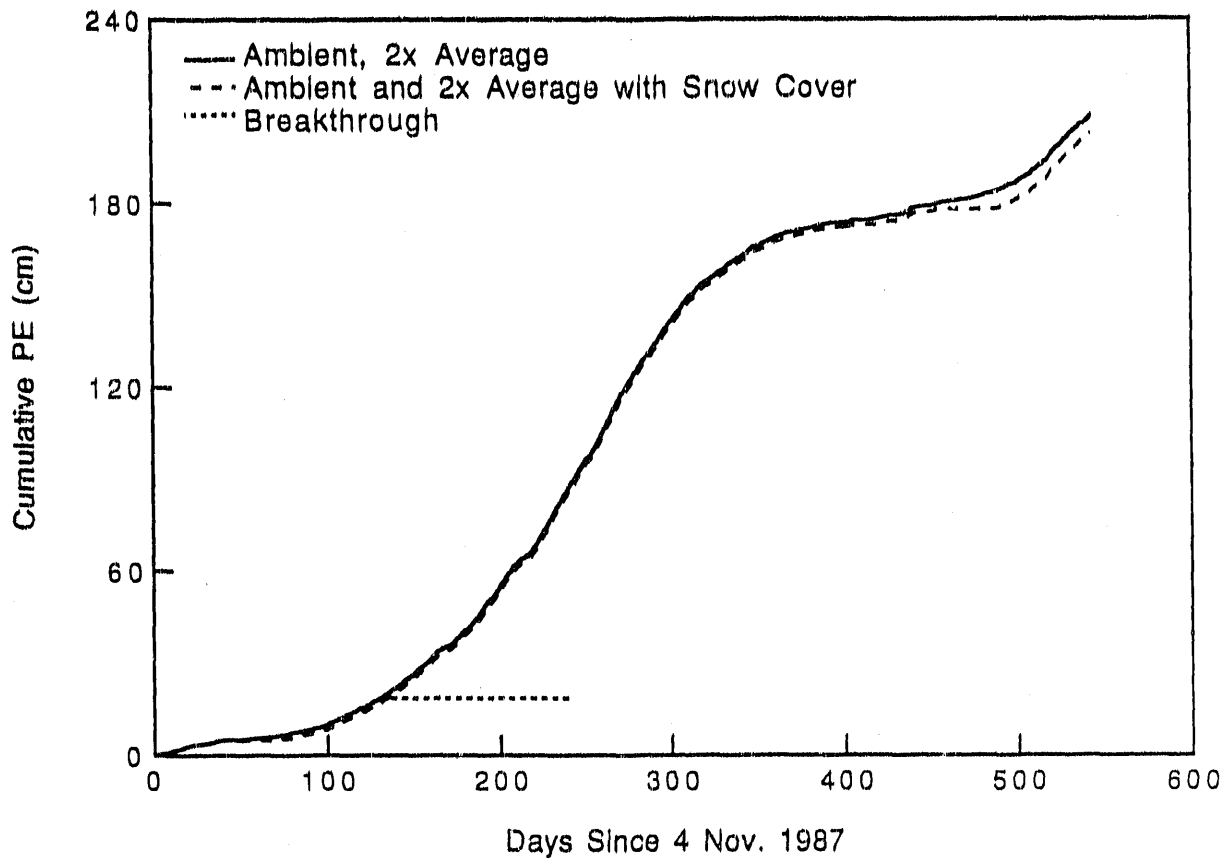


FIGURE 5.5. Cumulative Potential Evaporation for the Ambient and 2x Average Precipitation Treatments Without and With a Snow Cover and the Precipitation to Breakthrough Treatment

5.3 RESULTS

5.3.1 Ambient Precipitation Treatment

On 2 November 1988, the measured water content profiles were the driest since the lysimeters were installed. After that date, the measured water content profiles were the wettest on 14 March 1989. Except for the upper 50 cm of the profile on 14 March 1989, the simulated water contents on these dates were within $0.023 \text{ cm}^3/\text{cm}^3$ of the measured values (Fig. 5.6). On 14 March 1989, the simulations show a pulse of water that is smaller and higher in the profile than measured.

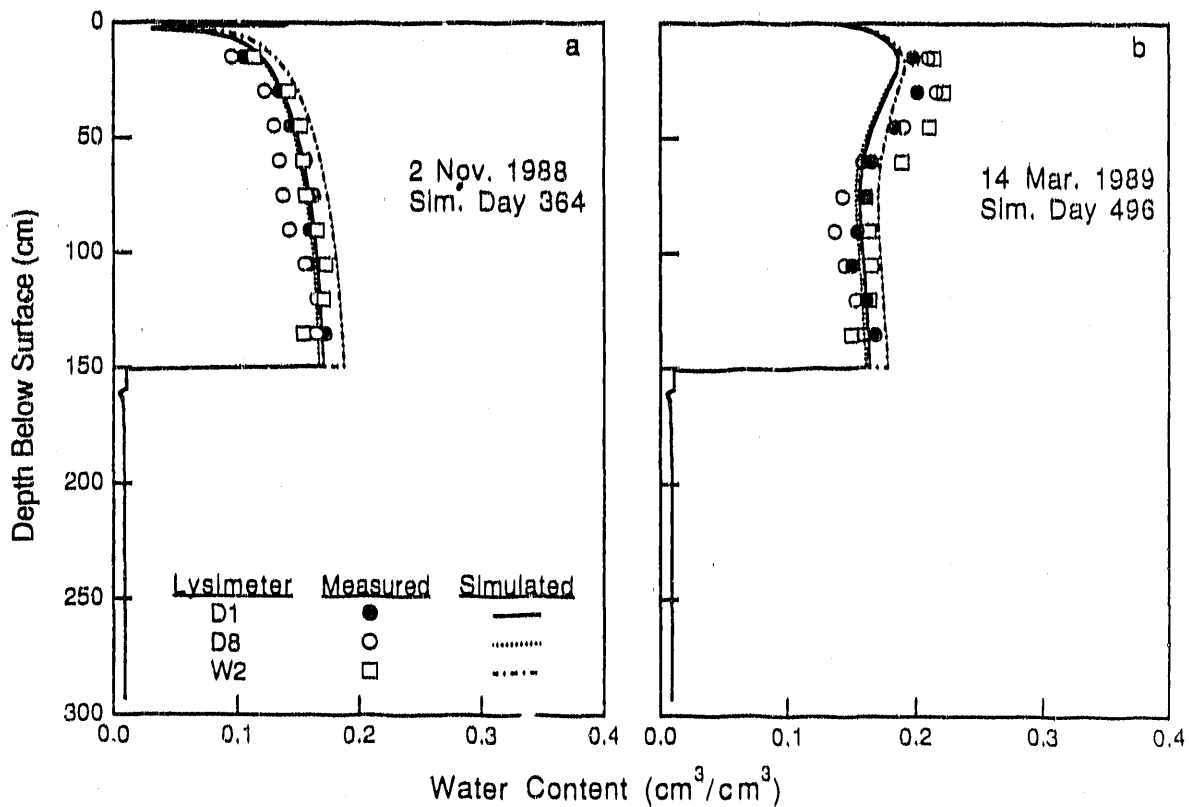


FIGURE 5.6. Measured and Simulated Water Contents for the Ambient Precipitation Treatment on 2 November 1988 and 14 March 1989

At each depth among the three lysimeters, the simulated water contents on 14 March 1989 are within $0.015 \text{ cm}^3/\text{cm}^3$ of each other, despite initial differences as large as $0.076 \text{ cm}^3/\text{cm}^3$. At the soil-sand interface, the simulated flux was upward during the entire simulation period. No measurable drainage occurred from these lysimeters.

Figure 5.7 shows that during both winters storage increased, whereas during the summer storage decreased. This pattern is typical of the Hanford Site, which receives 52% of its precipitation in the months of November through February, and 40% of that in the form of snow. Compared to the measured changes, the simulated storage changes were less during all seasons. This result indicates that more evaporation is simulated in the winter and

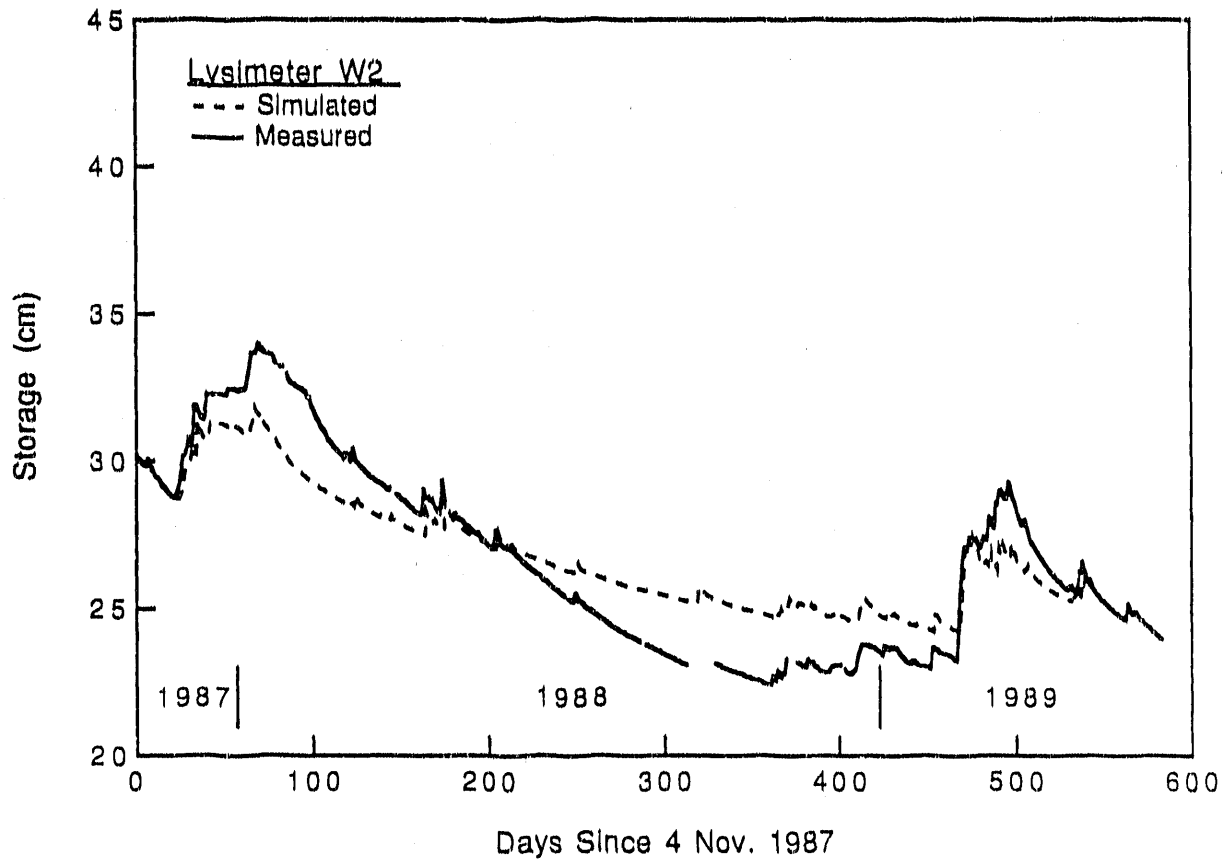


FIGURE 5.7. Measured and Simulated Storage for the Ambient Precipitation Treatment, Lysimeter W2

less evaporation during the remainder of the year than actually occurs. A comparison of predicted versus measured daily storage values yielded a root-mean-square error of 1.47 cm.

5.3.2 2x Average Precipitation Treatment

Figure 5.8 shows that the simulated water contents on 2 November 1988 are as much as $0.038 \text{ cm}^3/\text{cm}^3$ higher than measured, whereas on 14 March 1989, most of the simulated water contents are as much as $0.045 \text{ cm}^3/\text{cm}^3$ lower than measured. Immediately above the soil-sand interface, simulated water contents are as much as $0.067 \text{ cm}^3/\text{cm}^3$ less than measured.

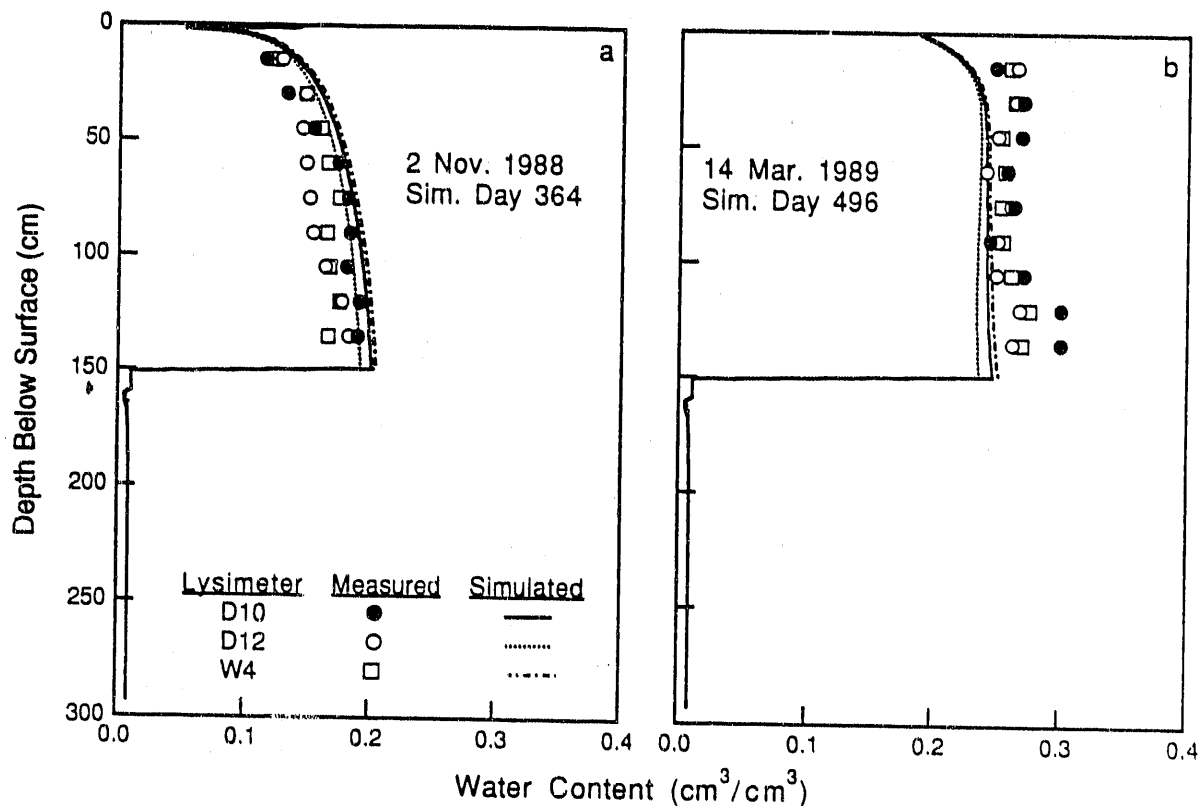


FIGURE 5.8. Measured and Simulated Water Contents for the 2x Average Precipitation Treatment on 2 November 1988 and 14 March 1989

At each depth among the three lysimeters, the simulated water contents on 14 March 1989 are within 0.015 cm³/cm³ of each other, despite initial differences as large as 0.040 cm³/cm³. The simulated flux at the soil-sand interface was upward until 7 January 1989. After that date, the downward flux into the sand reached its highest value (0.0087 cm/yr) on 11 March 1989. The simulated flux at the sand-gravel interface was upward at all times. Similar to the ambient treatment, no measurable drainage occurred from these lysimeters.

Similar to the ambient treatment, measured storage increased during both winters and decreased during the summer, and the simulated storage changes are

smaller than the measured changes throughout the simulated period (Fig. 5.9). This result provides additional evidence that UNSAT-H is simulating more evaporation in the winter and less evaporation during the remainder of the year than actually occurs. A comparison of predicted versus measured daily storage values yielded a root-mean-square error of 2.21 cm.

Additional simulations of lysimeter W4 were conducted to ascertain model sensitivities that might explain the difference between measured and simulated storage. In separate simulations, the value of h_{max} was set to 15,300 cm, historically known as the wilting point for plants, and calculated each day as

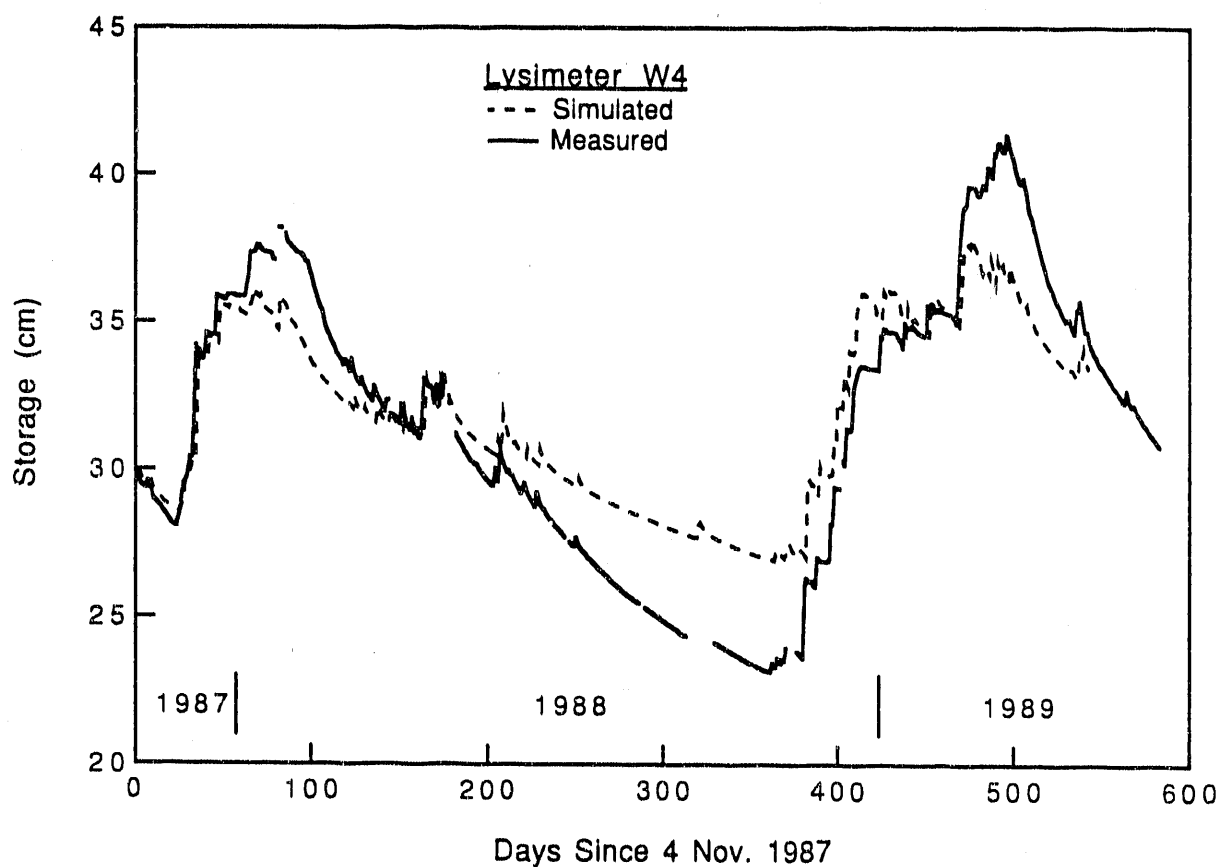


FIGURE 5.9. Measured and Simulated Storage for the 2x Average Precipitation Treatment, Lysimeter W4

a function of the mean daily air temperature and vapor density. Neither change resulted in a storage difference greater than 0.5 cm from the original simulation (Fig. 5.9).

Another possibility for the discrepancy between measured and simulated storage values is temperature. For a sandy loam soil, Constantz (1982) reported a hundredfold increase in hydraulic conductivity at a water content of $0.3 \text{ cm}^3/\text{cm}^3$ when the temperature was increased from 2 to 45°C . For a water content of $0.2 \text{ cm}^3/\text{cm}^3$, he observed a tenfold increase in conductivity for the same temperature increase. The values of liquid conductivity (K_L) and isothermal vapor conductivity (K_{vh}) were individually adjusted within the entire silt loam layer according to the mean air temperature for each day. For K_L , we used the standard viscosity correction that Hopmans and Dane (1986) determined to be appropriate for soil. For K_{vh} , we made the soil's saturated vapor density (ρ_{vs}) and relative humidity (RH) (see Eq. [8] of Fayer and Jones 1990) functions of the air temperature. Both K_L and K_{vh} changes resulted in storage differences of less than 0.1 cm from the original simulation. Although temperature also affects water retention (Constantz 1982; Nimmo and Miller 1986), we did not test that effect for this report.

Sensitivity tests that indicated important effects involved variations in K_s and ℓ , the presence of a snow cover, and a reduction in PE. The effects of each change are described below.

Saturated Conductivity

During the curve-fitting process for the silt loam, 95% confidence intervals for the fitted value of K_s were generated using the RETC code (van Genuchten 1985). The values encompassing the lower and upper intervals are 2.16 and 5.76 cm/h, respectively, or approximately 1.8 cm/h about the mean value. In terms of K_s , these values represent $0.54 K_s$ and $1.43 K_s$, respectively. The results in Fig. 5.10 show that the value of $0.54 K_s$ allowed for increased storage (i.e., reduced evaporation) during all months; the value of $1.43 K_s$ allowed for decreased storage (i.e., increased evaporation) during all months.

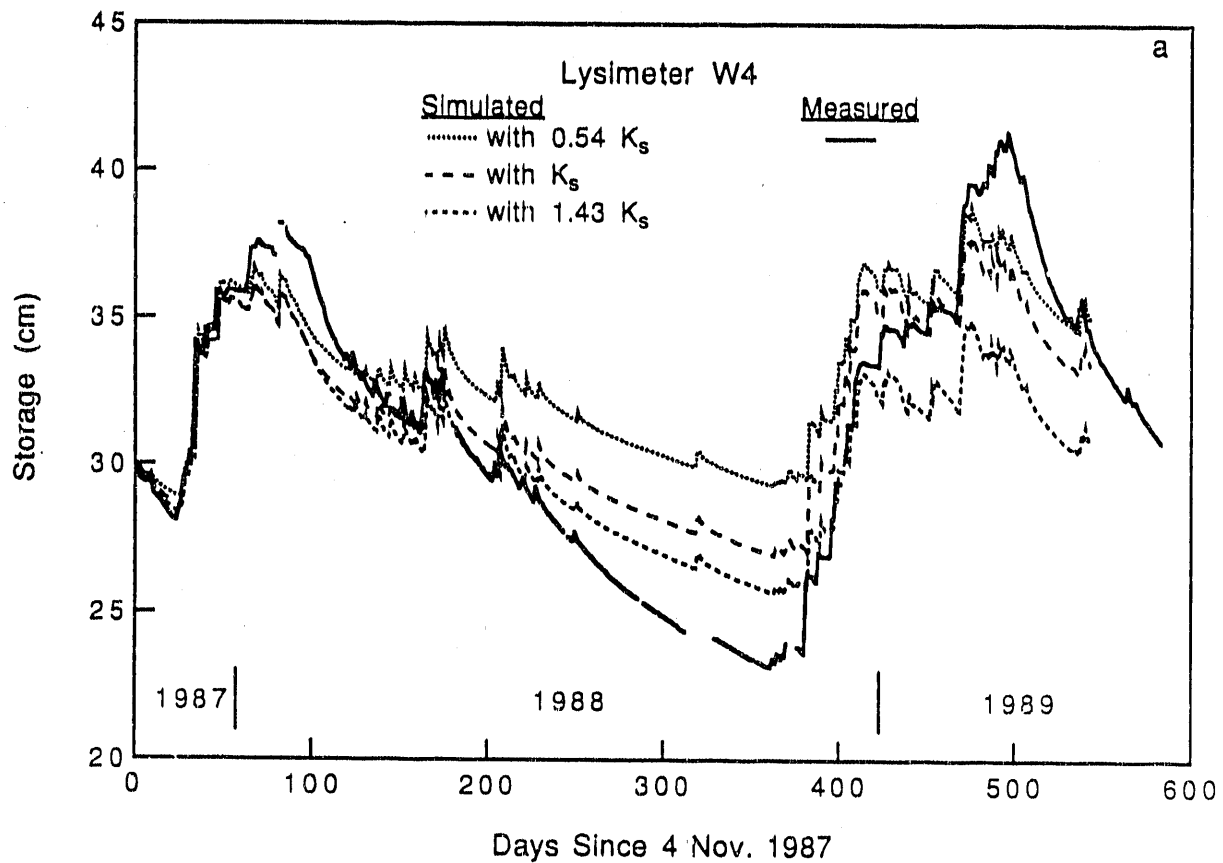


FIGURE 5.10. Measured and Simulated Storage for the 2x Average Precipitation Treatment, Lysimeter W4, Showing the Effects of a) 95% Confidence Intervals for K_s , b) $\ell = 0$, c) Snow Cover, and d) 0.7 PE

Pore Interaction Term

Having no measured values of K_L under dry conditions to guide the selection of an appropriate value for the pore interaction term, ℓ , we decided to explore the effect of a value of zero, i.e., no pore interaction. In Figure 2 of Mualem (1976a), an ℓ [corresponding to n (Mualem 1976a)] value of zero was nearly as valid as the value of 0.5 reported to be the best average value for a variety of soils. A lower value of ℓ yields a higher value of K_L (progressively more so as the soil dries), which increases evaporation. Thus, with $\ell = 0$, simulated storage decreased (i.e., evaporation increased) by 2.5 cm during the period from late spring to early fall of 1988 but did not change

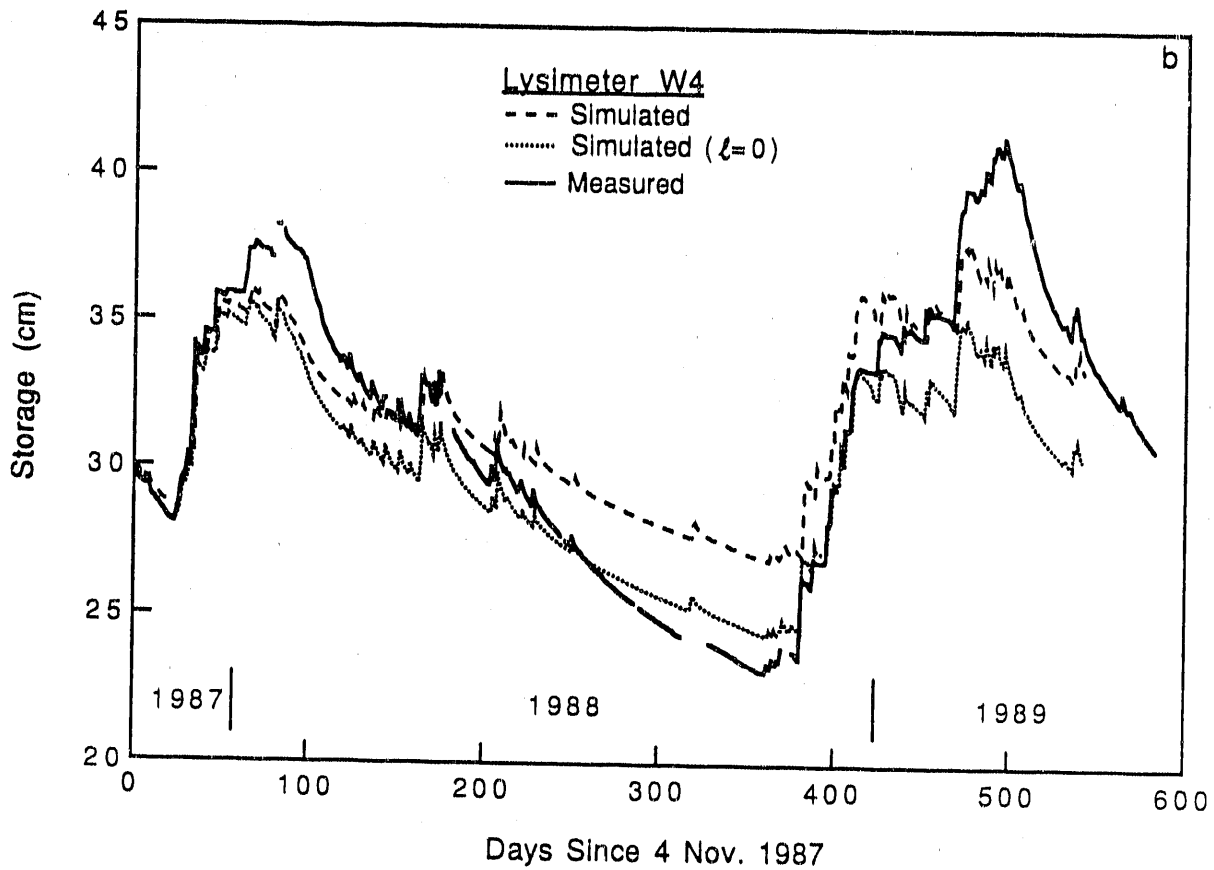


FIGURE 5.10. (contd)

appreciably during the two winters (Fig. 5.10). The reason for the seasonal effect is that the winter water contents were sufficiently high that K_L values were minimally affected by the change in l . In contrast, in the summer, water contents were sufficiently low that K_L was significantly affected by the change in l .

Snow Cover

During each winter, a snow cover persisted for several weeks (Table 5.4). During that time, the model simulated more evaporation than was measured. The high albedo of snow can significantly reduce PE. In addition to the snow

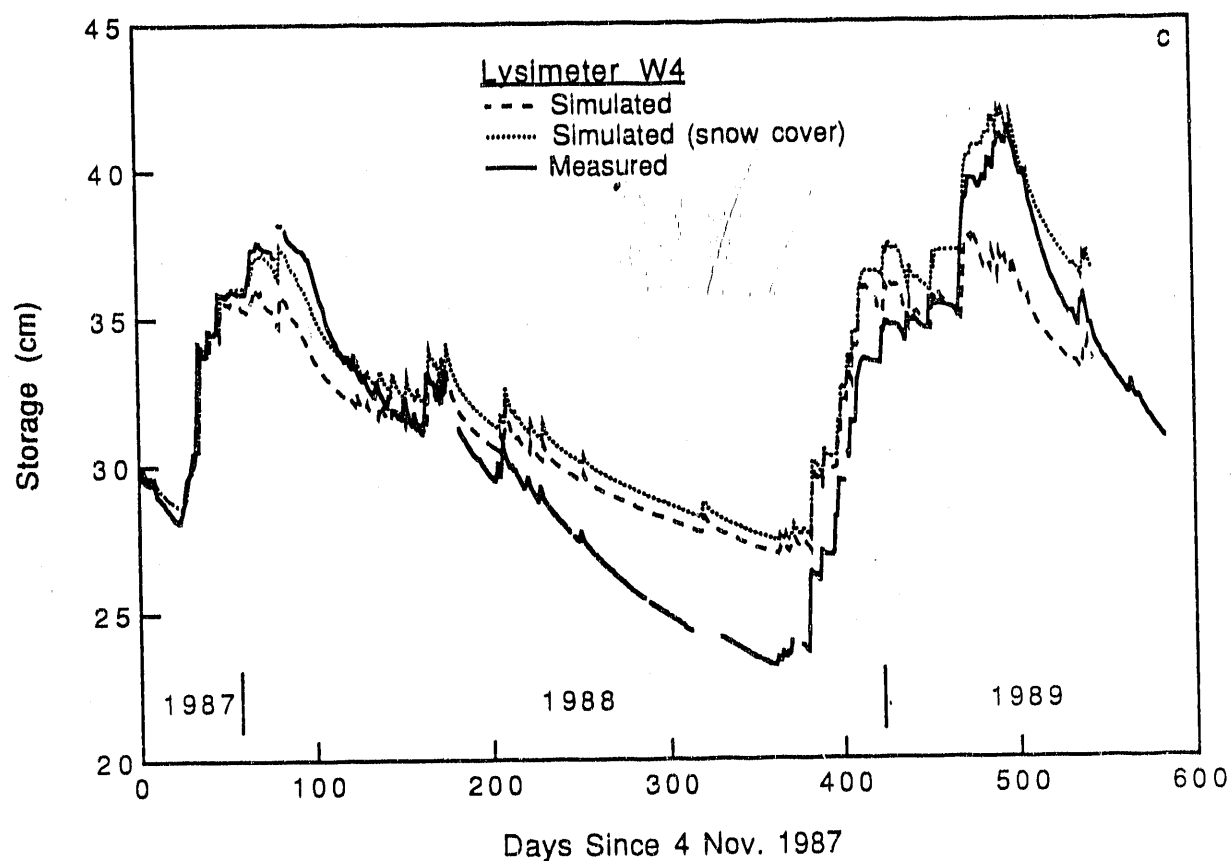


FIGURE 5.10. (contd)

cover, average daily soil temperatures measured with thermocouples in lysimeters W2 and W4 indicated that the 0°C isotherm reached the 10-cm depth during the 1987-1988 winter and the 50-cm depth during the 1988-1989 winter. Frozen soil impedes evaporation by reducing water flow to the evaporative surface from below and by reducing the vapor density at the surface, thus lowering the gradient that drives evaporation.

Although not explicitly included in the model, a snow cover was approximated by setting PE = 0 for the snow cover periods in Table 5.4 (the effect of soil freezing could have been roughly approximated in the same manner). This reduction in PE amounted to 6.3 cm, which represents about 3% of the total PE

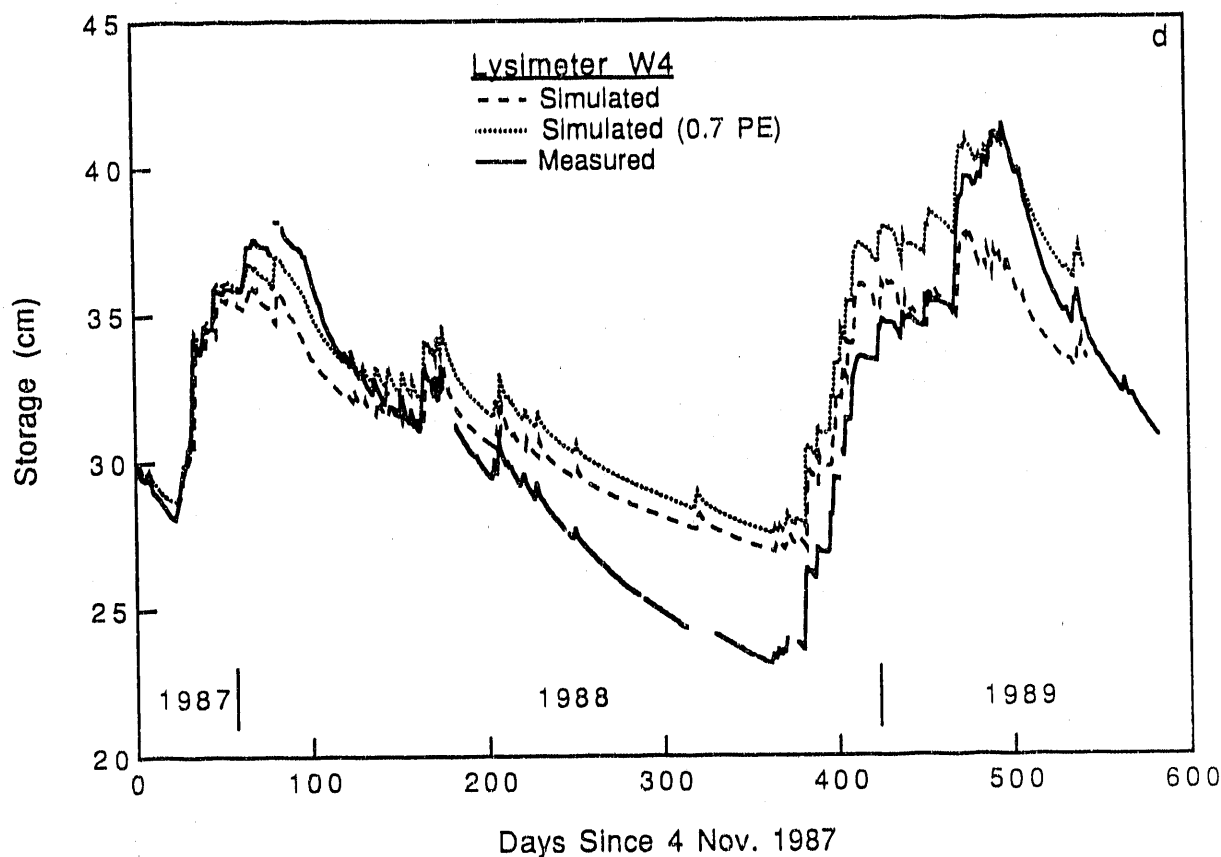


FIGURE 5.10. (contd)

TABLE 5.4. Periods of Extended Snow Cover and Mean Daily Air Temperature Equal to or Below 0°C

Simulation Days	Snow Cover		Mean Air Temperature Equal To or Below 0°C		
	Starting Date	Ending Date	Simulation Days	Starting Date	Ending Date
42 to 72	16 Dec 87	15 Jan 88	39 to 68	13 Dec 87	10 Jan 88
411 to 422	19 Dec 88	30 Dec 88	408 to 420	16 Dec 88	28 Dec 88
455 to 488	1 Feb 89	6 Mar 89	455 to 466	1 Feb 89	12 Feb 89

for the simulation. Sublimation and the redistribution of water in response to soil freezing were assumed to be negligible. The results in Fig. 5.10 show that storage increased 2.0 cm in the first winter and 5.0 cm in the second

winter relative to the original simulation (Fig. 5.9). The effects of the increased storage in winter persisted through the summer in the form of slightly higher storage, on the order of 0.5 cm. A similar response was noted for simulations of lysimeter W2.

Potential Evaporation

Knowing that the model was overpredicting evaporation in the winter, particularly when air temperatures are $\leq 0^{\circ}\text{C}$ (Table 5.4), and that the Penman equation in Doorenbos and Pruitt (1977) has not been tested at the Hanford Site, we elected to reduce PE by 30% (i.e., 0.7 PE). The lower PE resulted in less simulated evaporation in the months from late fall to early spring (Fig. 5.10). Very little difference in evaporation was observed during the period from late spring to early fall. Subsequent review of the results showed that evaporation during these times was rarely at the PE rate, whereas the winter evaporation rates were often at PE rates, thus explaining why reduced PE had the greatest effect during winter.

Example Calibration

To demonstrate the potential for calibrating the model to match the data, we conducted a final simulation of lysimeter W4 using 1.43 K_s , ℓ equal to zero, a snow cover, and 0.7 PE. The result in Fig. 5.11 shows that the model can be calibrated to significantly improve the match with the measured storage values. The root-mean-square error was 0.81 cm, which represents a 63% reduction from the original simulation in Fig. 5.9.

5.3.3 Precipitation to Breakthrough Treatment

Simulations using the silt loam desorption curve produced higher water contents at the 30-cm depth and lower water contents (by as much as $0.089 \text{ cm}^3/\text{cm}^3$) at the 135-cm depth than measured (Fig. 5.12). By 30 June 1988, the suction head at the sand-gravel interface had been lowered to 64 cm, a value at which a significant flux (i.e., 0.05 cm/yr) cannot enter the gravel. Given the high suction at the interface, these simulations with the desorption curve produced no drainage from the lysimeters.

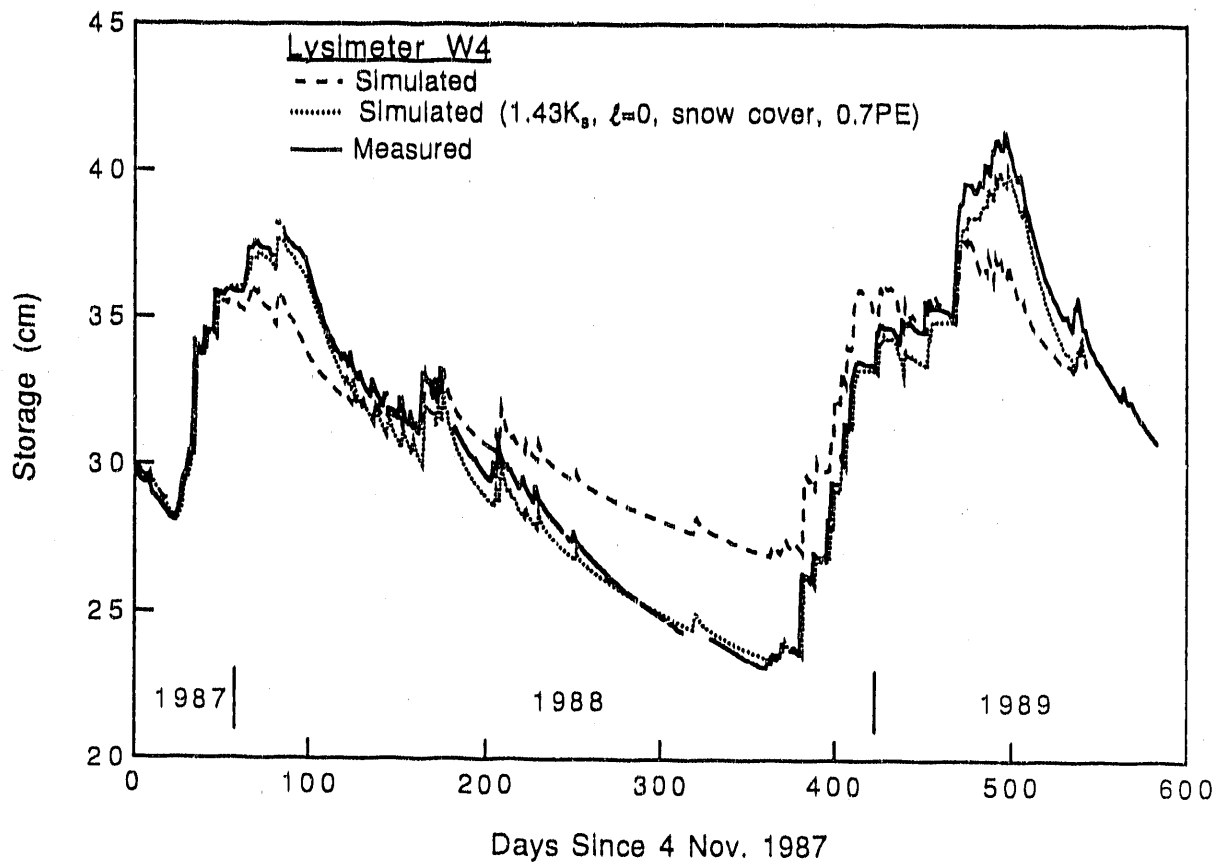


FIGURE 5.11. Measured and Simulated Storage for the 2x Average Precipitation Treatment, Lysimeter W4. Shown are the original simulation and the simulation with 1.43 K_s , $l = 0$, a snow cover, and 0.7 PE

The simulations were repeated using the silt loam sorption curve, assuming that this curve better represented the soil water status during the period after the lysimeters were covered on 14 March 1988 and wetted to breakthrough. Before being covered, these lysimeters were subjected to precipitation and evaporation that likely caused the water status in the silt loam to cycle along scanning curves between the main wetting and drying curves. For this series of simulations, however, the silt loam was assumed to be on the sorption branch only. The results were intended to demonstrate the importance of hysteresis in soil water retention to modeling of the protective barrier.

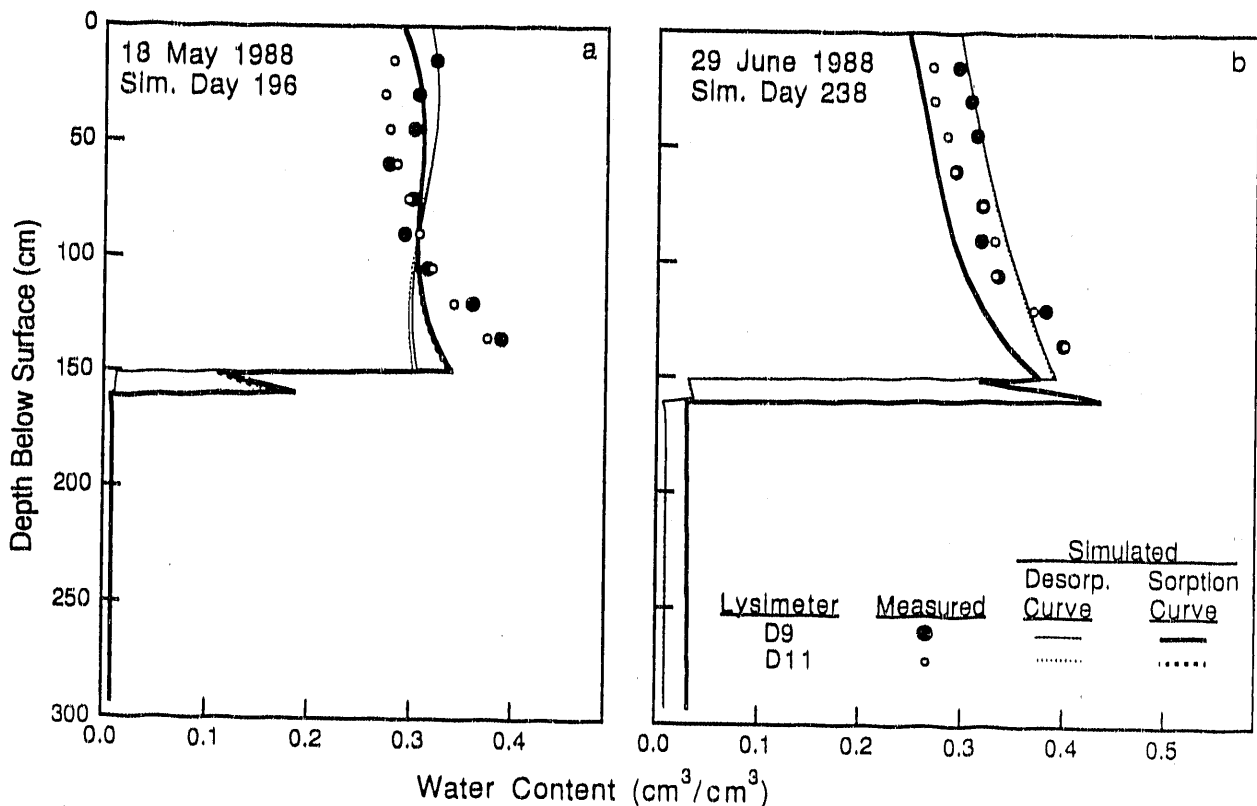


FIGURE 5.12. Measured and Simulated Water Contents for the Precipitation to Breakthrough Treatment on 18 May 1988 and 29 June 1988

Simulations with the sorption curve produced water content profiles that were in slightly better agreement with the measurements on 18 May 1988 than the simulations with the desorption curve (Fig. 5.12a). The maximum difference from the measurements on that date was $0.061 \text{ cm}^3/\text{cm}^3$ at the 135-cm depth. On 29 June 1988, the simulated water contents were all less than measured (and less than those simulated with the desorption curve), with the maximum difference from the measurements again being $0.061 \text{ cm}^3/\text{cm}^3$ at the 135-cm depth (Fig. 5.12b).

In the simulations, the onset of significant water movement (i.e., $>0.05 \text{ cm/yr}$) into the sand layer occurred around Day 168 (20 April 1988), when suction heads at the silt loam-sand interface decreased below 260 cm. Storage in the 0- to 165-cm-depth range (equivalent to the depth of the weighing

lysimeters) was 40.0 cm at this time. The onset of significant water movement into the gravel layer occurred around Day 186 (8 May 1988), when suction heads at the sand-gravel interface decreased below 60 cm. Storage in the 0- to 165-cm-depth range was 43.9 cm at this time. Toward the end of the simulations, when drainage was occurring, the suction heads at the silt loam-sand and sand-gravel interfaces were approximately 13 and 3 cm, respectively. The measurements of suction head at the silt loam-sand interface ranged between 2 and 8 cm during the same period.

The results in Fig. 5.13 show that simulated drainage appeared 11 to 12 days after measured drainage, which is acceptable given the 239-day duration of these simulations. The measured drainage values were 1.15 and 0.62 cm from lysimeters D9 and D11, respectively, on 28 June 1988. Use of the sorption curve for the silt loam resulted in simulated drainage of 1.51 and 1.31 cm.

The sensitivity of simulated drainage to uncertainty in the field-saturated conductivity value, K_{fs} , was evaluated using variations of 1.8 cm/h about the K_{fs} value. This variation represented the size of the confidence interval calculated during curve fitting of the laboratory desorption data. Although not based on field data, the variation is sufficient to demonstrate sensitivity. The results showed that using 1.56 K_{fs} for the silt loam caused drainage to occur three days earlier than when using K_{fs} . In contrast, using 0.56 K_{fs} delayed the start of drainage by 11 days in lysimeter D9 and resulted in no drainage from lysimeter D11 (although, if the simulations were continued 1 to 2 more days, drainage would surely have occurred). Using 1.56 K_{fs} , the simulated drainage values from lysimeters D9 and D11 were 1.98 and 1.77 cm, respectively. Using 0.56 K_{fs} , the simulated drainage values were zero. For the two lysimeters, the simulated drainage values bracket the measured values. These results demonstrate the sensitivity of cumulative drainage to just one soil hydraulic parameter.

5.4 DISCUSSION AND SUMMARY

A summary of the water balance parameters for every simulation is given in Table 5.5. In several cases, the simulation of small amounts of drainage

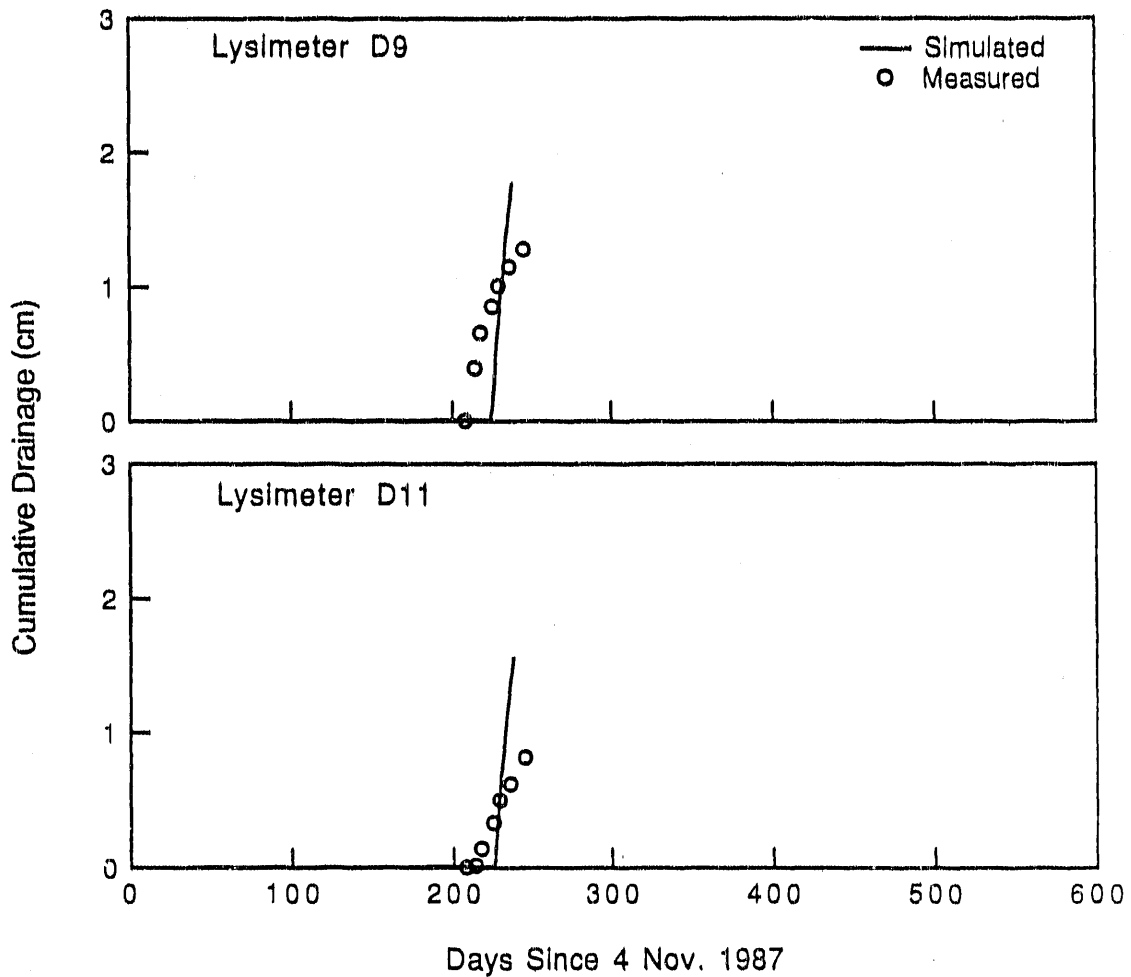


FIGURE 5.13. Measured and Simulated Drainage for the Precipitation to Breakthrough Treatment Using the Silt Loam Sorption Curve

(e.g., 0.01 to 0.02 cm) reflects the effect of initial matric potential values of -10 cm in the gravel along with a unit gradient condition at the bottom boundary. This drainage did not originate from the silt loam layer.

Comparisons of simulation results show that differences in initial conditions of as much as $0.017 \text{ cm}^3/\text{cm}^3$ were reduced to $< 0.001 \text{ cm}^3/\text{cm}^3$ by 29 June 1988 within the silt loam and sand layers of the two lysimeters. As with the other treatments, the simulations within the breakthrough treatment

TABLE 5.5. Summary of Water Balance Parameters for Each Simulation

Lysimeter	Precipitation Treatment	Total H ₂ O Added (cm)	Evaporation (cm)	Final Storage (cm)	Drainage (cm)	Mass Balance Error (cm)
D1	Ambient	26.19	26.58	25.27	0.02	0.031
D8	Ambient	26.19	26.66	24.93	0.02	0.029
W2	Ambient	26.19	30.66	25.68	0.00	-0.005
D10	2x Average	55.28	50.13	34.22	0.02	0.009
D12	2x Average	55.13	48.10	33.49	0.02	0.021
W4	2x Average	54.65	51.20	33.41	0.00	-0.002
W4 ^(a)	2x Average	54.65	52.89	31.72	0.00	-0.006
W4 ^(b)	2x Average	54.65	48.53	36.06	0.00	0.013
W4 ^(c)	2x Average	54.65	54.18	30.43	0.00	-0.010
W4 ^(d)	2x Average	54.65	48.16	36.46	0.00	-0.012
W4 ^(e)	2x Average	54.65	48.14	36.48	0.00	-0.022
W4 ^(f)	2x Average	54.65	51.19	33.46	0.00	-0.049
D9	Breakthrough	30.50	7.53	52.12	0.01	0.011
D9 ^(g)	Breakthrough	30.50	6.52	51.34	1.76	0.048
D9 ^(g,h)	Breakthrough	30.50	6.91	50.51	2.19	0.045
D9 ^(g,i)	Breakthrough	30.50	6.03	53.33	0.26	0.045
D11	Breakthrough	30.50	7.84	51.88	0.01	0.006
D11 ^(g)	Breakthrough	30.50	6.81	51.34	1.55	0.042
D11 ^(g,h)	Breakthrough	30.50	7.21	50.51	1.98	0.039
D11 ^(g,i)	Breakthrough	30.50	6.27	53.33	0.01	0.039

- (a) Simulated with 1.43 K_s.
 (b) Simulated with 0.54 K_s.
 (c) Simulated with a snow cover.
 (d) Simulated with $\ell = 0$.
 (e) Simulated with 0.7 PE.
 (f) Simulated with 1.43 K_s, $\ell = 0$, snow cover, and 0.7 PE.
 (g) Simulated with sorption curve for silt loam.
 (h) Simulated with 1.43 K_s.
 (i) Simulated with 0.54 K_s.

converged toward a single solution, indicating that initial conditions become less important when simulating longer durations. In contrast, measured water contents at specific depths for the conditions of a given treatment do not converge on a single value, as do the simulations. This result suggests that the lysimeters have some degree of heterogeneity in hydraulic properties despite attempts to fill them uniformly. Whether the degree of heterogeneity is sufficient to significantly affect the simulation results, if given information on the heterogeneity, remains to be tested.

Without any calibration to field data, the UNSAT-H model reproduced much of the water balance changes that were observed in the field. Differences between measured and simulated values of water content and storage were largest in winter (when evaporation was overpredicted) and summer (when evaporation was underpredicted). Sensitivity tests demonstrated the importance of the hydraulic conductivity function (specifically, K_s and ℓ), snow cover, and potential evaporation to successful modeling of storage in a protective barrier. When these parameters and processes were adjusted (though not optimized), the root-mean-square error for the 2x average treatment was reduced by 63%. This result suggests that a more rigorous calibration in the future will likely reduce the error further.

For the breakthrough treatment, simulated drainage was obtained only by using field-measured sorption and saturated conductivity data. This result demonstrates that hysteresis is important to successful modeling of drainage through protective barriers. Hysteresis may also be important to successful modeling of evaporation. Using computer simulations, Hillel (1977) demonstrated that hysteresis suppresses evaporation. For the Gilat fine sandy loam, Hillel's results show a 5 to 17% reduction in cumulative evaporation over a 10-day period using scanning-loop transition between the primary sorption and desorption branches.

The results presented in this paper show how the uncalibrated model performed and indicate areas for model improvement. Subsequent work will be focused on unsaturated conductivity measurements at suction head values well above 200 cm of water, hysteresis, snow cover, frozen soil, and the calculation of potential evaporation. This work will include long-term comparisons

such as presented here as well as short-term comparisons using hourly data from the weighing lysimeters. Once all major processes operating within the barrier are identified and incorporated, parameters used to simulate the protective barrier will be optimized by calibrating with a subset of the available lysimeter data. We believe that additional measurements, model enhancements, and calibration can lead to the successful prediction of drainage rates as low as 0.05 cm/yr through layered soil in a semiarid climate.

6.0 REFERENCES

- Adams, M. R., and N. R. Wing. 1986. Protective Barrier and Warning Marker System Development Plan. RHO-RE-PL-35P, Rockwell Hanford Operations, Richland, Washington.
- Brutsaert, W. F. 1971. "A Functional Iteration Technique for Solving the Richards Equation Applied to Two-Dimensional Infiltration Problems." Water Resour. Res. 7(6):1583-1596.
- Campbell, G. S. 1985. Soil Physics with BASIC. Elsevier, New York.
- Constantz, J. 1982. "Temperature Dependence of Unsaturated Hydraulic Conductivity of Two Soils." Soil Sci. Soc. Am. J. 46:466-470.
- Davis, L. A., and S. P. Neuman. 1983. Documentation and User's Guide: UNSAT2 - Variably Saturated Flow Model. NUREG/CR-3390, prepared by Water, Waste and Land, Inc., Fort Collins, Colorado, for the U.S. Nuclear Regulatory Commission, Washington, D.C.
- DOE. See U.S. Department of Energy.
- Doorenbos, J., and W. O. Pruitt. 1977. Guidelines for Predicting Crop Water Requirements. FAO Irrigation Paper No. 24, 2nd ed., pp. 1-107, Food and Agricultural Organization of the United Nations, Rome, Italy.
- Fayer, M. J. 1987. Model Assessment of Protective Barrier Designs: Part II. PNL-6297, Pacific Northwest Laboratory, Richland, Washington.
- Fayer, M. J. 1990. Test Plan for Hydrologic Modeling of Protective Barriers. PNL-7152, Pacific Northwest Laboratory, Richland, Washington.
- Fayer, M. J., and T. L. Jones. 1990. UNSAT-H Version 2.0: Unsaturated Soil Water and Heat Flow Model. PNL-6779, Pacific Northwest Laboratory, Richland, Washington.
- Fayer, M. J., W. Conbere, R. R. Heller, and G. W. Gee. 1985. Model Assessment of Protective Barrier Designs. PNL-5604, Pacific Northwest Laboratory, Richland, Washington.
- Freeman, H. D., and G. W. Gee. 1989a. Hanford Protective Barriers Program Asphalt Barrier Studies - FY 1988. PNL-6874, Pacific Northwest Laboratory, Richland, Washington.
- Freeman, H. D., and G. W. Gee. 1989b. Hanford Protective Barriers Program: Status of Asphalt Barrier Studies - FY 1989. PNL-7153, Pacific Northwest Laboratory, Richland, Washington.

Freeman, H. D., G. W. Gee, and J. F. Relyea. 1989. Field Study Plan for Alternate Barriers. PNL-6840, Pacific Northwest Laboratory, Richland, Washington.

Gee, G. W., R. R. Kirkham, J. L. Downs, and M. D. Campbell. 1989. The Field Lysimeter Test Facility (FLTF) at the Hanford Site: Installation and Initial Tests. PNL-6810, Pacific Northwest Laboratory, Richland, Washington.

Glass, R. J., T. S. Steenhuis, and J. Y. Parlange. 1989. "Mechanism for Finger Persistence in Homogeneous, Unsaturated, Porous Media: Theory and Verification." Soil Science 148(1):60-70.

Gupta, S. K., K. K. Tanji, D. R. Nielsen, J. W. Biggar, C. S. Simmons, and J. L. MacIntyre. 1978. Field Simulation of Soil-Water Movement with Crop Water Extraction. Water Science and Engineering Paper No. 4013, Department of Land, Air, and Water Resources, University of California, Davis, California.

Healy, R. W. 1987. Simulation of Trickle Irrigation, an Extension to the U.S. Geological Survey's Computer Program VS2D. Water-Resources Investigations Report 87-4086, U.S. Geological Survey, Denver, Colorado.

Healy, R. W., and A. W. Warrick. 1988. "A Generalized Solution to Infiltration from a Surface Point Source." Soil Sci. Soc. Am. J. 52:1245-1251.

Hillel, D. 1977. Computer Simulation of Soil-Water Dynamics. International Development Research Center, Ottawa, Canada.

Hillel, D. 1980. Fundamentals of Soil Physics. Academic Press, New York.

Hillel, D., and R. S. Baker. 1988. "A Theory of Fingering." Soil Science 146(1):51-56.

Hopmans, J. W., and J. H. Dane. 1986. "Temperature Dependence of Soil Hydraulic Properties." Soil Sci. Soc. Am. J. 50:4-9.

Klute, A., and C. Dirksen. 1986. "Hydraulic Conductivity and Diffusivity: Laboratory Methods." In Methods of Soil Analysis, Part 1, 2nd ed, A. Klute, pp. 687-734. Agronomy Monograph 9, American Society of Agronomy and Soil Science Society of America, Madison, Wisconsin.

Lappala, E. G., R. W. Healy, and E. P. Weeks. 1987. Documentation of Computer Program VS2D to Solve the Equations of Fluid Flow in Variably Saturated Porous Media. Water-Resources Investigations Report 83-4099, U.S. Geological Survey, Denver, Colorado.

Lu, A. H., S. J. Phillips, and M. R. Adams. 1982. "Finite Element Model Evaluation of Barrier Configurations to Reduce Infiltration into Waste Disposal Structures: Preliminary Results and Design Considerations." In Proceedings of the Symposium on Waste Management, pp. 559-575, University of Arizona, Tucson, Arizona.

Magnusen, S. O., R. G. Baca, and A. J. Sondrup. 1990. Independent Verification and Benchmark Testing of the PORFLO-3 Computer Code, Version 1.0. EGG-BG-9175, Idaho National Engineering Laboratory, Idaho Falls, Idaho.

Miller, D., and W. C. Bungler. 1963. "Moisture Retention by Soil with Coarse Layers in the Profile." Soil Sci. Soc. Am. Proc. 27:586-589.

Mualem, Y. 1976a. A Catalogue of the Hydraulic Properties of Soils. Research Progress Report No. 442, Technion, Israel Institute of Technology, Haifa, Israel.

Mualem, Y. 1976b. "A New Model for Predicting the Hydraulic Conductivity of Unsaturated Porous Media." Water Resour. Res. 12(3):513-522.

Nimmo, J. R., and E. E. Miller. 1986. "The Temperature Dependence of Isothermal Moisture vs. Potential Characteristics of Soils." Soil Sci. Soc. Am. J. 50:1105-1113.

Pruess, K. 1987. TOUGH User's Guide. LBL-20700, Lawrence Berkeley Laboratory, University of California, Berkeley, California.

Rockhold, M. L., M. J. Fayer, and G. W. Gee. 1988. Characterization of Unsaturated Hydraulic Conductivity at the Hanford Site. PNL-6488, Pacific Northwest Laboratory, Richland, Washington.

Runchal, A. K., and B. Sagar. 1989. PORFLO-3: A Mathematical Model for Fluid Flow, Heat and Mass Transport in Variably Saturated Geologic Media. WHC-EP-0041/Rev.0, Westinghouse Hanford Company, Richland, Washington.

Stone, W. A., J. M. Thorp, O. P. Gifford, and D. J. Hoitink. 1983. Climatological Summary for the Hanford Area. PNL-4622, Pacific Northwest Laboratory, Richland, Washington.

Travis, B. J. 1984. TRACR3D: A Model of Flow and Transport in Porous/Fractured Media. LA-9667-MS, Los Alamos National Laboratory, Los Alamos, New Mexico.

U.S. Department of Energy (DOE). 1987. Final Environmental Impact Statement, Disposal of Hanford Defense High-Level, Transuranic and Tank Wastes, Hanford Site, Richland, Washington. DOE/EIS-0113 (Vol. 3), Washington, D.C.

van Genuchten, R. 1978. Calculating the Unsaturated Hydraulic Conductivity with a New Closed-Form Analytical Model. Water Resources Program, Department of Civil Engineering, Princeton University, Princeton, New Jersey.

van Genuchten, M. Th. 1985. RETC.F77: A Program to Analyze Observed Soil Water Tension and Hydraulic Conductivity Data. U.S. Salinity Laboratory Special Report, Riverside, California.

Warrick, A. W. 1974. "Time-Dependent Linearized Infiltration. I. Point Sources." Soil Sci. Soc. Am. Proc. 38:383-386.

Weast, R. C. 1982. Handbook of Chemistry and Physics. CRC Press, Inc., Boca Raton, Florida.

Wooding, R. A. 1968. "Steady Infiltration from a Shallow Circular Pond." Water Resour. Res. 4:1259-1273.

APPENDIX A

DETERMINATION OF FLTF SOIL HYDRAULIC PROPERTIES

APPENDIX A

DETERMINATION OF FLTF SOIL HYDRAULIC PROPERTIES

For long-term simulations of the protective barrier, the hydraulic properties of the materials must be well characterized. Gee et al. (1989) report the results of extensive measurements of water retention and saturated conductivity for soil contained in the lysimeters at the Field Lysimeter Test Facility (FLTF). To supplement those measurements, a steady-state column experiment was conducted in FY 1988 to provide simultaneous measurements of water content, matric potential, and unsaturated conductivity (a previously unmeasured property).

A.1 METHOD

Unsaturated hydraulic conductivities as a function of water content and matric potential were determined using a modification of the steady-state flux method (Klute and Dirksen 1986). In this modification, the flux of water into soil columns is controlled with equipment described by Wierenga et al. (1986). Figure A.1 shows a schematic of the steady-state flux method experimental apparatus.

Details of the experimental procedure are described by Rockhold, Fayer, and Gee (1988). Two acrylic columns (Figure A.1) were packed with FLTF soil to a bulk density of 1.37 g/cm^3 . Water was pumped at a known rate (less than the saturated conductivity) to the top of the columns and allowed to drain through the sample. A vacuum box at the lower end of the column maintained a given matric potential at the lower plate. The flux to the top and the potential at the bottom were adjusted such that matric potentials at the two measuring points along the column were equal (i.e., unit gradient conditions prevailed). At that time, the column was weighed to determine the water content. The conductivity associated with that water content and the measured matric potentials was equivalent to the input flux. The flux was then decreased to the next desired rate, the pressure in the vacuum box adjusted, and the procedure repeated.

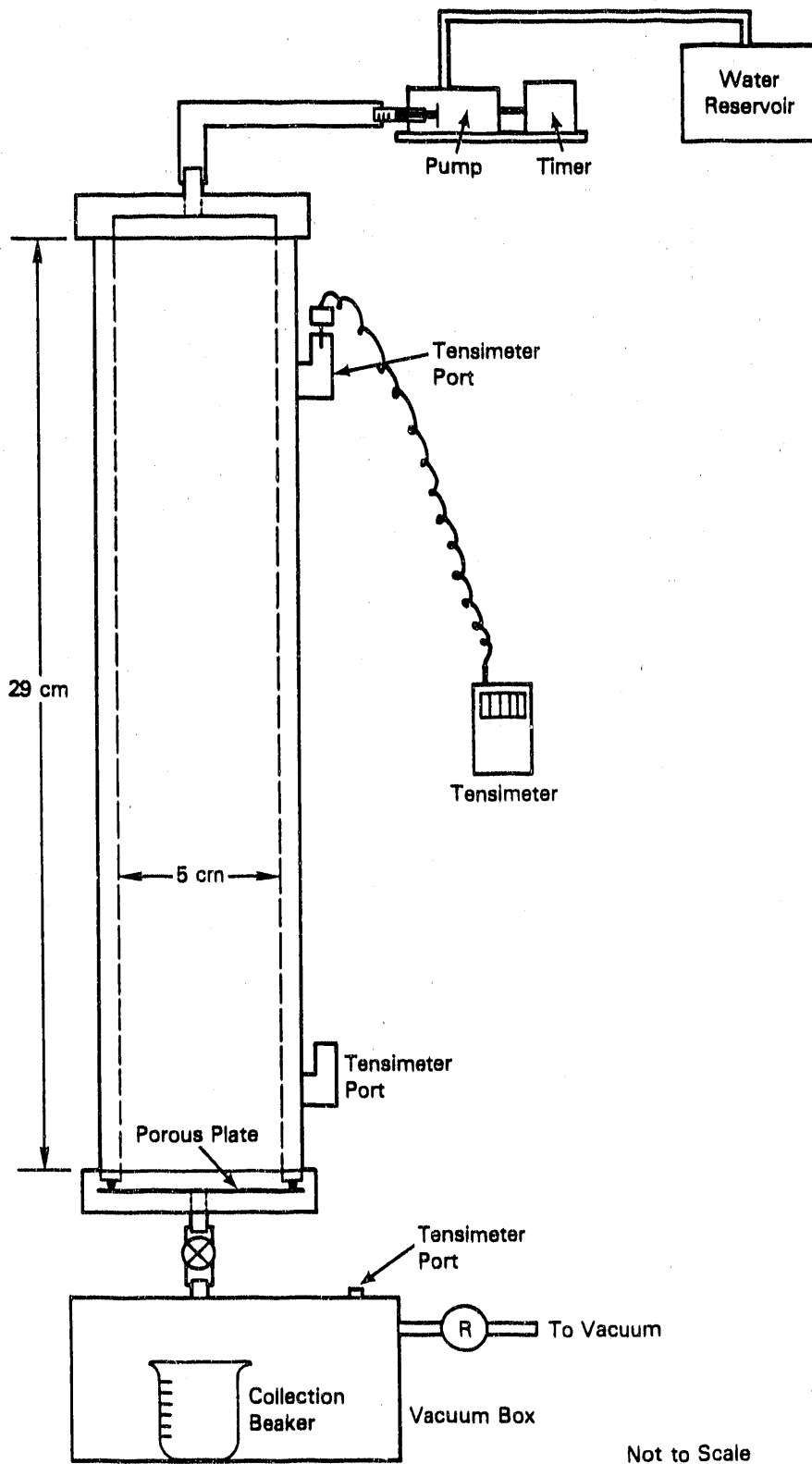


FIGURE A.1. Steady-State Flux Apparatus

A.2 RESULTS

Table A.1 contains the results of the steady-state flux experiment. Several problems were encountered during the steady-state flux method experiment. During the saturation process, some horizontal cracks in the soil were noted. These cracks disappeared once the columns were saturated, but began to reappear after the air-entry potential had been reached during desorption. At that time, the soil pulled slightly away from the acrylic column walls. Both phenomena may have resulted from the packing method or may simply be characteristic of this soil material. Because the horizontal cracks were just hairlines, the effect on the data was estimated to be minimal. Shrinkage from the column wall was estimated to reduce the flow area, thus altering the calculated conductivity values, by less than 10%.

Halfway through the steady-state flux experiment, a syringe-stroke counter indicated that the pump was not cycling at the frequency to which the pump timer was set. For the remainder of the experiment, a time-averaged flux was calculated from the number of strokes indicated by the counter during a given time period and the syringe output per stroke. This calculation was checked by measuring the weight changes of beakers placed below each column to determine the actual volume of outflow. The inability to maintain a constant flux probably allowed the soil column to depart from the primary desorption curve on occasion. The effect on the data was estimated to be minimal because the step changes in flux were small.

The flux density at each flow rate was calculated from V/At , where V is the volume of water passing through the column of cross-sectional area A in time t . The hydraulic conductivity is equal to the flux density if a unit hydraulic gradient was attained. The vacuum supply used varied by approximately ± 4 mb, even with a regulator valve between the main vacuum source and the vacuum chamber. Therefore, exact unit gradient conditions were difficult to attain. When the tensiometers in the columns indicated unequal matric potentials, the arithmetic mean of the matric potentials was used. If the actual potential gradients at the time of measurement were used, the calculated conductivity values would be anywhere from 50% less to 100% greater than the values reported in Table A.1.

TABLE A.1. Soil Hydraulic Properties Determined with the Steady-State Flux Technique for a Composite of Selected FLTF Soil Samples

Column E, $\rho_b = 1.45 \text{ g/cm}^3$			Column F, $\rho_b = 1.44 \text{ g/cm}^3$		
Water Content (cm^3/cm^3)	Matric Potential (-cm)	Hydraulic Conductivity (cm/s)	Water Content (cm^3/cm^3)	Matric Potential (-cm)	Hydraulic Conductivity (cm/s)
0.481	≈ 0	2.74×10^{-4}	0.471	≈ 0	5.50×10^{-4}
0.472	104	6.47×10^{-5}	0.438	152	2.61×10^{-5}
0.458	119	2.19×10^{-5}	0.422	176	1.97×10^{-5}
0.450	139	1.82×10^{-5}	0.416	181	1.16×10^{-5}
0.446	161	1.77×10^{-5}	0.397	186	1.11×10^{-5}
0.417	177	1.22×10^{-5}	0.392	198	1.10×10^{-5}
0.392	190	1.01×10^{-5}	--	--	--

The measurements of unsaturated hydraulic conductivity by the steady-state flux method required approximately 13 to 14 weeks, which included approximately 2 weeks to fully saturate the samples.

A.3 FUNCTION FIT

The van Genuchten (1978) functions for water content (θ) and unsaturated hydraulic conductivity (K) are

$$\theta = \theta_r + (\theta_s - \theta_r) [1 + (\alpha h)^n]^{-m} \quad (\text{A.1})$$

and

$$K = \frac{K_s \{1 - (\alpha h)^{n-1} [1 + (\alpha h)^n]^{-m}\}^2}{[1 + (\alpha h)^n]^{m/2}} \quad (\text{A.2})$$

where θ_r = residual water content
 θ_s = saturated water content
 h = matric potential
 K_s = saturated hydraulic conductivity
 α, m, n = curve-fitting parameters.

The conductivity function is based on Mualem's (1976) conductivity model, which calculated hydraulic conductivity from the water retention curve. van Genuchten (1978) derived a closed-form solution to the Mualem (1976) model assuming $m = 1 - 1/n$ [see Rockhold, Fayer, and Gee (1988) for more details].

The RETC.F77 computer program (van Genuchten 1985) was used to simultaneously fit a mathematical function to the laboratory-determined water retention data and the hydraulic conductivity data determined by the falling head method. These data can be found in Tables 6.3, 6.5, and 6.6 of Gee et al. (1989). Figure A.2 shows the water retention data and the curve fit to the data. Figure A.3 shows the hydraulic conductivity/water content data determined by the falling head method and the resulting curve fit.

For the water retention data (which are plotted in Figure A.2), the steady-state flux test yielded a higher air-entry value. During the saturation process, the columns were pressurized in an attempt to force some of the entrapped air into solution. This step resulted in some compaction of the soil so that the average bulk density increased from 1.37 g/cm^3 to approximately 1.44 g/cm^3 . Differences between the water retention characteristics measured by the steady-state flux method and by the other laboratory procedures may be caused in part by the bulk density differences. At the lowest matric potential values tested (-200 cm), the measured water contents are more closely aligned with the previous laboratory values.

The unsaturated conductivity data from the steady-state flux test are shown in Figure A.3 along with the data from the previous laboratory tests and the van Genuchten function. Even though only a small range of water content was covered (0.38 to $0.47 \text{ cm}^3/\text{cm}^3$), the unsaturated hydraulic conductivity data shown in Figure A.3 match the previous laboratory values as well as the van Genuchten curve. A useful next step would be to measure unsaturated conductivities at water contents lower than $0.38 \text{ cm}^3/\text{cm}^3$ to verify that the van Genuchten function is valid in that region.

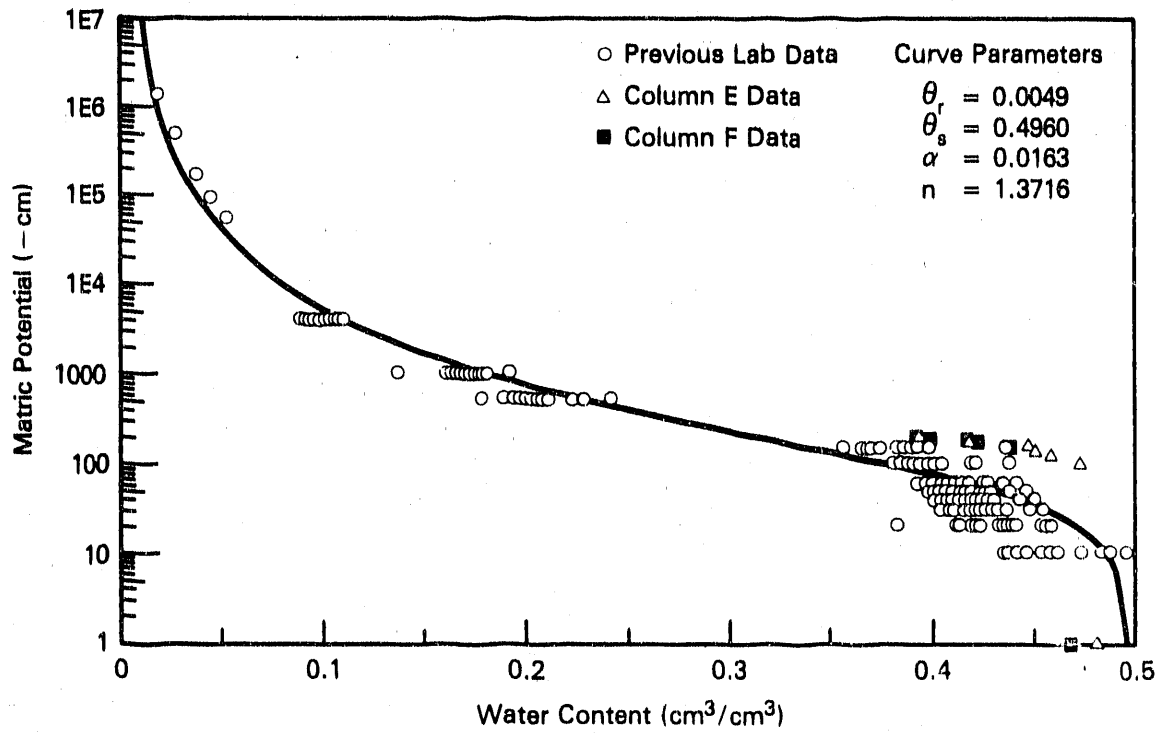


FIGURE A.2. Measured Water Retention Data and van Genuchten Function Fit for FLTF Soil

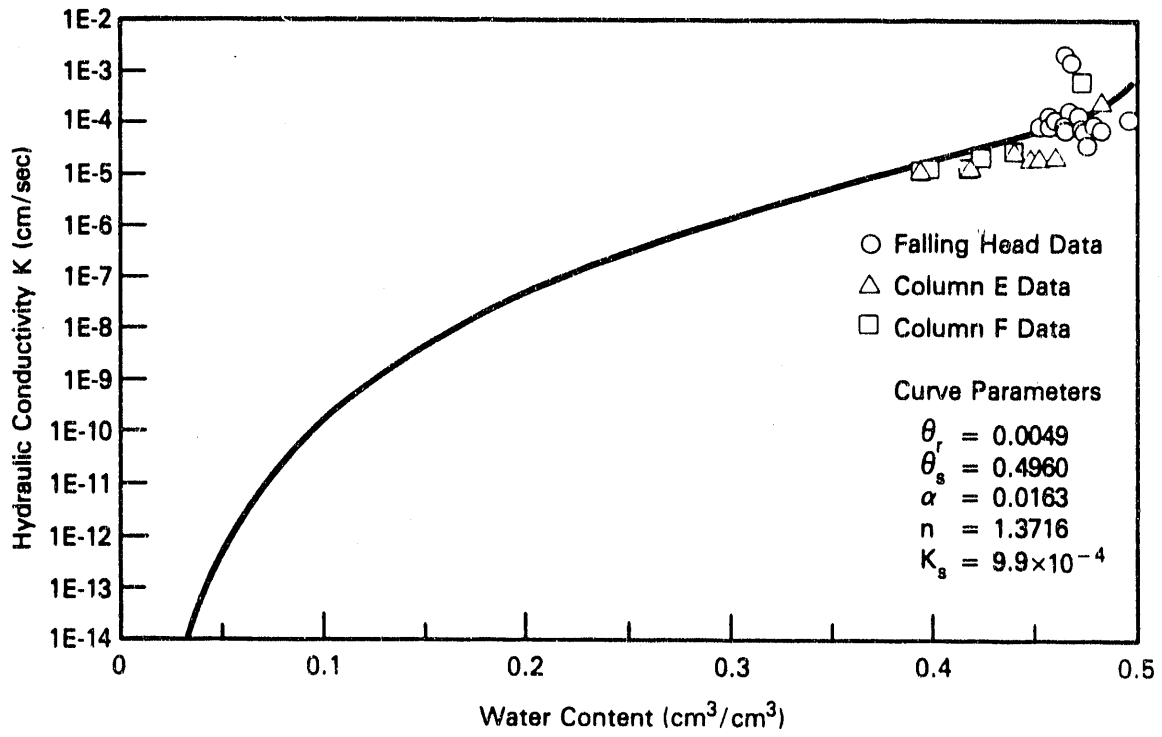


FIGURE A.3. Measured Hydraulic Conductivity Data and van Genuchten Function Fit for FLTF Soil

A.4 REFERENCES

Gee, G. W., R. R. Kirkham, J. L. Downs, and M. D. Campbell. 1989. The Field Lysimeter Test Facility (FLTF) at the Hanford Site: Installation and Initial Tests. PNL-6810, Pacific Northwest Laboratory, Richland, Washington.

Klute, A., and C. Dirksen. 1986. "Hydraulic Conductivity and Diffusivity: Laboratory Methods." In Methods of Soil Analysis, Part I. Agronomy Monograph No. 9, 2nd ed., American Society of Agronomy, Madison, Wisconsin.

Mualem, Y. 1976. "A New Model for Predicting the Hydraulic Conductivity of Unsaturated Porous Media." Water Resour. Res. 12(3):513-522.

Rockhold, M. L., M. J. Fayer, and G. W. Gee. 1988. Characterization of Unsaturated Hydraulic Conductivity at the Hanford Site. PNL-6488, Pacific Northwest Laboratory, Richland, Washington.

van Genuchten, R. 1978. Calculating the Unsaturated Hydraulic Conductivity with a New Closed-Form Analytical Model. Water Resources Program, Department of Civil Engineering, Princeton University, Princeton, New Jersey.

van Genuchten, M. Th. 1985. Program to Analyze Observed Soil Water Tension and Hydraulic Conductivity Data. U.S. Salinity Laboratory Special Report, Riverside, California.

Wierenga, P. J., L. W. Gelhar, C. S. Simmons, G. W. Gee, and T. J. Nicholson. 1986. Validation of Stochastic Flow and Transport Models for Unsaturated Soils: A Comprehensive Field Study. NUREG/CR-4622, U.S. Nuclear Regulatory Commission, Washington, D.C.

APPENDIX B

GENERATION OF LONG-TERM WEATHER VARIABLES

APPENDIX B

GENERATION OF LONG-TERM WEATHER VARIABLES

Weather (in the form of meteorological parameters) is the upper boundary condition for simulations of the protective barrier using the UNSAT-H code (Fayer and Jones 1990). Precipitation becomes a flux of water into the barrier and evaporation becomes a flux of water out of the barrier. In addition, meteorological parameters are used to simulate the rate of water uptake from the soil by plants. At the Hanford Site, the longest continuous weather record from the Hanford Meteorological Station dates back to 1944 (Stone et al. 1983). Hourly weather observations, which began in 1944, are available on magnetic tape at least as far back as 1957. The data of interest to modeling are the surface observations of precipitation, solar radiation, cloud cover, air temperature, relative humidity, and wind speed. The hourly precipitation can be input directly to UNSAT-H or reduced to a daily value before input. The remaining data are preprocessed to produce a single value for the potential evapotranspiration for the day.

The hourly-data record is less than 50 years long, yet the time periods being considered for disposal are 10,000 years. To simulate longer periods of time, or to simulate short periods with different weather (i.e., other realizations), it is necessary to generate sequences of weather variables consistent with observations at the Hanford Meteorological Station. One method is the weather generation model WGEN (Richardson and Wright 1984). Two computer codes are associated with this model. The first code, WGENPAR, uses actual weather data (specifically, daily values of precipitation, maximum and minimum air temperature, and solar radiation) and fits statistical functions to the data. The generated statistical parameters are then fed into the second code, WGEN. The WGEN code generates yearly sequences of weather variables that have the same statistical characteristics as the actual weather data.

The WGEN model operates by generating precipitation for a given day independent of the other weather variables. Maximum and minimum air temperature and solar radiation for a given day are then generated and

conditioned as functions of whether the day was wet or dry. According to Richardson and Wright (1984), "The model is designed to preserve the dependence in time, the correlation between variables, and the seasonal characteristics in actual weather data for the location."

Use of WGEN or a similar model allows weather sequences of any length to be generated and used in simulations. These sequences would, of course, reflect the statistical variations present in the climate from which the parameters were obtained. The added benefit of this technique is that some statistics could be varied on the basis of information from the climate change task of the Protective Barriers Program. For example, the statistical parameters for precipitation could be altered to yield 30% more precipitation annually, or perhaps shift the precipitation toward the summer months. Air temperatures and solar radiation, which are predicted partly on the basis of precipitation status, would change accordingly.

Daily weather data from the Hanford Meteorological Station for the years 1958 to 1987 were input to the WGENPAR code. The code fit functions to the data, and the parameters of the fit are shown in Table B.1 [the reader is referred to Richardson and Wright (1984) for descriptions of the parameters]. These parameters were then input to WGEN and a 30-year record was generated. To facilitate comparison between the observed data and generated weather variables, the code WGENSTAT was written to calculate a number of summary statistics. The summary statistics used for the comparison are nearly identical to those used by Richardson and Wright (1984). Table B.2 shows the comparison.

Figures B.1, B.2, and B.3 show comparisons of selected weather statistics from Table B.2. The comparisons indicate that the WGEN code reasonably reproduces sequences of weather variables that retain the statistics of Hanford weather. The next step should be to analyze the comparisons for statistical significance. If any statistical differences do exist, the functions used in WGEN should be examined for possible replacement with functions more suited to the Hanford weather record.

As part of the test for significance, generating a much longer sequence of weather variables would allow testing of extreme values. For example, generation of a 100- to 200-year sequence of weather variables would enable study

TABLE B.1. Weather-Generation Parameters Generated With WGENPAR Using Hanford Meteorological Station Data from the Period 1958-1987 (actual format for input to WGEN)

WGEN Input File		Input Description										
GENERATED RAINFALL, TMAX, TMIN, AND RAD. - HMS 1958-1987 (NO CORRECTION FACTORS)		Title										
30	146.57	0	No. of Years, Latitude, Contrl.									
0.439	0.516	0.388	0.317	0.301	0.252	0.294	0.258	0.337	0.319	0.444	0.484	Rainfall Generation Parameters
0.195	0.166	0.163	0.121	0.122	0.123	0.055	0.059	0.085	0.094	0.198	0.256	Rainfall Generation Parameters
0.984	0.921	0.998	0.937	0.857	0.854	0.931	0.837	0.856	0.931	0.959	0.998	Rainfall Generation Parameters
0.107	0.102	0.075	0.096	0.127	0.112	0.108	0.106	0.119	0.092	0.118	0.109	Rainfall Generation Parameters
65.222	26.066	0.154	-0.088									Maximum Air Temperature Param.
59.619												Maximum Air Temperature Param.
42.627	18.157	0.204	-0.129									Minimum Air Temperature Param.
380.628	284.041											Solar Radiation Parameters
246.837												Solar Radiation Parameters

TABLE B.2. Comparison of Observed and Generated Weather Variables for the Hanford Meteorological Station from the Period 1958-1987

	<u>Jan</u>	<u>Feb</u>	<u>Mar</u>	<u>Apr</u>	<u>May</u>	<u>Jun</u>	<u>Jul</u>	<u>Aug</u>	<u>Sep</u>	<u>Oct</u>	<u>Nov</u>	<u>Dec</u>	<u>Annual Mean</u>
<u>Mean Monthly Precipitation (in.)</u>													
Observed	0.85	0.68	0.49	0.41	0.50	0.40	0.22	0.20	0.35	0.32	0.89	1.11	6.42
Generated	0.78	0.82	0.52	0.39	0.50	0.49	0.24	0.22	0.35	0.35	0.79	1.23	6.68
<u>Number of Days with Precipitation</u>													
Observed	8.03	7.20	6.53	4.53	4.60	4.23	2.23	2.27	3.40	3.77	7.87	10.23	64.90
Generated	7.87	7.70	6.77	4.20	4.63	4.70	2.20	2.17	3.23	3.27	6.87	10.23	63.83
<u>Number of Days with Precipitation >0.25 in</u>													
Observed	0.73	0.67	0.33	0.33	0.60	0.37	0.33	0.20	0.37	0.27	1.03	1.17	6.40
Generated	0.70	0.57	0.23	0.27	0.47	0.40	0.23	0.27	0.37	0.27	0.93	1.37	6.07
<u>Average Maximum Air Temperature (°F)</u>													
Observed	36.64	45.22	55.41	63.44	73.29	82.10	89.88	90.21	80.19	67.00	49.85	38.54	64.31
Generated	38.32	40.14	48.34	60.74	74.32	84.94	90.27	88.51	79.76	66.71	52.96	41.92	63.91
<u>Average No. of Days >95°F</u>													
Observed	0.00	0.00	0.00	0.00	0.30	3.03	8.87	9.50	1.30	0.00	0.00	0.00	23.00
Generated	0.00	0.00	0.00	0.03	0.30	2.67	5.83	4.77	1.07	0.00	0.00	0.00	14.67
<u>Average Minimum Air Temperature (°F)</u>													
Observed	24.08	29.13	34.22	39.56	47.47	56.12	61.64	61.82	53.63	42.45	33.38	26.51	42.50
Generated	24.73	26.40	31.66	40.08	49.33	57.08	60.47	59.54	52.96	44.22	34.63	27.25	42.36
<u>Average No. of Days <32°F</u>													
Observed	23.40	15.93	9.97	2.67	0.13	0.00	0.00	0.00	0.03	1.63	11.23	21.70	86.70
Generated	25.27	20.80	15.90	4.97	0.40	0.00	0.00	0.00	0.00	1.80	11.27	22.20	102.60
<u>Average Daily Solar Radiation (Lv)</u>													
Observed	105.8	176.9	309.3	440.1	554.6	611.3	641.5	557.5	422.6	280.9	136.7	85.6	360.2
Generated	100.5	171.4	304.0	452.9	575.2	628.4	626.6	531.8	402.2	255.9	130.6	80.2	355.0

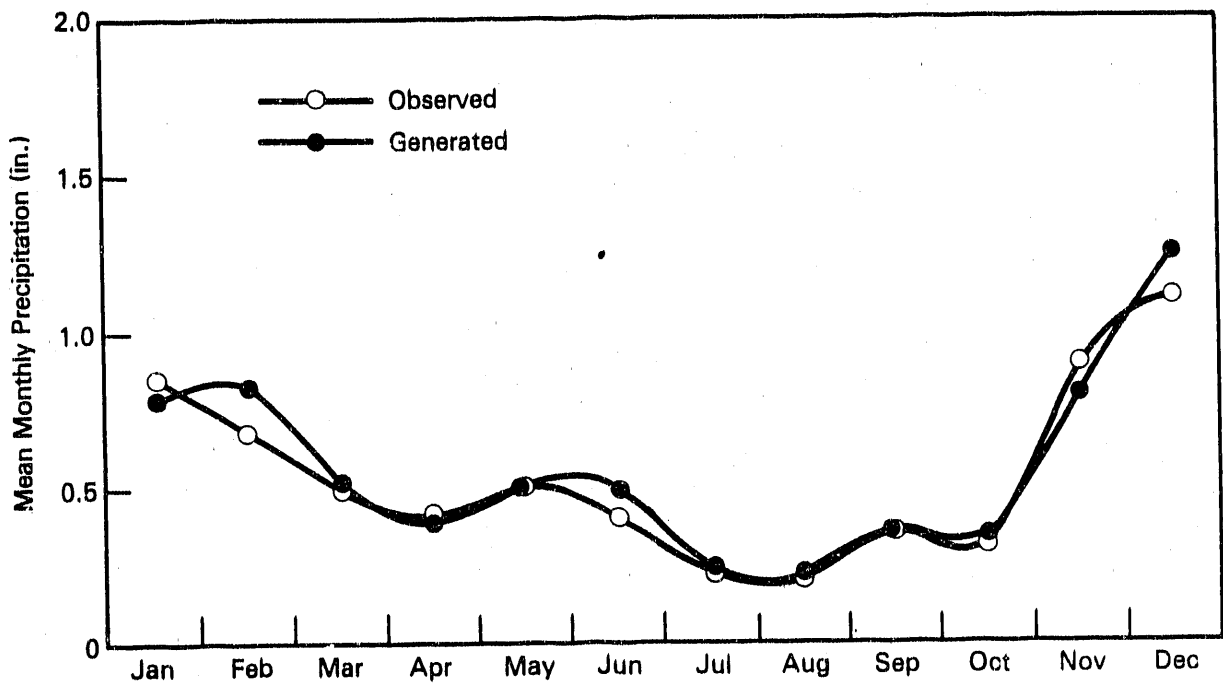


FIGURE B.1. Comparison of Observed and Generated Mean Monthly Precipitation

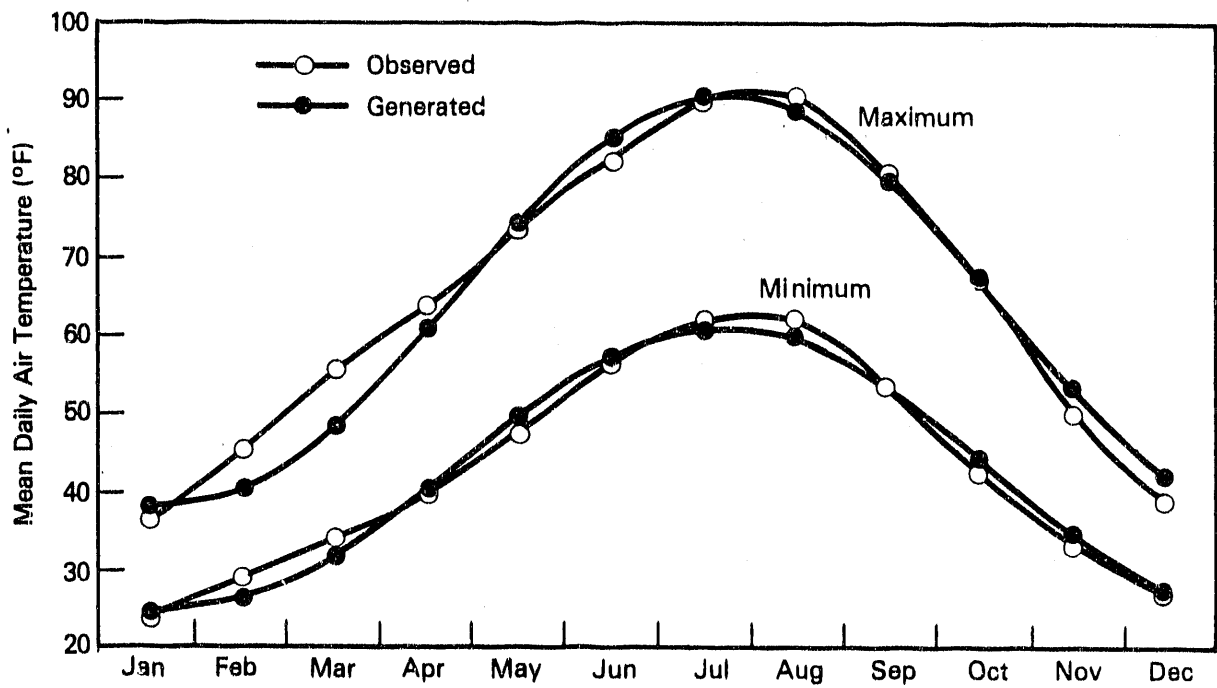


FIGURE B.2. Comparison of Observed and Generated Mean Monthly Maximum and Minimum Air Temperatures

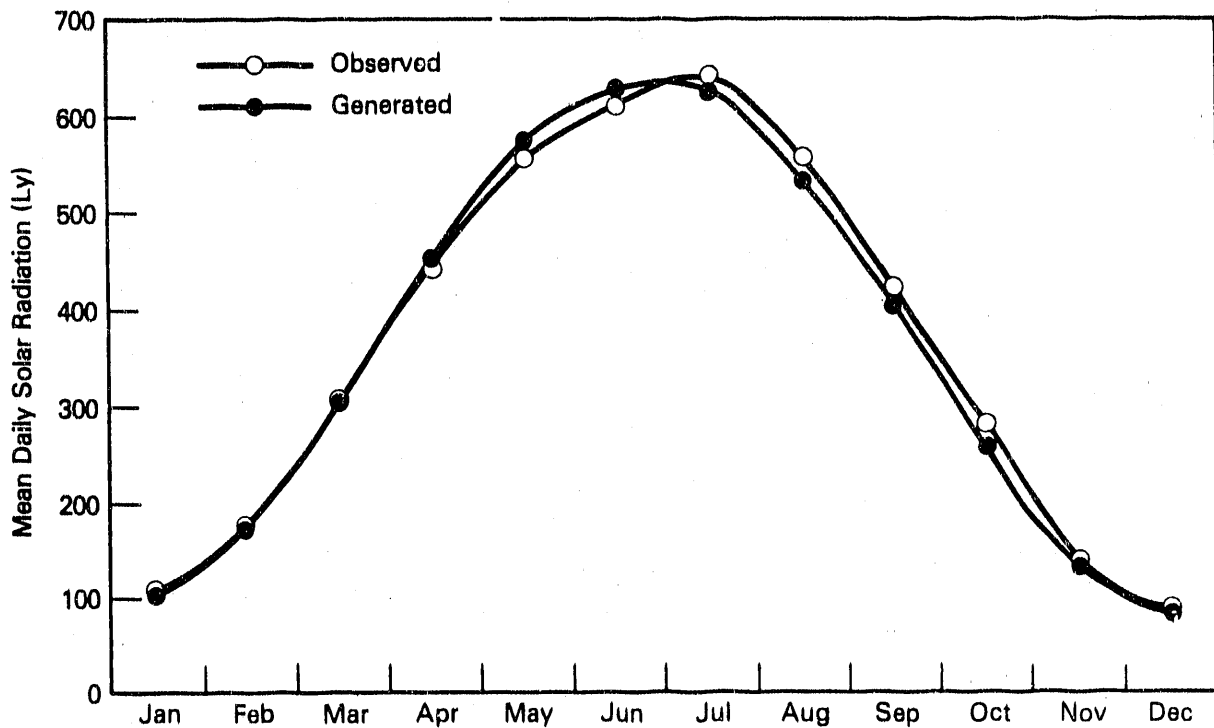


FIGURE B.3. Comparison of Observed and Generated Mean Monthly Solar Radiation

of the occurrence of extreme precipitation events as well as extreme annual precipitation amounts. Also, such a long record might be used to show the long-term variation in short-term averages (e.g., 10-year moving averages).

Two weather parameters currently not provided by WGEN are relative humidity and wind speed. Some estimate of both would be needed to calculate evapotranspiration in the UNSAT-H model. One approach would be to regress the daily mean values from the meteorological record on variables such as days since precipitation, time of year, and temperature. This approach would tie relative humidity and wind speed to the generated variables, thus making the generated weather sequence more complete.

REFERENCES

Fayer, M. J., and T. L. Jones. 1990. UNSAT-H Version 2.0: Unsaturated Water and Heat Flow Model. PNL-6779, Pacific Northwest Laboratory, Richland, Washington.

Richardson, C. W., and D. A. Wright. 1984. WGEN: A Model for Generating Daily Weather Variables. ARS-8, U.S. Department of Agriculture, Agricultural Research Service, Temple, Texas.

Stone, W. A., J. M. Thorp, O. P. Gifford, and D. J. Hoitink. 1983. Climatological Summary for the Hanford Area. PNL-4622, Pacific Northwest Laboratory, Richland, Washington.

APPENDIX C

GENERALIZED SOLUTION TO INFILTRATION
FROM A SURFACE POINT SOURCE

APPENDIX C

GENERALIZED SOLUTION TO INFILTRATION FROM A SURFACE POINT SOURCE

Healy and Warrick (1988) presented a generalized solution for infiltration from a surface point source. They substituted dimensionless variables into Richard's equation and solved the new equation numerically with an extension of the VS2D finite-difference computer code for a variety of soil types and source strengths (Healy 1987). The resulting dimensionless wetting-front locations and wetted soil volumes were fitted to empirical equations. Dimensional results for specific locations and times were obtained by applying scaling factors to the results of the empirical equations. This appendix describes the generalized solution and contains listings of the input and output files and source code for the Generalized Solution to Infiltration from a Surface Point Source (GSIPS) code.

By assuming axial symmetry in three dimensions, Richards' equation can be written as

$$\frac{\partial \theta}{\partial t} = \frac{1}{r} \frac{\partial}{\partial r} \left(rK \frac{\partial h}{\partial r} \right) + \frac{\partial}{\partial z} \left(K \frac{\partial h}{\partial z} \right) + Q\delta(r - r_o, z - z_o) \quad (C.1)$$

where θ = volumetric moisture content (dimensionless)

h = total hydraulic head (L), which is equivalent to $h_p + h_z$

h_p = pressure head (L)

h_z = elevation head (L)

K = unsaturated hydraulic conductivity (LT^{-1})

r = radial distance (L)

z = depth (L)

Q = volumetric flux (L^3T^{-1})

$\delta(r - r_0, z - z_0)$ = Dirac delta function (L^{-3}); equals 0 if $r \neq r_0$ or $z \neq z_0$, where (r_0, z_0) is the location of the point source; equals ∞ if $r = r_0$ and $z = z_0$ and $t = \text{time (T)}$.

The following definitions of dimensionless variables are made:

$$h^* = \alpha h \quad (C.2)$$

$$z^* = \alpha z \quad (C.3)$$

$$r^* = \alpha r \quad (C.4)$$

$$K^* = K/K_s \quad (C.5)$$

$$t^* = \alpha K_s t / (\theta_s - \theta_r) \quad (C.6)$$

$$Q^* = \alpha^2 Q / K_s \quad (C.7)$$

$$\delta^* = \delta / \alpha^3 \quad (C.8)$$

$$W = (\theta - \theta_r) / (\theta_s - \theta_r) \quad (C.9)$$

where α = scaling factor for length (L^{-1})

θ_s = volumetric moisture content at saturation (dimensionless)

θ_r = residual volumetric moisture content (dimensionless)

K_s = saturated hydraulic conductivity (LT^{-1}).

The terms Q and Q^* can refer to any externally imposed source or sink. Healy and Warrick (1988) used Q and Q^* to represent the rate of flow from a surface

point source for which r_0 and z_0 are taken to be zero. Equation (C.1) can then be written in dimensionless form as

$$\frac{\partial W}{\partial t^*} = \frac{1}{r^*} \frac{\partial}{\partial r^*} \left(r^* K^* \frac{\partial h^*}{\partial r^*} \right) + \frac{\partial}{\partial z^*} \left(K^* \frac{\partial h^*}{\partial z^*} \right) + Q^* \delta^*(r^*, z^*) \quad (C.10)$$

The constitutive relations between effective saturation (W) and pressure head and relative hydraulic conductivity (K^*) and pressure head are defined by van Genuchten (1978):

$$W = \left[\frac{1}{1 + h_p^{*n}} \right]^m \quad (C.11a)$$

and

$$K^* = W^{1/2} [1 - (1 - W^{1/m})^m]^2 \quad (C.11b)$$

where h_p^* is dimensionless pressure head, and m and n are curve-fitting parameters such that $m = 1 - 1/n$.

Initial conditions are assumed to be uniform and are given in terms of effective saturations:

$$W(r^*, z^*) = W_i = 0.01, \quad t^* = 0 \quad (C.12)$$

The point source in Equation (C.10) is represented by the following time-dependent boundary condition, which is approximated by a combination of Dirichlet and Neuman boundary conditions:

$$h_p^*(r^*, z^*) = 0, \quad 0 < t^*, \quad z^* = 0, \quad 0 < r^* \leq \rho(t^*) \quad (C.13)$$

where $\rho(t^*)$ is the dimensionless radius of the ponded area (the wetted radius) such that the flow from the saturated circular disk of radius $\rho(t^*)$ is equal to Q^* . The other boundary conditions are 1) constant effective saturations

(equal to the initial value) at an infinite distance from the source and 2) no flow across the land surface at distances greater than $\rho(t^*)$ from the origin. These are described by

$$\lim_{r^*, z^* \rightarrow \infty} W(r^*, z^*) = W_i, \quad 0 < t^* \quad (C.14)$$

$$\partial h^* / \partial z^* = 0, \quad 0 < t^*, \quad z^* = 0, \quad \rho(t^*) < r^* \quad (C.15)$$

The finite-difference approximation of Equation (C.10) was solved numerically (Healy 1987). Small spatial and temporal discretizations were used in order to minimize discretization errors. The computational grid contained 4224 nodes with 66 nodes in the radial direction and 64 nodes in the vertical direction, representing a depth of 5.50 and a radius of 5.50. This was large enough to ensure that the saturations at the radial and vertical boundaries remained equal to the initial saturation. Variable grid spacing was used, with the distance between adjacent nodes (z^*) ranging from 0.005 to 0.25. Grid spacing was identical in both the radial and vertical directions. The size of the initial time step for these simulations was 1×10^{-6} . The size of the time step was allowed to increase during the simulations, but was always held ≤ 0.1 .

Healy and Warrick (1988) arbitrarily assumed the wetting front to be defined by the set of points (r^*, z^*) such that $W(r^*, z^*) = 1.25 \cdot W_i$. From the results of each simulation, three locations of the wetting front and the volume of soil that was wetted at various times were fit to the following cubic equations in terms of dimensionless time:

$$D1 = At^{*1/2} + Bt^* + Ct^{*3/2} \quad (C.16)$$

$$D2 = Dt^{*1/2} + Et^* + Ft^{*3/2} \quad (C.17)$$

$$D3 = Gt^{*1/2} + Ht^* + It^{*3/2} \quad (C.18)$$

$$V^* = Jt^{*1/2} + Kt^* = Lt^{*3/2} \quad (C.19)$$

where $D1$ = dimensionless distance from origin to wetting front
along the vertical line $r^* = 0$

$D2$ = dimensionless distance from origin to wetting front
along the diagonal line $r^* = z^*$

$D3$ = dimensionless distance from the origin to wetting front
along the horizontal line $z^* = 0$ (land surface)

V^* = dimensionless wetted volume

A to L = coefficients dependent on n and Q^* .

Values of the coefficients in Equations (C.16-C.19) are listed in Table C.1 for six different values of n and five different values of Q^* . Approximately 50 different points in time were used for fitting each of these equations. The average mean squared error of prediction (MSE) was 0.000337 for Equation (C.16), 0.000555 for Equation (C.17), 0.00511 for Equation (C.18), and 0.000784 for Equation (C.19).

This generalized solution to infiltration from a surface point source is implemented in the GSIPS code. Table C.1 is the coefficient matrix used by the program. Example input and output files corresponding to the verification test problems in Section 3.0 are provided in Figures C.1 and C.2. A listing of the GSIPS code is provided at the end of this appendix.

TABLE C.1. Coefficient Matrix Used by the GSIPS Code

Q*	N	A	B	C	D	E	F	G	H	I	J	K	L
0.05	1.50	0.872	-0.513	0.135	0.711	-0.435	0.124	0.880	-0.542	0.142	-0.014	0.191	-0.010
0.05	1.75	0.903	-0.533	0.142	0.758	-0.471	0.138	0.897	-0.555	0.150	-0.008	0.202	-0.003
0.05	2.00	0.921	-0.521	0.134	0.779	-0.447	0.121	0.906	-0.545	0.143	-0.012	0.238	-0.008
0.05	2.50	0.936	-0.504	0.128	0.803	-0.459	0.130	0.922	-0.552	0.143	-0.011	0.264	-0.007
0.05	3.50	0.993	-0.558	0.151	0.816	-0.414	0.105	0.949	-0.596	0.158	-0.002	0.271	0.001
0.05	5.00	0.974	-0.510	0.142	0.839	-0.454	0.126	0.906	-0.554	0.142	-0.004	0.226	0.013
0.10	1.50	1.03	-0.605	0.161	0.835	-0.477	0.133	1.10	-0.729	0.199	-0.013	0.326	-0.022
0.10	1.75	1.08	-0.643	0.175	0.896	-0.521	0.146	1.10	-0.702	0.186	-0.013	0.365	-0.017
0.10	2.00	1.10	-0.640	0.174	0.912	-0.499	0.135	1.11	-0.699	0.187	0.009	0.338	0.20
0.10	2.50	1.13	-0.662	0.188	0.949	-0.505	0.134	1.12	-0.710	0.191	0.001	0.407	0.003
0.10	3.50	1.07	-0.474	0.119	0.925	-0.406	0.095	1.06	-0.596	0.142	-0.031	0.479	0.015
0.10	5.00	1.17	-0.652	0.197	0.984	-0.500	0.133	1.10	-0.722	0.190	0.004	0.426	0.024
0.50	1.5	1.26	-0.571	0.159	1.27	-0.670	0.172	1.90	-1.44	0.416	0.042	0.921	0.100
0.50	1.75	1.35	-0.604	0.162	1.38	-0.790	0.216	1.87	-1.42	0.42	0.028	1.02	0.129
0.50	2.00	1.44	-0.670	0.182	1.36	-0.712	0.184	1.84	-1.37	0.402	0.014	1.12	0.145
0.50	2.50	1.52	-0.728	0.201	1.45	-0.796	0.220	1.78	-1.30	0.367	0.023	1.17	0.191
0.50	3.50	1.53	-0.656	0.182	1.51	-0.862	0.247	1.75	-1.25	0.359	-0.034	1.32	0.191
0.50	5.00	1.54	-0.586	0.161	1.48	-0.780	0.221	1.72	-1.25	0.353	0.055	1.16	0.278
1.00	1.5	1.25	-0.333	0.081	1.56	-0.896	0.252	2.44	-1.88	0.540	-0.028	1.89	0.094
1.00	1.75	1.41	-0.45	0.109	1.58	-0.844	0.23	2.33	-1.74	0.499	-0.105	2.16	0.097
1.00	2.00	1.53	-0.525	0.128	1.65	-0.884	0.245	2.27	-1.65	0.462	-0.096	2.21	0.178
1.00	2.50	1.63	-0.541	0.125	1.69	-0.902	0.251	2.21	-1.6	0.458	-0.143	2.5	0.139
1.00	3.50	1.67	-0.559	0.142	1.70	-0.904	0.260	2.15	-1.60	0.46	-0.153	2.40	0.242
1.00	5.00	1.73	-0.532	0.138	1.73	-0.863	0.239	2.10	-1.58	0.444	-0.106	2.44	0.286
5.00	1.5	1.18	0.158	-0.022	1.86	-0.672	0.188	5.17	-4.91	1.57	0.163	8.12	-0.204
5.00	1.75	1.42	0.101	-0.054	2.05	-0.735	0.178	4.46	-3.66	1.04	0.01	8.54	-0.07
5.00	2.00	1.58	0.005	-0.028	2.22	-0.911	0.227	4.28	-3.48	0.986	-0.21	9.44	-0.232
5.00	2.50	1.81	-0.232	0.068	2.35	-1.00	0.253	4.07	-3.24	0.906	-0.004	9.19	0.141
5.00	3.5	1.96	-0.255	0.077	2.45	-1.08	0.284	3.91	-3.15	0.886	-0.164	9.72	0.186
5.00	5.0	1.98	-0.196	0.073	2.48	-1.08	0.28	3.72	-2.97	0.822	-0.139	9.45	0.382

55.44 0.307 0.09 0.093 3.6956 400.0 3 KS,WCS,WCR,ALPHA,N,Q,# OF TIMESTEPS
 0.05 0.1 0.15 TIMESTEPS

FIGURE C.1. Example Input File for the GSIPS Code

ALPHA = 0.9300E-01 Q = 0.4000E+03 KS = 0.5544E+02
 QSTAR = 0.6240E-01 TSTAR = 0.1188E+01
 INTERPOLATION FOR QSTAR AND N
 DV = 0.6526E+00 DD = 0.5627E+00 DH = 0.5526E+00 VS = 0.3747E+00
 TIME = 0.050 V = 0.7017E+01 D = 0.6050E+01 H = 0.5942E+01 VOL. = 0.4658E+03
 QSTAR = 0.6240E-01 TSTAR = 0.2376E+01
 INTERPOLATION FOR QSTAR AND N
 DV = 0.8134E+00 DD = 0.6979E+00 DH = 0.6488E+00 VS = 0.7610E+00
 TIME = 0.100 V = 0.8746E+01 D = 0.7505E+01 H = 0.6977E+01 VOL. = 0.9460E+03
 QSTAR = 0.6240E-01 TSTAR = 0.3564E+01
 INTERPOLATION FOR QSTAR AND N
 DV = 0.9687E+00 DD = 0.8181E+00 DH = 0.7503E+00 VS = 0.1152E+01
 TIME = 0.150 V = 0.1042E+02 D = 0.8796E+01 H = 0.8068E+01 VOL. = 0.1433E+04

FIGURE C.2. Example Output File from the GSIPS Code

REFERENCES

Healy, R. W. 1987. Simulation of Trickle Irrigation, an Extension to the U.S. Geological Survey's Computer Program VS2D. U.S. Geological Survey Water-Resources Investigations Report 87-4086, Denver, Colorado.

Healy, R. W., and A. W. Warrick. 1988. "A Generalized Solution to Infiltration from a Surface Point Source." Soil Sci. Soc. Am. J. 52:1245-1251.

van Genuchten, R. 1978. Calculating the Unsaturated Hydraulic Conductivity with a New Closed-Form Analytical Model. Water Resources Program, Department of Civil Engineering, Princeton University, Princeton, New Jersey.

PROGRAM GSIPS

```
C ///////////////////////////////////////////////////////////////////
C //
C //                               GSIPS
C //
C //      A GENERALIZED SOLUTION TO INFILTRATION
C //      FROM A SURFACE POINT SOURCE
C //
C //      REFERENCE: R.W. HEALY AND A.W. WARRICK
C //      SOIL SCI. SOC. AM. J. 52:1245-1251 (1988)
C //
C //      M.L. ROCKHOLD, MARCH 1990
C ///////////////////////////////////////////////////////////////////
```

```
C
C   KS   = SATURATED HYDRAULIC CONDUCTIVITY (UNITS OF L/T)
C   WCS  = SATURATED WATER CONTENT (DIMENSIONLESS)
C   WCR  = RESIDUAL WATER CONTENT (DIMENSIONLESS)
C   ALPHA = VAN GENUCHTEN MODEL ALPHA (UNITS OF 1/L)
C   N     = " " N (DIMENSIONLESS)
C   Q     = VOLUMETRIC FLUX (UNITS OF L**3/T)
C   TIME  = TIME (UNITS CONSISTENT WITH KS AND Q)
C   STEPS = NUMBER OF TIME STEPS
C   TSTAR = DIMENSIONLESS TIME VARIABLE
C   QSTAR = DIMENSIONLESS FLUX VARIABLE
```

```
C -----
C
C   CHARACTER*80 FNAME, ONAME
C   DIMENSION QS(5),ND(5,6),D(4,2),DTMP(2),VAL(5,6,12),TIME(10),DV(4)
C   REAL ND, QS, QSTAR, TSTAR, VAL, X, Y, XO, YO, X1, Y1, TIME, V, DIAG, H,
C   & VOL, INTERP, N, KS, ALPHA, Q, OD, WD, VO, VW, WST, AOIT
C   INTEGER I, J, K, STEPS, A, ANS, M, P, R
```

```
C -----
C --- LINEAR INTERPOLATION FUNCTION
```

```
C
C   INTERP(X,X0,X1,Y0,Y1)=((X-X1)/(X0-X1))*Y0+((X-X0)/(X1-X0))*Y1
```

```
C
C   WRITE(6,100)
100 FORMAT(/1X,'ENTER INPUT FILE NAME ==> ', $)
   READ(5,200) FNAME
200 FORMAT(A80)
   OPEN(UNIT=1, FILE=FNAME, STATUS='OLD')
   WRITE(6,300)
300 FORMAT(/1X,'ENTER OUTPUT FILE NAME ==> ', $)
   READ(5,200) ONAME
   OPEN(UNIT=2, FILE=ONAME, STATUS='NEW')
   READ(1,*) KS,WCS,WCR,ALPHA,N,Q,STEPS
   READ(1,*) (TIME(A),A=1,STEPS)
   OPEN(UNIT=3,NAME='HEALY.INP',TYPE='OLD',READONLY)
```

```

READ(3,*)
DO 500 I = 1,5
  DO 500 J = 1,6
    READ(3,*) QS(I),ND(I,J),(VAL(I,J,K),K=1,12)
500 CONTINUE
CLOSE(UNIT=3)
QSTAR = ALPHA**2*Q/KS
WRITE(6,108)ALPHA,Q,KS,QSTAR
WRITE(2,108)ALPHA,Q,KS,QSTAR
DO 900 A = 1, STEPS
  TSTAR = ALPHA*KS*TIME(A)/(WCS-WCR)
  WRITE(6,109)TSTAR
  WRITE(2,109)TSTAR
  IF (TSTAR .GT. 5.0) THEN
    WRITE(6,161)
    GO TO 900
  ENDIF

```

C
C
C
C

--- ASSIGN INDEX I FOR VALUE OF QSTAR

```

I = 10
IF (QSTAR.LT.0.05) THEN
  WRITE(6,110)
ELSE IF (QSTAR.EQ.0.05) THEN
  I = 1
ELSE IF (QSTAR.GT.0.05.AND.QSTAR.LT.0.1) THEN
  I = 6
ELSE IF (QSTAR.EQ.0.1) THEN
  I = 2
ELSE IF (QSTAR.GT.0.1.AND.QSTAR.LT.0.5) THEN
  I = 7
ELSE IF (QSTAR.EQ.0.5) THEN
  I = 3
ELSE IF (QSTAR.GT.0.5.AND.QSTAR.LT.1.0) THEN
  I = 8
ELSE IF (QSTAR.EQ.1.0) THEN
  I = 4
ELSE IF (QSTAR.GT.1.0.AND.QSTAR.LT.5.0) THEN
  I = 9
ELSE IF (QSTAR.EQ.5.0) THEN
  I = 5
ELSE IF (QSTAR.GT.5.0) THEN
  WRITE(6,120)
ENDIF
IF (I .EQ. 10) THEN
  WRITE(6,160)
  GO TO 900
ENDIF

```

C
C
C
C

--- ASSIGN INDEX J FOR VALUE OF N

```
J = 12
IF (N.LT.1.5) THEN
  WRITE(6,130)
ELSE IF (N.EQ.1.5) THEN
  J = 1
ELSE IF (N.GT.1.5.AND.N.LT.1.75) THEN
  J = 7
ELSE IF (N.EQ.1.75) THEN
  J = 2
ELSE IF (N.GT.1.75.AND.N.LT.2.0) THEN
  J = 8
ELSE IF (N.EQ.2.0) THEN
  J = 3
ELSE IF (N.GT.2.0.AND.N.LT.2.5) THEN
  J = 9
ELSE IF (N.EQ.2.5) THEN
  J = 4
ELSE IF (N.GT.2.5.AND.N.LT.3.5) THEN
  J = 10
ELSE IF (N.EQ.3.5) THEN
  J = 5
ELSE IF (N.GT.3.5.AND.N.LT.5.0) THEN
  J = 11
ELSE IF (N.EQ.5.0) THEN
  J = 6
ELSE IF (N.GT.5.0) THEN
  WRITE(6,140)
ENDIF
IF (J.EQ.12) THEN
  WRITE(6,160)
  GO TO 900
ENDIF
```

C
C
C
C

--- COMPUTE DIMENSIONLESS DISTANCES AND WETTED VOLUMES

```
IF (I.LT.6.AND.J.LT.7) THEN
  K = 1
  DO 610 M = 1,4
    DV(M) = VAL(I,J,K)*TSTAR**0.5+VAL(I,J,K+1)*TSTAR
    &      +VAL(I,J,K+2)*TSTAR**1.5
    K=K+3
610  CONTINUE
    WRITE(6,119)
    WRITE(2,119)
```

```

C
C -----
C --- INTERPOLATE FOR QSTAR AND N
C -----
      ELSE IF (I.GE.6.AND.J.GE.7) THEN
        DO 640 P = 5,4,-1
          K = 1
          DO 630 M = 1,4
            DO 620 R = 6,5,-1
              DTMP(R)=VAL(I-P,J-R,K)*TSTAR**0.5+VAL(I-P,J-R,K+1)
              & *TSTAR+VAL(I-P,J-R,K+2)*TSTAR**1.5
620          CONTINUE
              D(M,P)=INTERP(N,ND(I-P,J-6),ND(I-P,J-5),DTMP(6),DTMP(5))
              K=K+3
              DV(M)=INTERP(QSTAR,QS(I-5),QS(I-4),D(M,5),D(M,4))
630          CONTINUE
640          CONTINUE
              WRITE(6,127)
              WRITE(2,127)

C
C -----
C --- INTERPOLATE FOR N ONLY
C -----
      ELSE IF (I.LT.6.AND.J.GE.7) THEN
        K=1
        DO 660 M = 1,4
          DO 650 R = 6,5,-1
            DTMP(R)=VAL(I,J-R,K)*TSTAR**0.5+VAL(I,J-R,K+1)*TSTAR
            & +VAL(I,J-R,K+2)*TSTAR**1.5
650          CONTINUE
            DV(M)=INTERP(N,ND(I,J-6),ND(I,J-5),DTMP(6),DTMP(5))
            K=K+3
660          CONTINUE
              WRITE(6,128)
              WRITE(2,128)

C
C -----
C --- INTERPOLATE FOR QSTAR ONLY
C -----
      ELSE IF (I.GE.6.AND.J.LT.7) THEN
        K=1
        DO 680 M = 1,4
          DO 670 R = 5,4,-1
            DTMP(R)=VAL(I-R,J,K)*TSTAR**0.5+VAL(I-R,J,K+1)
            & *TSTAR+VAL(I-R,J,K+2)*TSTAR**1.5
670          CONTINUE
            DV(M)=INTERP(QSTAR,QS(I-5),QS(I-4),DTMP(5),DTMP(4))
            K=K+3
680          CONTINUE
              WRITE(6,129)
              WRITE(2,129)

```

```

      ENDIF
C
      IF (DV(1) .GT. 4.5) THEN
        WRITE(6,162)
        WRITE(2,162)
        GO TO 900
      ENDIF

C
C -----
C --- COMPUTE ACTUAL DISTANCES AND VOLUMES
C -----
      V = DV(1)/ALPHA
      DIAG = DV(2)/ALPHA
      H = DV(3)/ALPHA
      VOL = DV(4)/ALPHA**3
      WRITE(2,600)TIME(A),V,DIAG,H,VOL
      WRITE(6,600)TIME(A),V,DIAG,H,VOL

C
C
108 FORMAT(/1X,'ALPHA = ',E10.4,' Q = ',E10.4,' KS = ',E10.4,
      &' QSTAR = ',E10.4)
109 FORMAT(/1X,'TSTAR = ',E10.4)
110 FORMAT(1X,'QSTAR IS LESS THAN MINIMUM VALUE OF 0.05 ')
119 FORMAT(1X,'DIRECT TABLE LOOK-UP; NO INTERPOLATION')
120 FORMAT(1X,'QSTAR IS GREATER THAN MAXIMUM VALUE OF 5.0 ')
127 FORMAT(1X,'INTERPOLATION FOR QSTAR AND N')
128 FORMAT(1X,'INTERPOLATION FOR N ONLY')
129 FORMAT(1X,'INTERPOLATION FOR QSTAR ONLY')
130 FORMAT(1X,'N IS LESS THAN MINIMUM VALUE OF 1.5 ')
140 FORMAT(1X,'N IS GREATER THAN MAXIMUM VALUE OF 5.0 ')
160 FORMAT(1X,'VALUES OUTSIDE OF TABLE LIMITS')
161 FORMAT(1X,'COEFFICIENTS NOT VALID FOR TSTAR > 5.0 ')
162 FORMAT(1X,'COEFFICIENTS NOT VALID FOR DV > 4.5')
600 FORMAT(1X,'TIME = ',F5.3,' V = ',E10.4,' D = ',E10.4,
      &' H = ',E10.4,' VOL. = ',E10.4)
900 CONTINUE
      STOP
      END

```

DISTRIBUTION

<u>No. of Copies</u>		<u>No. of Copies</u>	
12	DOE Office of Scientific and Technical Information	3	Battelle Memorial Institute Project Management Division 505 King Avenue Columbus, OH 43201 ATTN: W. A. Carbeiner W. S. Madia Technical Library
5	DOE Idaho Operations Office 550 Second Street Idaho Falls, ID 83401 ATTN: J. P. Hamric S. T. Hirschberger J. L. Lyle O. D. Markham T. E. Reynolds		G. S. Campbell Agronomy Department Washington State University Pullman, WA 99164
6	DOE Office of Civilian Radioactive Waste Management Forrestal Building Washington, DC 20585 ATTN: L. H. Barrett, RW-33 C. R. Cooley, RW-40 J. R. Hilley, RW-30 S. H. Kale, RW-20 D. E. Shelor, RW-32 R. Stein, RW-23		D. Hillel Department of Plant and Soil Science 12A Stockbridge Hall University of Massachusetts Amherst, MA 01003
4	DOE Office of Defense Waste & Transporation Management GTN Washington, DC 20545 ATTN: T. C. Chee, DP-123 K. A. Chorey, DP-123 G. H. Daly, DP-124 J. E. Lytle, DP-12	2	Idaho National Engineering Laboratory P.O. Box 1625 Idaho Falls, ID 83415 ATTN: J. B. Sisson Technical Library
4	DOE Office of Remedial Action & Waste Technology GTN Washington, DC 20545 ATTN: J. A. Coleman, NE-24 T. W. McIntosh, NE-24 W. R. Voight, NE-20 H. F. Walter, NE-24	2	Jacobs Engineering Group, Inc. 5301 Central Avenue NE Suite 1700 Albuquerque, NM 87108 ATTN: N. B. Larson C. Reith
		2	Los Alamos National Laboratory P.O. Box 663 Los Alamos, NM 87545 ATTN: T. E. Hakonson J. W. Nyhan

No. of
Copies

No. of
Copies

ONSITE

- 4 DOE Richland Field Office
J. J. Broderick
R. D. Freeburg
M. J. Furman
J. M. Hennig
- 15 Westinghouse Hanford Company
M. R. Adams
H. Babad
J. D. Berger
L. C. Brown
J. W. Cammann
R. A. Carlson
J. D. Davis
W. F. Heine
K. N. Jordan
D. R. Myers
K. L. Petersen
S. J. Phillips
M. R. Sackschewsky
J. C. Sonnichsen
N. R. Wing
- EPA - Hanford Project Office
D. R. Sherwood, A7-70
- 42 Pacific Northwest Laboratory
L. L. Cadwell
M. D. Campbell
J. C. Chatters
J. L. Downs

- M. J. Fayer (10)
H. D. Freeman
G. W. Gee (2)
D. J. Holford
C. T. Kincaid
R. R. Kirkham
G. V. Last
M. W. Ligothke
S. O. Link
W. J. Martin
W. E. Nichols
W. T. Pennell
M. L. Rockhold
L. E. Rogers
C. S. Simmons
J. L. Smoot
D. L. Stewart
G. P. Strelle
J. M. Thomas
W. H. Walters
R. E. Wildung
Publishing Coordination
Technical Report Files (5)

Routing

- R. M. Ecker
J. W. Falco
M. J. Graham
R. L. Skaggs
P. C. Hays (last)

END

**DATE
FILMED**

5 / 6 / 92

